The Roles of Actin and Microtubule-based Motor Proteins in T Cell Activation

Chang K. Yi

A dissertation submitted to the faculty of the University of North Carolina at Chapel Hill in partial fulfillment of the requirements for the degree of Doctor of Philosophy in the Department of Biology

Chapel Hill
2012

Approved by,

Dr. John A. Hammer III

Dr. Xufeng S. Wu

Dr. Kerry S. Bloom

Dr. Stephen Rogers

Dr. Lawrence E. Samelson

Dr. Kevin Slep

ABSTRACT

Chang K. Yi: The Roles of Actin and Microtubule-based Motor Proteins in T Cell Activation
(Under the direction of Dr. John A. Hammer III)

T cell activation is a critical process in our body's fight against infection and disease. The activation process begins upon encounter with stimulatory antigen presenting cells (APCs), which leads to the rapid polarization of various cellular components in T cells. At the membrane of the contact site, T cell receptors (TCRs), adhesion molecules, and other accessory components become differentially clustered and rearranged to form a supra-molecular structure called the immunological synapse. While both actin retrograde flow and myosin IIA activity have been implicated in immunological synapse formation, their relative organization and dynamics at the immunological synapse, and their relative contributions toward the reorganization of receptor clusters have not been fully understood. In this study, we show that the immunological synapse is essentially a radially symmetric migrating cell, as previously hypothesized, and provide direct proof that classical lamellipodial and lamellar actin networks localize at dSMAC and pSMAC regions, respectively. Moreover, our experiments using actin and myosin II inhibitors reveal that actin retrograde flow and actomyosin II contraction work coordinately to drive the inward movements of receptor clusters at the immunological synapse.

Concomitant with immunological synapse formation, the microtubule organizing center (MTOC) polarizes rapidly toward the contact site with the APC to position the secretory apparatus for directed secretion. Due to the lack of spatial and temporal control in most previous studies, the kinetics of MTOC repositioning have not been well characterized in T cells. In addition, the specific roles of dynein and dynein regulatory proteins during T

cell activation have not been defined. In this study, we show using an optical trap-controlled T cell activation method that TCR and LFA-1 signaling are both required for robust MTOC repositioning. Moreover, we report that the repositioning process is bi-phasic, with distinct kinetics at each phase of MTOC movement. Lastly, inhibition experiments using dominant negative constructs show that dynein and LIS1 are required for both phases of MTOC repositioning. In conclusion, the actin and microtubule cytoskeletal systems mediate many distinct aspects of T cell activation, and are critical components of the overall adaptive immune response.

To my loving parents

With deepest admiration and gratitude

ACKNOWLEDGEMENTS

We shall not cease from exploration
And the end of all our exploring
Will be to arrive where we started
And know the place for the first time.

- T.S. Eliot

It has been an incredible honor to have received training at NIH, one of the premier research institutions in the world, and to have interacted with many gifted scientists through the UNC partnership program. First, I would like to thank the members of my committee, Drs. Kerry Bloom, Stephen Rogers, Lawrence Samelson, and Kevin Slep for their invaluable input and support through the years. Also, I thank my mentor, Dr. John Hammer, for his guidance and friendship. His passion for scientific rigor and integrity, and his deep sense of humanity have impacted me greatly. Next, I would like to thank the chairperson of my committee, Dr. Xufeng Wu, for her innumerable contributions to my graduate experience. Her magnanimous heart, adventurous spirit, and keen scientific mind have inspired me on a regular basis. Our exuberant, ad lib discussions over “cool” results will surely be missed.

This dissertation would not have been possible without the constant support and care from my family. Words cannot express the deep respect and appreciation I feel toward my parents, Kwang Taek and Chong Hee Yi, who have dedicated their lives toward my growth as a student and as an individual. I’m inspired by their immigrant journey, and the many sacrifices they’ve made along the way. This dissertation has been, in no small part, a labor of love in celebration of their journey. Lastly, and most importantly, I thank my wife, Chanmi Yi, for her support and encouragement throughout my graduate career. She has

been a constant source of warmth and joy, enriching the often monotonous experience of basic research. Thank you for making the journey worthwhile.

TABLE OF CONTENTS

LIST OF FIGURES

LIST OF ABBREVIATIONS

ADAP	Adhesion and degranulation-promoting protein
ADP	Adenosine diphosphate
APC	Antigen presenting cell
ATP	Adenosine triphosphate
BB	Blebbistatin
CC1	Coiled coil region 1
CD	Cytochalasin D
CN	Control
cSMAC	Central SMAC
CTL	Cytotoxic T Lymphocyte
DAG	Diacylglycerol
DNS	Data not shown
dSMAC	Distal SMAC
ELC	Essential light chain
FMNL1	Formin-like 1
FRAP	Fluorescence recovery after photobleaching
GEF	Guanine exchange factor
GFP	Green flourescent protein
HC	Heavy chain
IC	Intermediate chain
ICAM-1	Intercellular adhesion molecule-1
IS	Immunological synapse
ITAM	Immunoreceptor-based tyrosine activation motif
Jas	Jasplakinolide
LAT	Linker for activation of T cells

LC	Light chain
LFA-1	Lymphocyte function-associated antigen-1
LIC	Light intermediate chain
LM	Lamella
LP	Lamellipodia
MC	Microcluster
MPM	Modulated polarization microscopy
MT	Microtubule
MTOC	Microtubule organizing center
pMHC	Peptide-bound major histocompatibility complex
pSMAC	Peripheral SMAC
PTK	Protein tyrosine kinase
RFP	Red flourescent protein
SH2	Src-homology 2
shRNA	Short hairpin ribonucleic acid
siRNA	Short interference ribonucleic acid
SMAC	Supra-molecular activation cluster
TCR	T cell receptor
WT	Wild type

CHAPTER 1

INTRODUCTION

I. Overview

The actin and microtubule cytoskeleton are known to play critical roles in T cell function. They are involved in signaling of antigen receptors, formation of the immunological synapse, and focused delivery of effector molecules, which are necessary for targeted cell death and communication between lymphocytes. In addition, these cytoskeletal systems play important roles in numerous fundamental cellular processes such as directed cell migration and asymmetric cell division. Thus, the investigation of the role of actin and MTs in T cells is relevant not just for the study of cell-mediated immunity, but also for the discovery of common biological mechanisms in cytoskeletal function and regulation.

II. Lymphocytes and adaptive immunity

Lymphocytes are essential for adaptive immunity against infection from pathogens, and the emergence of immune-related diseases, such as AIDS, has served to underscore their importance. Adaptive immunity refers to the body's ability to generate a specific immune response toward particular microbes and microbial toxins, and its ability to mount an amplified response upon future exposure to those same pathogens. In adaptive immunity, the response is largely carried out by two types of cells: B and T lymphocytes. The B lymphocytes are responsible for the production of antibodies which mediate humoral immunity, whereas the cooperative action by various subsets of T lymphocytes constitutes cell-mediated immunity (Abbas and Lichtman, 2006).

T Lymphocytes are equipped with specialized receptors, T cell receptors (TCRs), which engage peptide-bound major histocompatibility complexes (pMHCs) on the surface of antigen presenting cells (APCs). There are two subsets of T cells, distinguished by the presence of either CD4 or CD8 glycoprotein on the cell surface. $CD4^+$ T cells are called helper T cells because of their role in helping B cells produce antibodies, as well as in helping phagocytes destroy harmful microbes, $CD8^+$ T cells are called cytotoxic T lymphocytes (CTL's) because of their role in lysing infected cells (Abbas and Lichtman, 2006).

All T cells have their origin in the thymus, where progenitors differentiate into T cells after migration from the bone marrow. These "naïve" T cells then leave the thymus and circulate between peripheral lymphoid organs where they encounter multiple APCs. After recognition of antigen, naive T cells proliferate and differentiate into two different types of T cells: effector and memory cells. Effector helper T cells secrete cytokines to activate macrophages and B cells, whereas effector CTLs develop the ability to kill infected cells. Effector T cells are usually short-lived while memory T cells can continue to survive long after differentiation. Although memory cells are functionally "silent," they can give rise to a large population of effector cells upon re-encountering the same antigen, which is the basis for the rapid, amplified nature of the secondary immune response (Abbas and Lichtman, 2006).

III. Signaling pathways of T cell activation

a. TCR signal transduction

Underlying T cell activation is the outside-in signal transduction mediated by the TCR signaling complex. The TCR signaling complex consists of α-, β-, and ζ- TCR chains and a repertoire of CD3 subunits, which associate with the TCR to form the functional signaling complex (Chan *et al.*, 1994; Samelson, 2002; Guy and Vignali, 2009). Recognition and

binding of pMHC by the α-and β- TCR chains initiates the signal transduction cascade by recruiting Src-family of protein tyrosine kinases (PTKs) Lck and Fyn to phosphorylate the immunoreceptor-based tyrosine activation motifs (ITAMs) on the CD3 subunits and the ζ-chain of the TCR complex (Fig. 1) (Chan *et al.*, 1994; Samelson, 2002; Billadeau *et al.*, 2007; Guy and Vignali, 2009). This leads to the binding and activation of a Syk-family PTK, ZAP-70, which in turn phosphorylates key adaptor proteins, including the transmembrane protein LAT (linker for activation of T cells) (Fig. 1) (Samelson, 2002; Billadeau *et al.*, 2007). LAT also contains several ITAMs which can bind Src homology (SH2)-containing molecules such as PLCγ1 and SLP76, and functions as a protein scaffold for the recruitment of multiple downstream effectors involved in TCR signal transduction (Fig. 1) (O'Shea, 2000; Samelson, 2002; Billadeau *et al.*, 2007).

b. Integrin regulation and signaling

In addition to TCR signaling, full activation of T cells requires the engagement of co-stimulatory and adhesion molecules (Guy and Vignali, 2009). A major example is the β_2-integrin, LFA-1 (lymphocyte function-associated antigen-1; $\alpha_L\beta_2$), which binds ICAM-1 (intercellular adhesion molecule-1) on the surface of APCs (Kinashi, 2005). LFA-1 is involved in adhesion to APCs, and is critical for the effector function of T cells during activation (Kinashi, 2005). In contrast to the TCR, LFA-1 integrins are initially regulated by inside-out signaling, and require T cell stimulation by antigen or cytokines to become activated (Baker and Koretzky, 2008). In non-stimulated T cells, LFA-1 integrins adopt a low-affinity, bent conformation, and lack the ability to form multivalent clusters. However, engagement of the T cell antigen receptor alters the avidity of LFA-1 by opening the heterodimer into a high-affinity ligand binding state, as well as allowing the formation of multivalent LFA-1 clusters (Kinashi, 2005). This TCR-dependent increase in LFA-1 avidity requires LAT recruitment of PLCγ1, which leads to calcium flux and diacylglycerol (DAG)

Figure 1. **Illustration of the TCR signaling cascade** (Billadeau *et al*., 2007).

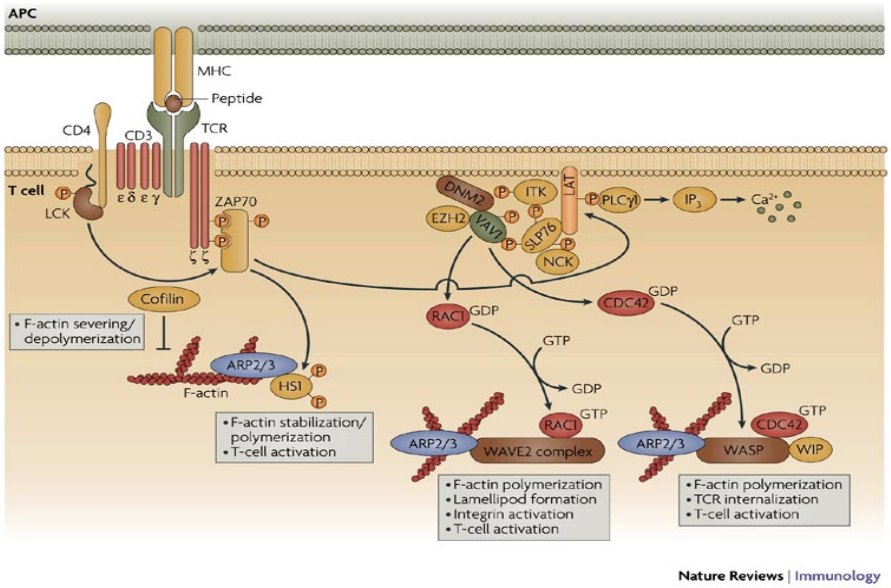

production, and SLP76, which activates VAV1, an important guanine exchange factor (GEF) involved in actin reorganization (Fig 1) (Billadeau *et al.*, 2007; Baker and Koretzky, 2008). Also, SLP76 associates with ADAP (adhesion and degranulation-promoting protein), an adaptor molecule required for integrin function in T cells (Baker and Koretzky, 2008). Once activated, LFA-1 contributes to the outside-in co-stimulatory signal to enhance T cell activation and effector function.

IV. Immunological Synapse

a. Identity and function of SMAC domains

APC engagement also leads to dramatic changes at the cellular level in T lymphocytes. Upon binding their respective ligands on the surface of the APC, antigen receptors and adhesion proteins undergo differential clustering and rearrangement at the synaptic junction to form segregated, concentric domains known as supra-molecular activating clusters (SMACs) (Monks *et al.*, 1998; Grakoui *et al.*, 1999; Fooksman *et al.*, 2010). The resulting bull's-eye pattern of SMACs is a hallmark of the immunological synapse (IS), and provides the structural basis for signaling and secretion at the T cell-APC interface. The center area of the IS, known as the central SMAC (cSMAC), is marked by the accumulation of TCRs, which are bound to pMHCs on the surface of the APC (Monks *et al.*, 1998). The surrounding ring of the bull's eye, known as the peripheral SMAC (pSMAC), is marked by LFA-1 clusters, which are bound to ICAM-1 receptors present on the APC surface (Monks *et al.*, 1998). The outermost ring, known as the distal SMAC (dSMAC), is marked by CD45, as well as an enrichment of F-actin (Freiberg *et al.*, 2002; Sims *et al.*, 2007).

Recent studies argue that TCR signaling is degraded at the cSMAC, and that active signaling actually takes place at the periphery of the IS (Yokosuka *et al.*, 2005; Varma *et al.*, 2006; Vardhana *et al.*, 2010). Thus, the pSMAC region may serve dual functions during T

cell activation: as a zone of adhesion between the T cell and the APC, and as a zone of active TCR signaling at the IS. Meanwhile, the dSMAC is thought to function as a zone of exclusion from the IS, owing to the localization of receptors with large ecto-domains and/or inhibitory effect on TCR signaling (Freiberg *et al.*, 2002).

Substitution of the APC surface with a supported planar lipid bilayer displaying stimulatory molecules has been shown to replicate the signaling activity and spatial organization of the IS, and has become an important tool in the study of T cell activation (Grakoui *et al.*, 1999; Dustin, 2009). Alternatively, glass coverslips coated with stimulatory molecules can be used to engage and activate T cells (Bunnell *et al.*, 2003). However, since the stimulatory ligands are immobilized on the coverslip substrate, antigen receptors and adhesion molecules on the T cell surface cannot rearrange to form the bull's eye pattern of SMACs, as observed after engagement to APC and planar bilayer substrates. This difference between the coverslip and planar bilayer substrates has been utilized in our imaging studies to distinguish the reorganization of molecules occurring at the membrane from that of the synaptic cortex.

b. TCR MCs and the regulation of TCR signaling

T cells display remarkable sensitivity to antigen despite the relatively weak affinity of TCRs for pMHCs and low numbers of available ligand on the APC surface (Shaw and Dustin, 1997; Huppa and Davis, 2003). It is known that stimulation by a single pMHC on the APC surface is sufficient for transient activation of T cells, and that engagement of ~10 pMHC molecules can result in sustained activation (Irvine *et al.*, 2002). This sensitivity is, in part, enabled by the T cell co-receptor, as helper T cells lacking the CD4 co-receptor require higher numbers of pMHC for activation and show reduced ability to form a mature IS (Irvine *et al.*, 2002).

However, sensitization of individual TCRs cannot account for the prolonged TCR signaling observed during T cell activation (on the order of hours), as their association with antigen is short-lived (on the order of seconds) (Huppa and Davis, 2003). Rather, this requires amplification of signal from the transiently engaged TCRs through a multi-protein structure at the membrane called the TCR microcluster (MC). Within seconds of T cell engagement to the anti-CD3-bound substrate, TCR MCs form at the contact site (Grakoui *et al.*, 1999; Bunnell *et al.*, 2002). These MCs are estimated to contain ~100 TCR molecules, and act as a platform for the recruitment and activation of downstream signaling molecules (Campi *et al.*, 2005; Varma *et al.*, 2006). Studies using artificial substrates have shown concentrated tyrosine phosphorylation activity, as well as dynamic localization of ZAP70, Lck, and LAT to these MCs, indicating that the TCR MC functions as a basic signaling unit during T cell activation (Bunnell *et al.*, 2002; Campi *et al.*, 2005; Yokosuka *et al.*, 2005; Varma *et al.*, 2006). Paradoxically, either signal amplification or degradation can be observed at TCR MCs, depending on the strength of antigenic peptide utilized (Lee *et al.*, 2003). Based on this result, A. Shaw and colleagues propose that TCR signaling is actively tuned at the IS, allowing amplification of weak signals and dampening of strong signals (Cemerski and Shaw, 2006).

Further regulation of TCR signaling occurs via active transport of TCR MCs. During IS formation, TCR MCs form at the periphery and are transported toward the center of the IS through an actin-dependent mechanism (Campi *et al.*, 2005; Varma *et al.*, 2006; Kaizuka *et al.*, 2007). However, once accumulated at the cSMAC, these MCs disassociate from downstream signaling molecules, lose their tyrosine phosphorylation activity, and are internalized for recycling back to the IS periphery (Yokosuka *et al.*, 2005; Varma *et al.*, 2006). Thus, it is through the continuous formation and cycling of TCR MCs that TCR signaling is sustained for full T cell activation.

V. The role of actin and myosin IIA in IS formation

a. Non-muscle myosin IIA

Non-muscle myosin II (referred to here as myosin II), a subclass of myosin motor proteins, is expressed in all eukaryotic non-muscle cells and is involved in many crucial functions of the cell, including cell polarity, migration, and cytokinesis. It is composed of two heavy chains (HCs), two regulatory light chains (RLCs), and two essential light chains (ELCs). The globular N-terminal head region of the HCs contains the binding site for actin and catalytic sites for ATP hydrolysis, and generates the force required for myosin II contractile activity. Adjacent to the head is a neck region that binds the regulatory and essential LCs, and acts as a level arm to amplify the small ATP-hydrolysis induced conformational changes in the head, allowing the myosin to step. Following the neck is a long coiled-coil rod domain that mediates dimerization of the HCs, and a short-helical tail that contain multiple phosphorylation sites for regulation of myosin II activity. The rod domains of multiple myosin II dimers self-associate to form bipolar filaments, which can then bind and exert tension on actin filaments to form contractile structures in cells (Vicente-Manzanares *et al.*, 2009).

Three myosin II HC genes exist in mammalian cells (MYH9, MYH 10, and MYH14), giving rise to three myosin II isoforms (myosin IIA, IIB, and IIC, respectively) that differ in structure, regulation, localization and function. *In vitro* experiments have shown that myosin IIA displays the highest rate of ATPase hydrolysis and the fastest rate of actin filament displacement. Myosin IIA plays critical roles in leading edge protrusion and adhesion in migrating cells and is the dominant isoform expressed in mammalian T cells (Jacobelli *et al.*, 2004; Morin *et al.*, 2008; Vicente-Manzanares *et al.*, 2009).

b. Actin networks in migrating cells

The actin cytoskeleton is required for numerous fundamental cellular processes and has been studied in a broad spectrum of cellular systems (Gardel *et al.*, 2010). In particular, characterization of actin networks at the leading edge of migrating cells has yielded important understanding of their dynamics and function in recent decades. At the leading edge is the lamellipodia (LP), where a branched network of dendritic F-actin filaments undergoes rapid actin retrograde flow, driven by actin polymerization at the front and depolymerization at the rear of the LP (Pollard and Borisy, 2003; Ponti *et al.*, 2004). Polymerization of actin requires addition of ATP-bound actin monomers to the "barbed" ends of growing filaments, and Arp2/3, which creates free barbed ends by *de novo* nucleation of actin filaments off the sides of pre-existing filaments (Pollard and Borisy, 2003). On the other hand, ADF cofilin (which can also create free barbed ends by severing existing actin filaments) promotes depolymerization of actin at the "pointed" ends of actin filaments (Pollard and Borisy, 2003). The resulting actin retrograde flow provides the protrusive 'pushing' force against the leading edge membrane when the cell is engaged to a substrate, and is the kinetic signature of the LP actin network.

Proximal to the LP is the lamella (LM), where transverse arcs containing actin and myosin IIA filaments undergo slow contraction toward and disassembly at the cell rear (Medeiros *et al.*, 2006; Wilson *et al.*, 2010). The contraction of acto-myosin IIA filaments provides the 'pulling' force for actin networks at the cell cortex, and is the kinetic signature of the LM actin network. Focal adhesion complexes enriched with integrins and associated signaling proteins also form in the LM, and are known to mediate the linkage between the cortical actin networks and the extracellular matrix (Gardel *et al.*, 2010). In combination with actin polymerization-driven protrusion in the LP, contraction of acto-myosin IIA filaments against these focal adhesion complexes results in the net forward movement of the cell body during cell migration.

c. The roles of actin and myosin IIA in T cell function

Actin networks also regulate various aspects of T cell activation. *In vivo* studies have shown that the initial stages of migration, polarization, and synapse formation require the actin cytoskeleton (Billadeau *et al.*, 2007). More recently, *in vitro* experiments utilizing supported planar bilayer and immobilized coverslip substrates have revealed an intricate link between receptor-ligand complexes and cortical F-actin at the IS (Barda-Saad *et al.*, 2005; Campi *et al.*, 2005). Upon contact with a stimulatory surface, sub-micron-sized TCR MCs form and signal downstream to activate actin polymerization (Bunnell *et al.*, 2001; Varma *et al.*, 2006). This leads to increased cell spreading and further nucleation of TCR and LFA-1 clusters. On laterally mobile substrates, these newly formed TCR and LFA-1 clusters subsequently undergo actin-dependent centripetal transport to accumulate at their respective SMAC regions, forming the bull's eye pattern of the IS (Kaizuka *et al.*, 2007). However, the rate of actin retrograde flow is reported to be two-fold higher than that of receptor cluster movements (Kaizuka *et al.*, 2007), and TCR MCs are able to move around physical barriers in the bilayer substrate without cortical F-actin reorganization (DeMond *et al.*, 2008), suggesting an inherent "slippage" in the mechanism of coupling between receptor clusters and cortical actin . Moreover, receptor clusters appear to be differentially linked to cortical actin networks as pre-formed LFA-1, but not TCR, clusters are destabilized by Latrunculin B treatment (Campi *et al.*, 2005; Kaizuka *et al.*, 2007). While the molecular interactions mediating these linkages are unknown, centripetal flow of cortical actin has emerged as the likely driving mechanism behind receptor transport at the IS.

The synaptic interface of T lymphocytes is analogous to the leading edge of migrating cells, as previously noted by M. Dustin and colleagues. Based on the motility of T cells on the planar bilayer substrate, as well as the localization of LP and LM markers at the IS, the dSMAC and pSMAC regions were predicted to be functionally equivalent to the LP and LM networks, respectively (Dustin *et al.*, 2007; Sims *et al.*, 2007). There is evidence of

LP network involvement in IS formation. Regulators of dendritic actin nucleation, such as Arp2/3 and the WAVE/WASP complex, are known to be recruited and activated by VAV1 during TCR signal transduction (Fig. 1) (Billadeau *et al.*, 2007). Dynamic ruffling has been described at the contact site between T cells and APCs, and rapid actin treadmilling has been observed at the IS as imaged by ectopic expression of GFP-actin (Bunnell *et al.*, 2001; Kaizuka *et al.*, 2007). Additionally, inhibition of actin polymerization is known to disrupt the inward movement of receptor clusters at the IS (Campi *et al.*, 2005; Varma *et al.*, 2006; Kaizuka *et al.*, 2007). In contrast, it is not known whether a classical LM network functions at the IS, as no one has described acto-myosin II arcs or focal adhesion complexes at the IS. Consistent with these observations, R. Vale and colleagues have proposed that a single LP actin network exists at the IS, and that actin retrograde flow drives the inward movement of receptor clusters at the IS (Kaizuka *et al.*, 2007).

Myosin IIA is known to regulate the migration and adhesion of T cells (Jacobelli *et al.*, 2004; Morin *et al.*, 2008), and has been implicated in the secretion of lytic granules in natural killer cells (Andzelm *et al.*, 2007). However, the role of myosin IIA in T cell activation is unclear as conflicting reports exist regarding the regulation and function of myosin IIA in IS formation. Jacobelli *et al*. reported that IS formation does not require myosin IIA, as TCR and LFA-1 receptors reorganized into the bull's eye pattern of cSMAC and pSMAC regions in blebbistatin-treated T cells (Jacobelli *et al.*, 2004). On the other hand, recent report by M. Dustin and colleagues showed that myosin IIA is required for IS formation, as inhibition of myosin IIA, using blebbistatin and siRNA knockdown of myosin IIA heavy chain, disrupted the directed movement of TCR MCs as well as cSMAC formation (Ilani *et al.*, 2009). However, actin and myosin IIA were not dynamically imaged at the IS, and the relative contribution of actin retrograde flow and myosin II contractility to IS formation was not quantitatively analyzed in these studies, thus giving very little information about how actin and myosin II are involved in IS formation.

VI. The role of dynein in MTOC repositioning in T cells

a. Cytoplasmic Dynein

Dynein is a class of minus end-directed MT motor proteins involved in a wide range of cellular functions including cargo transport, asymmetric cell division, and cell polarity (Dujardin and Vallee, 2002; Kardon and Vale, 2009; Allan, 2011). In contrast to other classes of cytoskeletal motors, only a single dynein, cytoplasmic dynein, accommodates these diverse functions in non-axonemal cells. Cytoplasmic dynein (referred to here as dynein) is a large complex composed of a heavy chain (HC) and several non-catalytic subunits. The C-terminal portion of the HC contains a coiled-coil "stalk" extension that mediates binding to the MT and a ring-shaped "head" consisting of six AAA domains that functions as the catalytic site for ATP hydrolysis. In addition to the AAA domains, the "head" region contains a linker domain that shifts its position on the catalytic ring during the ATPase cycle, and possibly serves as the mechanical element in the dynein power stroke. The N-terminal "tail" portion is involved in the homo-dimerization of HCs and functions as a scaffold to recruit dimers of non-catalytic subunits: TCTEX 1, light chain 8 (LC8), LC7, intermediate chain (IC), and light intermediate chain (LIC). These non-catalytic subunits are implicated in the binding of selective cargo, and are known to associate with different adaptor proteins that regulate the activity of dynein in cells (Kardon and Vale, 2009).

b. Dynein adaptor proteins

Among the dynein adaptor proteins, two complexes have become of interest: dynactin and LIS1-NUDE/NUDEL. Like dynein, dynactin is a large complex comprised of multiple subunits, including p150 which mediates binding of dynactin to the dynein complex through its N-terminal coiled coil region (CC1). Dynactin is involved in the targeting of dynein to specific cellular regions, binding of dynein to cargo, and modulates the

processivity of dynein's movement on MTs. Regarding the latter role of dynactin, *in vitro* experiments showed that dynein processivity along MT tracks increased almost two-fold in the presence of dynactin. Initially, this enhancement in processivity was attributed to the increased tethering of the dynein-dynactin complex to MTs via the CAP-Gly MT-binding domain of p150, but subsequent *in vivo* studies showed that the CAP-Gly domain was dispensable for modulation of dynein processivity. At present, the mechanism by which dynactin affects dynein motility remains unclear (Kardon and Vale, 2009).

In addition to dynactin, LIS1 plays an important role in the regulation of dynein activity. LIS1 is thought to be an important cofactor for dynein, and forms a tripartite complex with dynein and the LIS1-binding partner, NUDE or NUDEL (in metazoans). LIS1 is composed of an N-terminal coiled-coil domain that mediates dimerization, and a C-terminal WD40 domain that binds to an ATPase domain (AAA^1) in the head region of the dynein HC, and possibly to the tail region of the HC as well as the p50 subunit of dynactin. In budding yeast, homologs of LIS1 and NUDE (Pac1 and Ndl1, respectively) are involved in the localization of dynein at the plus ends of MTs, and in the cortical anchoring of dynein at the bud cell during cell division. In metazoans, LIS1, NUDE, and NUDEL are required for dynein-mediated positioning of the nucleus, centrosome and the mitotic spindle, and are involved in the cortical anchoring of dynein during spindle repositioning (Kardon and Vale, 2009).

Furthermore, recent reports from R. Vallee and colleagues show that NUDE recruits LIS1 to the dynein complex to modulate force generation, distinct from dynactin-regulated dynein activity. Specifically, LIS1-NUDE associates with dynein to induce a sustained state of force generation under high load conditions (McKenney *et al.*, 2010). Association with LIS1-NUDE also improved the ensemble activity of multiple dynein motors, promoting dynein activity under high load conditions (McKenney *et al.*, 2010). Furthermore, NUDE and dynactin share a common binding site on the dynein IC subunit, suggesting that association

of dynein with LIS1-NUDE and dynactin is mutually exclusive (McKenney *et al.*, 2011). While it is unclear whether LIS1-NUDE and dynactin compete with other adaptors for association with dynein, these results are consistent with the emerging idea that differential binding to adaptor proteins allows dynein to accommodate a wide range of cargos and functions in the cell (Kardon and Vale, 2009).

c. MTOC repositioning in T cells

Concomitant with IS formation, APC engagement leads to rapid repositioning of the MTOC toward the contact site in T cells (Kupfer and Dennert, 1984). It is believed that MTOC repositioning serves as a key step in the directed secretion of effector molecules in T lymphocytes (Sancho *et al.*, 2002). In the case of target cell killing by CTLs, antigen recognition and subsequent TCR signaling leads to rapid MTOC polarization to the IS (Stinchcombe *et al.*, 2006). Lytic granules, then, move to the centrosome via dynein-mediated intracellular transport, and undergo docking and fusion at the synaptic membrane (Stinchcombe and Griffiths, 2007). Imaging studies by Stinchcombe *et al*. suggest that lytic granules localize to a specialized secretory domain of the IS and that the lytic contents are secreted into a sealed cleft between the CTL and target cell to cause lysis of the target cell (Stinchcombe *et al.*, 2006). In addition to the known functional role in directed secretion, a recent publication by Sanchez-Madrid and colleagues suggests that MTOC repositioning contributes to sustained T cell signaling and proper IS maturation (Martin-Cofreces *et al.*, 2008).

d. TCR-proximal events involved in MTOC repositioning

While MTOC repositioning is known to be dependent on TCR engagement, the downstream signaling pathways and mechanisms leading to repositioning are poorly understood. Among the known molecules required for MTOC repositioning, which include

Lck, ZAP70, LAT, SLP76, VAV1, and CDC4, most are involved in signaling immediately downstream of the TCR (Stowers *et al.*, 1995; Kuhne *et al.*, 2003; Billadeau *et al.*, 2007). Studies have also shown that TCR-proximal events, including calcium flux, are involved in MTOC repositioning in T cells (Kuhne *et al.*, 2003; Billadeau *et al.*, 2007). However, the cascade of TCR-proximal events leading to MTOC repositioning is unclear as M. Huse and colleagues reported, using a photoactivateable pMHC ligand system, that DAG, and not calcium flux, is required for MTOC repositioning (Quann *et al.*, 2009). In their signaling model, PLCγ1-directed cleavage of PIP_2 produces DAG, which then signals through atypical PKCs to recruit dynein to the contact site, leading to MTOC repositioning (Quann *et al.*, 2011). Further experiments using T cell-APC conjugates are needed to confirm the distinct roles of DAG and calcium flux in T cell activation.

In addition to DAG/ calcium influx, F-actin reorganization is thought to play an important role in MTOC repositioning (Sancho *et al.*, 2002; Billadeau *et al.*, 2007). CDC42, a key regulator of Arp2/3-mediated actin polymerization, is required for MTOC polarization in T cells (Stowers *et al.*, 1995), and has been implicated in the tethering of MT plus ends to actin filaments via its interaction with IQGAP1 in non-T cell systems (Fukata *et al.*, 2002). Based on these and other observations, G. Griffiths and colleagues proposed that the ring of lamellipodial actin in the dSMAC drives MTOC repositioning through CDC42-mediated tethering of MTs to the spreading actin ring (Stinchcombe *et al.*, 2006). However, Gomez *et al.* report that MTOC repositioning is independent of CDC42 and Arp2/3, and that MTOC repositioning occurs in the absence of a lamellipodial actin ring (Gomez *et al.*, 2007). Instead, they suggest that the formins mDIA1 and FMNL1 mediate the association between filopodial actin and MTs during actin-dependent MTOC repositioning. Further complicating the role of F-actin in MTOC repositioning is a study from Sedwick *et al*. They show utilizing a live-cell competition assay that the MTOC consistently repositions toward the site of TCR stimulation while F-actin polarizes toward the site of LFA-1 stimulation (Sedwick *et al.*, 1999).

They conclude that the signal pathways leading to actin reorganization contribute to MTOC repositioning by amplifying TCR signaling, rather than through a direct association between actin filaments and MTs. Given the conflicting reports regarding the role of actin in MTOC repositioning, more experiments are needed to understand the crosstalk between the actin and MT cytoskeleton during MTOC repositioning in T cells.

e. Cortical pulling model of MTOC repositioning in T cells

The most attractive model of MTOC repositioning in T cells to date is the one proposed by Martin Poenie's lab (Fig. 2). Using a technique called modulated polarization microscopy (MPM), they observe sliding of MTs near the CTL-target cell contact site coincident with MTOC movement toward the synapse (Kuhn and Poenie, 2002). When engaged by multiple target cells, the CTL's centrosome appears to oscillate back and forth between the targets in a linear fashion, suggesting that MTs become pulled at both sites of contact. Furthermore, MTs are seen anchored at and looping through the pSMAC region in CTL-target cell conjugates (Kuhn and Poenie, 2002). Based on these observations, the authors postulate that MTs become captured and pulled by a minus end-directed MT motor present in the pSMAC ring, resulting in MT sliding and net centrosome polarization to the IS. Since dynein is the major minus end-directed MT motor in cells, they speculate that cortically anchored dynein captures and pulls MTs in the pSMAC, analogous to its function in sliding MTs along the bud cortex in budding yeast (Adames and Cooper, 2000). However, the detailed localization of cortical dynein, the mechanism of its cortical anchoring, and the regulation of cortical dynein activity at the IS are still unknown.

Regarding the cortical pulling model of MTOC repositioning, questions are raised in light of other experimental results. First, there is a difference between the time frames involved in centrosome polarization and IS maturation. Studies utilizing planar lipid bilayers to engage T cells have shown that a mature IS, containing a defined pSMAC ring, forms 5-

Figure 2. Model of MTOC repositioning in T cells (Billadeau *et al*., 2007).

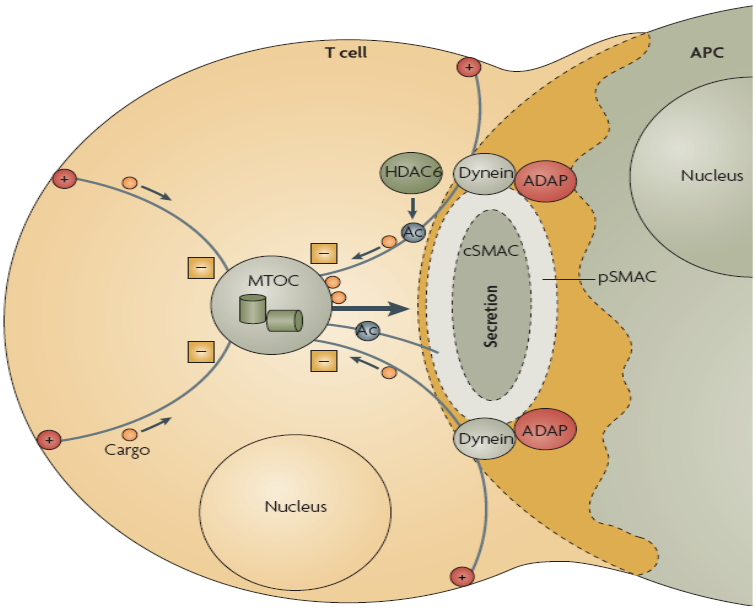

10 minutes after contact with stimulatory molecules (Grakoui *et al.*, 1999; Kaizuka *et al.*, 2007). In contrast, the MTOC is known to reposition to the contact site within 2-3 minutes after engagement with APC (Poenie *et al.*, 2004), suggesting that the centrosome movement precedes pSMAC formation. Second, a number of reports show that TCR ligation alone is enough to induce MTOC repositioning in T cells. T cells engaged by polystyrene beads as well as coverslip substrates coated with anti-TCR antibodies result in MTOC localization toward the contact area (Stowers *et al.*, 1995; Kuhne *et al.*, 2003). Therefore, MTOC repositioning does not require LFA-1 engagement, nor the lateral movement of antigen and adhesion receptors to form a segregated IS at the contact site.

Third, a follow-up study by M. Poenie's group implicated the involvement of ADAP, not LFA-1, in anchoring dynein at the contact site in T cells (Combs *et al.*, 2006). LFA-1-deficient Jurkat T cells were observed to reposition their MTOC normally, while inhibition of ADAP using shRNA knockdown disrupted MTOC translocation. Furthermore, cortically associated MTs localized to the dSMAC region of the IS along with ADAP, in contrast to the pSMAC localization observed previously. Lastly, ADAP was shown to associate with subunits of dynein in pull-down experiments, suggesting that ADAP serves as the cortical anchor for recruitment of dynein during MTOC repositioning. However, the functional role of ADAP is inconclusive, as mouse T cells do not require ADAP for MTOC repositioning and $ADAP^{-/-}$ mice do not exhibit significant immune defects. Identifying the cortical receptor for dynein at the synapse, therefore, will be an important pursuit in the overall goal of characterizing MTOC repositioning in T lymphocytes.

f. General mechanism of MTOC repositioning

Centrosome positioning is essential for many fundamental cellular processes. In interphase cells, MTOC positioning is known to play an important role in establishing overall cellular architecture and in the distribution of various organelles, including the endoplasmic

reticulum, Golgi apparatus, and endosomes. Additionally, MTOC polarization is thought to play a critical role in the differentiation of neural and epithelial cells, mitotic spindle organization in both symmetric and asymmetric cell division, wound healing, and in directed migration of fibroblasts, epithelial cells, astrocytes, and neurons (Manneville and Etienne-Manneville, 2006).

In most cells, the centrosome is thought to be physically linked to the nucleus near the center of the cell (Manneville and Etienne-Manneville, 2006). Two possible forces acting on MTs are thought to maintain the MTOC at that position. The first is a pushing force produced either by MT plus-end growth or centripetal actin retrograde flow (Burakov *et al.*, 2003). The second is a pulling force produced either by plus end-attachment coupled MT depolymerization or minus end-directed MT motor activity at the cortex (Burakov *et al.*, 2003). Laser ablation and RNAi experiments in single cell *C. elegans* embryos, as well as localized nocodazole experiments in mammalian interphase cells, have strongly suggested that MT motor-dependent pulling forces dominate in positioning the centrosome (Burakov *et al.*, 2003; Manneville and Etienne-Manneville, 2006).

Dynein has been shown to be a critical component of this cortical pulling force. Function blocking antibodies injected into interphase cells and wounded fibroblasts, respectively, show that dynein inhibition causes displacement of the centrosome from the cell center (Burakov *et al.*, 2003; Gomes *et al.*, 2005; Manneville and Etienne-Manneville, 2006). Furthermore, the recent report by Tsai *et al.* shows, using siRNA knockdown of dynein HC and LIS1, that dynein and LIS1 are required for pulling the MT network from the leading process during neural progenitor cell migration (Tsai *et al.*, 2007). The mechanism of MT pulling by cortical dynein is especially well characterized during cell division in budding yeast. Translocation of the nucleus and spindle into the bud neck is known to occur through a 'MT capture and sliding' mechanism, driven by dynein localized at the bud cortex via the cortical receptor, Num1 (Adames and Cooper, 2000; Gundersen, 2002). As

emerging evidence continues to solidify the conserved role of dynein in centrosome positioning, it seems plausible, then, that cortically targeted dynein at the IS could likewise drive MTOC repositioning in T lymphocytes.

VII. References

Abbas, A.K., and Lichtman, A.H. (2006). Basic immunology : functions and disorders of the immune system. Elsevier Saunders: Philadelphia, PA.

Adames, N.R., and Cooper, J.A. (2000). Microtubule interactions with the cell cortex causing nuclear movements in Saccharomyces cerevisiae. J Cell Biol *149*, 863-874.

Allan, V.J. (2011). Cytoplasmic dynein. Biochem Soc Trans *39*, 1169-1178.

Andzelm, M.M., Chen, X., Krzewski, K., Orange, J.S., and Strominger, J.L. (2007). Myosin IIA is required for cytolytic granule exocytosis in human NK cells. J Exp Med *204*, 2285-2291.

Baker, R.G., and Koretzky, G.A. (2008). Regulation of T cell integrin function by adapter proteins. Immunol Res *42*, 132-144.

Barda-Saad, M., Braiman, A., Titerence, R., Bunnell, S.C., Barr, V.A., and Samelson, L.E. (2005). Dynamic molecular interactions linking the T cell antigen receptor to the actin cytoskeleton. Nat Immunol *6*, 80-89.

Billadeau, D.D., Nolz, J.C., and Gomez, T.S. (2007). Regulation of T-cell activation by the cytoskeleton. Nat Rev Immunol *7*, 131-143.

Bunnell, S.C., Barr, V.A., Fuller, C.L., and Samelson, L.E. (2003). High-resolution multicolor imaging of dynamic signaling complexes in T cells stimulated by planar substrates. Sci STKE *2003*, PL8.

Bunnell, S.C., Hong, D.I., Kardon, J.R., Yamazaki, T., McGlade, C.J., Barr, V.A., and Samelson, L.E. (2002). T cell receptor ligation induces the formation of dynamically regulated signaling assemblies. J Cell Biol *158*, 1263-1275.

Bunnell, S.C., Kapoor, V., Trible, R.P., Zhang, W., and Samelson, L.E. (2001). Dynamic actin polymerization drives T cell receptor-induced spreading: a role for the signal transduction adaptor LAT. Immunity *14*, 315-329.

Burakov, A., Nadezhdina, E., Slepchenko, B., and Rodionov, V. (2003). Centrosome positioning in interphase cells. J Cell Biol *162*, 963-969.

Campi, G., Varma, R., and Dustin, M.L. (2005). Actin and agonist MHC-peptide complex-dependent T cell receptor microclusters as scaffolds for signaling. J Exp Med *202*, 1031-1036.

Cemerski, S., and Shaw, A. (2006). Immune synapses in T-cell activation. Curr Opin Immunol *18*, 298-304.

Chan, A.C., Desai, D.M., and Weiss, A. (1994). The role of protein tyrosine kinases and protein tyrosine phosphatases in T cell antigen receptor signal transduction. Annu Rev Immunol *12*, 555-592.

Combs, J., Kim, S.J., Tan, S., Ligon, L.A., Holzbaur, E.L., Kuhn, J., and Poenie, M. (2006). Recruitment of dynein to the Jurkat immunological synapse. Proc Natl Acad Sci U S A *103*, 14883-14888.

DeMond, A.L., Mossman, K.D., Starr, T., Dustin, M.L., and Groves, J.T. (2008). T cell receptor microcluster transport through molecular mazes reveals mechanism of translocation. Biophys J *94*, 3286-3292.

Dujardin, D.L., and Vallee, R.B. (2002). Dynein at the cortex. Curr Opin Cell Biol *14*, 44-49.
Dustin, M.L. (2009). Supported bilayers at the vanguard of immune cell activation studies. J Struct Biol *168*, 152-160.

Dustin, M.L., Starr, T., Varma, R., and Thomas, V.K. (2007). Supported planar bilayers for study of the immunological synapse. Curr Protoc Immunol *Chapter 18*, Unit 18 13.

Fooksman, D.R., Vardhana, S., Vasiliver-Shamis, G., Liese, J., Blair, D.A., Waite, J., Sacristan, C., Victora, G.D., Zanin-Zhorov, A., and Dustin, M.L. (2010). Functional anatomy of T cell activation and synapse formation. Annu Rev Immunol *28*, 79-105.

Freiberg, B.A., Kupfer, H., Maslanik, W., Delli, J., Kappler, J., Zaller, D.M., and Kupfer, A. (2002). Staging and resetting T cell activation in SMACs. Nat Immunol *3*, 911-917.

Fukata, M., Watanabe, T., Noritake, J., Nakagawa, M., Yamaga, M., Kuroda, S., Matsuura, Y., Iwamatsu, A., Perez, F., and Kaibuchi, K. (2002). Rac1 and Cdc42 capture microtubules through IQGAP1 and CLIP-170. Cell *109*, 873-885.

Gardel, M.L., Schneider, I.C., Aratyn-Schaus, Y., and Waterman, C.M. (2010). Mechanical integration of actin and adhesion dynamics in cell migration. Annu Rev Cell Dev Biol *26*, 315-333.

Gomes, E.R., Jani, S., and Gundersen, G.G. (2005). Nuclear movement regulated by Cdc42, MRCK, myosin, and actin flow establishes MTOC polarization in migrating cells. Cell *121*, 451-463.

Gomez, T.S., Kumar, K., Medeiros, R.B., Shimizu, Y., Leibson, P.J., and Billadeau, D.D. (2007). Formins regulate the actin-related protein 2/3 complex-independent polarization of the centrosome to the immunological synapse. Immunity *26*, 177-190.

Grakoui, A., Bromley, S.K., Sumen, C., Davis, M.M., Shaw, A.S., Allen, P.M., and Dustin, M.L. (1999). The immunological synapse: a molecular machine controlling T cell activation. Science *285*, 221-227.

Gundersen, G.G. (2002). Evolutionary conservation of microtubule-capture mechanisms. Nat Rev Mol Cell Biol *3*, 296-304.

Guy, C.S., and Vignali, D.A. (2009). Organization of proximal signal initiation at the TCR:CD3 complex. Immunol Rev *232*, 7-21.

Huppa, J.B., and Davis, M.M. (2003). T-cell-antigen recognition and the immunological synapse. Nat Rev Immunol *3*, 973-983.

Ilani, T., Vasiliver-Shamis, G., Vardhana, S., Bretscher, A., and Dustin, M.L. (2009). T cell antigen receptor signaling and immunological synapse stability require myosin IIA. Nat Immunol *10*, 531-539.

Irvine, D.J., Purbhoo, M.A., Krogsgaard, M., and Davis, M.M. (2002). Direct observation of ligand recognition by T cells. Nature *419*, 845-849.

Jacobelli, J., Chmura, S.A., Buxton, D.B., Davis, M.M., and Krummel, M.F. (2004). A single class II myosin modulates T cell motility and stopping, but not synapse formation. Nat Immunol *5*, 531-538.

Kaizuka, Y., Douglass, A.D., Varma, R., Dustin, M.L., and Vale, R.D. (2007). Mechanisms for segregating T cell receptor and adhesion molecules during immunological synapse formation in Jurkat T cells. Proc Natl Acad Sci U S A *104*, 20296-20301.

Kardon, J.R., and Vale, R.D. (2009). Regulators of the cytoplasmic dynein motor. Nat Rev Mol Cell Biol *10*, 854-865.

Kinashi, T. (2005). Intracellular signalling controlling integrin activation in lymphocytes. Nat Rev Immunol *5*, 546-559.

Kuhn, J.R., and Poenie, M. (2002). Dynamic polarization of the microtubule cytoskeleton during CTL-mediated killing. Immunity *16*, 111-121.

Kuhne, M.R., Lin, J., Yablonski, D., Mollenauer, M.N., Ehrlich, L.I., Huppa, J., Davis, M.M., and Weiss, A. (2003). Linker for activation of T cells, zeta-associated protein-70, and Src homology 2 domain-containing leukocyte protein-76 are required for TCR-induced microtubule-organizing center polarization. J Immunol *171*, 860-866.

Kupfer, A., and Dennert, G. (1984). Reorientation of the microtubule-organizing center and the Golgi apparatus in cloned cytotoxic lymphocytes triggered by binding to lysable target cells. J Immunol *133*, 2762-2766.

Lee, K.H., Dinner, A.R., Tu, C., Campi, G., Raychaudhuri, S., Varma, R., Sims, T.N., Burack, W.R., Wu, H., Wang, J., Kanagawa, O., Markiewicz, M., Allen, P.M., Dustin, M.L., Chakraborty, A.K., and Shaw, A.S. (2003). The immunological synapse balances T cell receptor signaling and degradation. Science *302*, 1218-1222.

Manneville, J.B., and Etienne-Manneville, S. (2006). Positioning centrosomes and spindle poles: looking at the periphery to find the centre. Biol Cell *98*, 557-565.

Martin-Cofreces, N.B., Robles-Valero, J., Cabrero, J.R., Mittelbrunn, M., Gordon-Alonso, M., Sung, C.H., Alarcon, B., Vazquez, J., and Sanchez-Madrid, F. (2008). MTOC translocation modulates IS formation and controls sustained T cell signaling. J Cell Biol *182*, 951-962.

McKenney, R.J., Vershinin, M., Kunwar, A., Vallee, R.B., and Gross, S.P. (2010). LIS1 and NudE induce a persistent dynein force-producing state. Cell *141*, 304-314.

McKenney, R.J., Weil, S.J., Scherer, J., and Vallee, R.B. (2011). Mutually exclusive cytoplasmic dynein regulation by NudE-Lis1 and dynactin. J Biol Chem *286*, 39615-39622.

Medeiros, N.A., Burnette, D.T., and Forscher, P. (2006). Myosin II functions in actin-bundle turnover in neuronal growth cones. Nat Cell Biol *8*, 215-226.

Monks, C.R., Freiberg, B.A., Kupfer, H., Sciaky, N., and Kupfer, A. (1998). Three-dimensional segregation of supramolecular activation clusters in T cells. Nature *395*, 82-86.

Morin, N.A., Oakes, P.W., Hyun, Y.M., Lee, D., Chin, Y.E., King, M.R., Springer, T.A., Shimaoka, M., Tang, J.X., Reichner, J.S., and Kim, M. (2008). Nonmuscle myosin heavy chain IIA mediates integrin LFA-1 de-adhesion during T lymphocyte migration. J Exp Med *205*, 195-205.

O'Shea, J.J. (2000). Something happens; a brief history of TCR signal transduction. Methods Mol Biol *134*, 197-207.

Poenie, M., Kuhn, J., and Combs, J. (2004). Real-time visualization of the cytoskeleton and effector functions in T cells. Curr Opin Immunol *16*, 428-438.

Pollard, T.D., and Borisy, G.G. (2003). Cellular motility driven by assembly and disassembly of actin filaments. Cell *112*, 453-465.

Ponti, A., Machacek, M., Gupton, S.L., Waterman-Storer, C.M., and Danuser, G. (2004). Two distinct actin networks drive the protrusion of migrating cells. Science *305*, 1782-1786.

Quann, E.J., Liu, X., Altan-Bonnet, G., and Huse, M. (2011). A cascade of protein kinase C isozymes promotes cytoskeletal polarization in T cells. Nat Immunol *12*, 647-654.

Quann, E.J., Merino, E., Furuta, T., and Huse, M. (2009). Localized diacylglycerol drives the polarization of the microtubule-organizing center in T cells. Nat Immunol *10*, 627-635.

Samelson, L.E. (2002). Signal transduction mediated by the T cell antigen receptor: the role of adapter proteins. Annu Rev Immunol *20*, 371-394.

Sancho, D., Vicente-Manzanares, M., Mittelbrunn, M., Montoya, M.C., Gordon-Alonso, M., Serrador, J.M., and Sanchez-Madrid, F. (2002). Regulation of microtubule-organizing center orientation and actomyosin cytoskeleton rearrangement during immune interactions. Immunol Rev *189*, 84-97.

Sedwick, C.E., Morgan, M.M., Jusino, L., Cannon, J.L., Miller, J., and Burkhardt, J.K. (1999). TCR, LFA-1, and CD28 play unique and complementary roles in signaling T cell cytoskeletal reorganization. J Immunol *162*, 1367-1375.

Shaw, A.S., and Dustin, M.L. (1997). Making the T cell receptor go the distance: a topological view of T cell activation. Immunity *6*, 361-369.

Sims, T.N., Soos, T.J., Xenias, H.S., Dubin-Thaler, B., Hofman, J.M., Waite, J.C., Cameron, T.O., Thomas, V.K., Varma, R., Wiggins, C.H., Sheetz, M.P., Littman, D.R., and Dustin, M.L. (2007). Opposing effects of PKCtheta and WASp on symmetry breaking and relocation of the immunological synapse. Cell *129*, 773-785.

Stinchcombe, J.C., and Griffiths, G.M. (2007). Secretory mechanisms in cell-mediated cytotoxicity. Annu Rev Cell Dev Biol *23*, 495-517.

Stinchcombe, J.C., Majorovits, E., Bossi, G., Fuller, S., and Griffiths, G.M. (2006). Centrosome polarization delivers secretory granules to the immunological synapse. Nature *443*, 462-465.

Stowers, L., Yelon, D., Berg, L.J., and Chant, J. (1995). Regulation of the polarization of T cells toward antigen-presenting cells by Ras-related GTPase CDC42. Proc Natl Acad Sci U S A *92*, 5027-5031.

Tsai, J.W., Bremner, K.H., and Vallee, R.B. (2007). Dual subcellular roles for LIS1 and dynein in radial neuronal migration in live brain tissue. Nat Neurosci *10*, 970-979.

Vardhana, S., Choudhuri, K., Varma, R., and Dustin, M.L. (2010). Essential role of ubiquitin and TSG101 protein in formation and function of the central supramolecular activation cluster. Immunity *32*, 531-540.

Varma, R., Campi, G., Yokosuka, T., Saito, T., and Dustin, M.L. (2006). T cell receptor-proximal signals are sustained in peripheral microclusters and terminated in the central supramolecular activation cluster. Immunity *25*, 117-127.

Vicente-Manzanares, M., Ma, X., Adelstein, R.S., and Horwitz, A.R. (2009). Non-muscle myosin II takes centre stage in cell adhesion and migration. Nat Rev Mol Cell Biol *10*, 778-790.

Wilson, C.A., Tsuchida, M.A., Allen, G.M., Barnhart, E.L., Applegate, K.T., Yam, P.T., Ji, L., Keren, K., Danuser, G., and Theriot, J.A. (2010). Myosin II contributes to cell-scale actin network treadmilling through network disassembly. Nature *465*, 373-377.

Yokosuka, T., Sakata-Sogawa, K., Kobayashi, W., Hiroshima, M., Hashimoto-Tane, A., Tokunaga, M., Dustin, M.L., and Saito, T. (2005). Newly generated T cell receptor microclusters initiate and sustain T cell activation by recruitment of Zap70 and SLP-76. Nat Immunol *6*, 1253-1262.

CHAPTER 2

ACTIN RETROGRADE FLOW AND ACTO-MYOSIN II ARC CONTRACTION DRIVE RECEPTOR CLUSTER DYNAMICS AT THE IMMUNOLOGICAL SYNAPSE IN JURKAT T CELLS

I. Abstract

Actin retrograde flow and acto-myosin II contraction have both been implicated in the inward movement of TCR microclusters and immunological synapse formation, but no study has integrated and quantified their relative contributions. Using Jurkat T cells expressing fluorescent myosin IIA heavy chain and F-Tractin, a novel reporter for F-actin, we now provide direct evidence that the dSMAC and pSMAC correspond to lamellipodial (LP) and lamellar (LM) actin networks, respectively, as hypothesized previously. Importantly, our images reveal concentric and contracting acto-myosin II arcs/rings at the LM/pSMAC. Moreover, the speeds of centripetally moving TCR microclusters correspond very closely to the rates of actin retrograde flow in the LP/dSMAC and acto-myosin II arc contraction in the LM/pSMAC. Using cytochalasin D and jasplakinolide to selectively inhibit actin retrograde flow in the LP/dSMAC, and blebbistatin to selectively inhibit acto-myosin II arc contraction in the LM/pSMAC, we demonstrate that both forces are required for centripetal TCR microcluster transport. Finally, we show that LFA-1 clusters accumulate over time at the inner aspect of the LM/pSMAC, and that this accumulation is dependent on acto-myosin II contraction. Thus, actin retrograde flow and acto-myosin II arc contraction coordinately drive receptor cluster dynamics at the immunological synapse.

II. Introduction

The activation of T lymphocytes involves antigen receptors, adhesion molecules, and other accessory components, all of which polarize rapidly toward the site of contact with the antigen presenting cell (Fooksman *et al.*, 2010). Upon binding their respective ligands on the surface of the APC, these proteins undergo differential clustering and rearrangement at the synaptic junction to form two segregated, concentric domains known as SMACs (Monks *et al.*, 1998; Grakoui *et al.*, 1999). The resulting bull's-eye pattern of SMACs is a hallmark of the IS, and provides the structural basis for signaling and secretion at the T cell-APC interface. The center area of the IS, known as the cSMAC, is marked by the accumulation of TCR MCs, which are bound to major histocompatibility complex proteins displaying antigenic peptide present on the surface of the APC (Campi *et al.*, 2005; Yokosuka *et al.*, 2005). The surrounding ring of the bull's eye, known as the pSMAC, is marked by clusters of the β2 integrin, LFA-1, which are bound to ICAM-1 receptors present on the APC surface (Monks *et al.*, 1998; Grakoui *et al.*, 1999). Recent studies argue that TCR signaling is degraded at the cSMAC, and that active signaling actually takes place at the periphery of the IS (Varma *et al.*, 2006; Vardhana *et al.*, 2010). Thus, the pSMAC region may serve dual functions during T cell activation: as a zone of adhesion between the T cell and the APC, and as a zone of active TCR signaling at the IS. Substitution of the APC surface with a glass-supported planar lipid bilayer displaying stimulatory molecules has been shown to replicate the signaling activity and spatial organization of the IS, and has become an important tool for studying T cell activation (Grakoui *et al.*, 1999; Dustin, 2009).

The creation of the bull's eye pattern exhibited by the mature IS requires the centripetal transport of both TCR MCs and integrin clusters, as well as their differential sorting at the pSMAC-cSMAC boundary. The vast majority of previous studies (see the Discussion for one recent exception) point to the inward flow of cortical F-actin at the IS as the major if not sole driving force behind centripetal receptor cluster movement (Billadeau *et*

al., 2007; Kaizuka *et al.*, 2007; DeMond *et al.*, 2008; Hartman *et al.*, 2009; Yu *et al.*, 2010). First, dynamic imaging of F-actin at the IS using GFP-actin as the reporter reveals very robust actin polymerization-driven retrograde actin flow at the perimeter of the IS (Bunnell *et al.*, 2001; Kaizuka *et al.*, 2007; Yu *et al.*, 2010). Moreover, this flow is radial symmetric, fully consistent with a symmetric centering force. Second, the inward movement of TCR MCs does not begin until leading edge actin polymerization converts from initial cell spreading to retrograde flow upon completion of spreading (DeMond *et al.*, 2008). Third, the centripetal movement of preformed TCR MCs completely ceases upon depolymerization of F-actin using latrunculin (Varma *et al.*, 2006; Kaizuka *et al.*, 2007).

Consistent with centripetal actin flow driving receptor cluster movement, simultaneous imaging of TCR MCs, integrin clusters and F-actin (using GFP-actin) at the periphery of bilayer-engaged Jurkat T cells showed that both types of clusters move inward with actin flow (Kaizuka *et al.*, 2007). Interestingly, the speed of centripetal TCR MC movement was reported to be ~40% that of actin retrograde flow, indicating significant slippage between cluster movement and actin flow (Kaizuka *et al.*, 2007). As predicted from previous images of the mature IS, TCR MCs were seen to accumulate at the cSMAC, while the inward movement of integrin clusters ceased at the pSMAC/cSMAC boundary (Kaizuka *et al.*, 2007; Hartman *et al.*, 2009). These two observations highlight three important questions regarding SMAC formation: what molecules link receptor clusters to actin flow, what are the physical/mechanical properties of this linkage, and how are TCR MCs and integrin clusters sorted at the pSMAC/cSMAC boundary (Hartman and Groves, 2011)? Regarding the second question, the apparent slippage between TCR MCs and actin flow observed by Kaizuka *et al*. (2007) was interpreted as evidence that the clusters spend variable periods of time completely detached from actin flow, by analogy with the duty cycle of a motor protein. Perhaps a more robust interpretation of slippage has come from elegant studies employing physical barriers placed within bilayers (DeMond *et al.*, 2008; Yu *et al.*,

2010), which argue strongly for a dissipative or frictional coupling mechanism in which numerous, transient, weak interactions between individual receptors within a cluster and actin keeps the cluster attached to actin but allows slippage.

Importantly, the peripheral ring of robust actin retrograde flow discussed above has been shown to lie immediately outside of the pSMAC, and as a consequence has been named the distal SMAC (dSMAC) (Freiberg *et al.*, 2002; Sims *et al.*, 2007). Based on this observation, and on the staining of the IS with various antibodies, M. Dustin proposed that the IS is in essence a symmetrical version of the actin cytoskeleton at the front of a migrating cell, where the dSMAC corresponds to the lamellipodium (LP) and the pSMAC corresponds to the lamellum (LM) (Dustin, 2007). Implicit in this comparison, therefore, is that the centripetal movement of receptor clusters may well be driven by a combination of the pushing force provided by polymerization-based actin retrograde actin flow in the LP and the pulling force provided by myosin II-based contraction of transverse actin bundles in the LM (Medeiros *et al.*, 2006; Gardel *et al.*, 2010; Wilson *et al.*, 2010).

With regard to the possible role of myosin II in the centripetal transport of TCR MCs, an early study using blebbistatin (BB) to inhibit myosin II argued that the myosin is not required for IS formation (Jacobelli *et al.*, 2004). In contrast, a subsequent study using both BB and siRNA knockdown of myosin IIA reported a dramatic inhibition of inward TCR MC movement, SMAC formation and IS stability (Ilani *et al.*, 2009). While convincing in many aspects, this study did not image the dynamics of F-actin or myosin II, determine the effect of myosin II inhibition on the rate of actin flow, define the organization of F-actin within the LM/pSMAC, or pinpoint the site of action of myosin II within the IS. Moreover, it did not parse out the relative contributions made by actin retrograde flow and myosin II-based contraction to the centripetal transport of TCR MCs. Armed with a novel reporter for F-actin, we sought here to address these and related, unresolved questions regarding the role of the actin cytoskeleton in IS formation.

III. Results

a. The region of the IS corresponding to the LM/pSMAC contains concentric actin arcs that are rich in myosin IIA

To examine in greater detail the organization of cortical F-actin at the IS, we utilized E6.1 Jurkat T cells stimulated by glass-supported planar lipid bilayers containing anti-CD3ε antibody and ICAM-1 (Kaizuka *et al.*, 2007) (see Methods). Anti-CD3ε antibody labeled with rhodamine-X and attached to biotinylated lipids in the bilayer via a streptavidin bridge distributes evenly in bilayers (data not shown [DNS]). Moreover, use of Fluorescence Recovery After Photobleaching (FRAP) to assess the lateral mobility of ICAM-1 tagged with Alexa-647 and attached to the bilayer via NTA-conjugated lipids indicated that the lipids in these bilayers are diffusing freely and uniformly (Fig. 3 A1-A3). Finally, after 5 min of engagement with the bilayer, the vast majority (93.8%, n=32 cells; Fig. 3 B) of Jurkat T cells formed the central accumulation of TCR MCs, as inferred from the distribution of the anti-CD3ε antibody in the bilayer, and the peripheral accumulation of the integrin LFA-1, as inferred from the distribution of ICAM-1 in the bilayer, that is characteristic of the bull's eye-patterned IS formed by primary T cells bound to bilayers containing peptide-MHC (Grakoui *et al.*, 1999).

To image the endogenous network of cortical F-actin at the plane of the IS, Jurkat T cells were stained with rhodamine-phalloidin (Fig. 4 A1-A4; two representative cells are shown; unless indicated otherwise, all fixations were performed 5 min after engagement with the bilayer). This staining revealed three visually distinct rings or zones of F-actin at the IS: an outer ring characterized by very intense F-actin staining interrupted by streaks, a middle ring characterized by concentric arcs of F-actin, and a central zone relatively free of F-actin (Fig. 4 A1 and A3, and the corresponding insets in A2 and A4, respectively: the cell in A1 shows the outer ring most clearly, while the cell in A3 shows the middle ring best).

Figure 3. Mobility of ICAM-1 in planar bilayers and efficiency of IS formation in Jurkat T cells.

(A1) Alexa-647-labeled ICAM-1 in the planar bilayer immediately after photo bleaching. The dark region corresponds to the ~5 μm-wide photo bleached spot in the bilayer. (A2) Alexa-647-labeled ICAM-1 molecules in the planar bilayer 3 min after photobleaching. (A3) Graph showing the recovery of Alexa-647-labeled ICAM-1 fluorescence in the bleached spot as a function of time (expressed as a ratio of Alexa-647-labeled ICAM-1 fluorescence intensity in the photo bleached region relative to a nearby, unbleached region). (B) Jurkat cells engaged on a planar bilayer containing Alexa-647-labeled ICAM-1 to indirectly visualize the distribution of LFA-1 clusters in the T cell (pseudo colored red), and Rhodamine-X-labeled anti-CD3ε antibody to indirectly visualize the distribution of TCR MCs in the T cell (pseudo colored green). This image was taken 7 min after bilayer engagement. The percentage of bilayer-engaged cells that displayed a bull's eye-patterned IS, as well as the total number of cells measured in three separate studies, are indicated below B. (C) Phalloidin staining at the contact site in Jurkat cells engaged on a planar bilayer containing only Alexa-647-labeled ICAM-1. All scale bars = 5 μm.

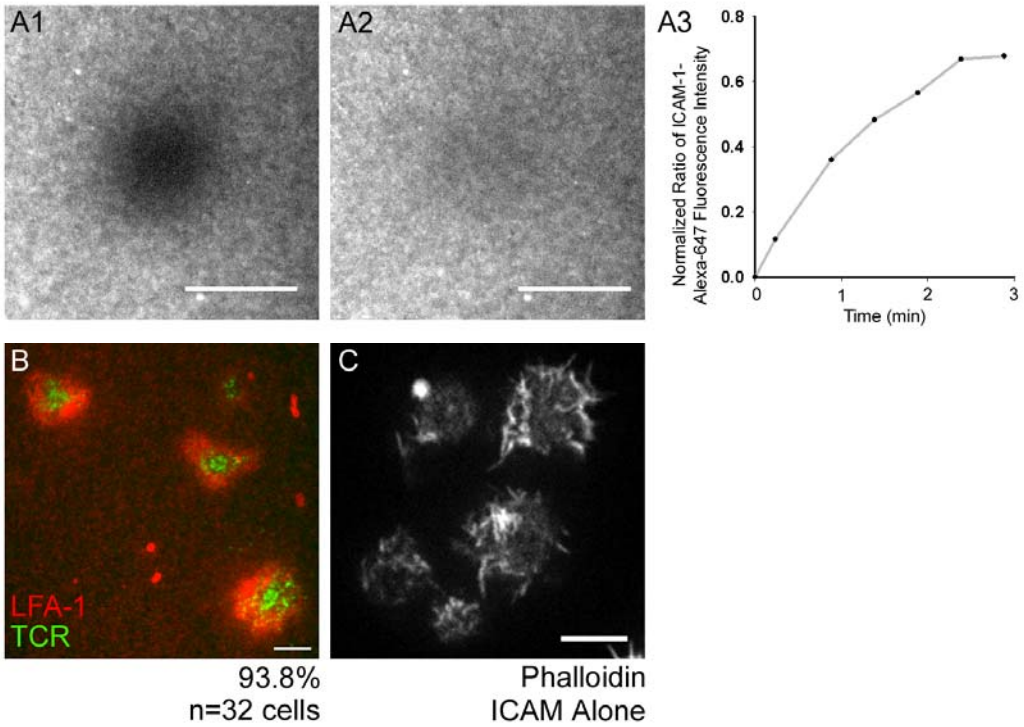

Importantly, the middle ring containing the concentric F-actin arcs overlaps extensively with the high concentration of ICAM-1 clusters that indirectly mark the position of the pSMAC (Fig. 4 B1, B3 and B5, and the corresponding insets in B2, B4 and B6). Moreover, the central zone that is essentially devoid of F-actin overlaps almost completely with the high concentration of TCR MCs that mark the mature cSMAC (Fig. 4 C1-C3).

To verify that the outer ring corresponds to the region of dramatic actin retrograde flow reported previously (Bunnell *et al.*, 2001; Kaizuka *et al.*, 2007), i.e. to what is essentially a LP actin network, we double-stained cells with phalloidin and an antibody against p34, a subunit of the Arp2/3 complex and a bona fide marker for the LP in migrating cells (Pollard and Borisy, 2003). Figure 4, Panels D1, D3 and D5, and the corresponding insets in D2, D4 and D6, show that this outer actin ring is indeed rich in the Arp2/3 complex, while the middle ring is not. This result is consistent with the assignment of this outer ring as a LP-like actin network. To verify that the middle actin ring corresponds to what is essentially a LM network of F-actin, we double-stained cells with phalloidin and an antibody against non-muscle myosin IIA, a bona fide marker for the LM in migrating cells (Medeiros *et al.*, 2006). Figure 4, Panels E1, E3 and E5, and the corresponding insets E2, E4 and E6, show that this middle ring is indeed rich in myosin IIA, while the outer ring is not. This result is consistent with the assignment of this middle ring as a LM-like network of F-actin. Together, these results argue that the outer ring, which exhibits very intense F-actin staining interrupted by streaks, corresponds to a LP actin network (i.e. the dSMAC [(Sims *et al.*, 2007)]), while the middle ring, which is comprised of concentric actin arcs and a high concentration of endogenous myosin IIA, and which overlaps extensively with the position of the integrin-rich pSMAC, corresponds to a LM actin network. These results confirm and extend those of Sims *et al.* (Sims *et al.*, 2007), who used antibodies against cofilin and Arp3 as markers for the LP/dSMAC, and an antibody against tropomyosin as a marker for LM/pSMAC.

Like SMAC formation, the formation of the LP and LM F-actin networks was

Figure 4. Localization of endogenous F-actin structures and corresponding LP/LM markers at the IS.

(A) Phalloidin staining of endogenous F-actin at the IS in representative Jurkat T cells stimulated on a supported planar bilayer (A1, A3) or on a glass coverslip coated with immobilized anti-CD3ε antibody (A5). (A2, A4, A6) Magnified images of the boxed regions (white) in A1, A3 and A5, respectively. The central zone, middle ring, and outer ring are indicated by brackets above A2, A4 and A6. (B) Overlap in localization of ICAM-1 with the middle ring of F-actin at the IS in a representative cell stimulated on a planar bilayer. Note that this particular image is a single frame from a movie of a cell expressing the F-actin reporter GFP-F-Tractin-P (see text) and not an image of a fixed, phalloidin-stained cell, as the distribution of ICAM-1 is disrupted by fixation. (B1) ICAM-1, (B3) GFP-F-Tractin-P in the same cell, and (B5) merged image between B1 (green) and B3 (red). (B2, B4, B6) Magnified images of the boxed regions (white) in B1, B3 and B5, respectively. The outer and middle rings are indicated by brackets above B2, B4 and B6. (C) Overlap in localization of TCR MCs with the actin-depleted central zone at the IS in a representative cell stimulated on a planar bilayer. (C1) Anti-CD3ε antibody-labeled TCR MCs, (C2) phalloidin-staining in the same cell, and (C3) merged image between C1 (green) and C2 (red). (D) Overlap in localization of the Arp2/3 complex with the outer ring of F-actin at the IS in a representative cell stimulated on a planar bilayer. (D1) Anti-p34 (Arp2/3 subunit) antibody staining, (D3) phalloidin-staining in the same cell, and (D5) merged image between D1 (green) and D3 (red). (D2, D4, D6) Magnified images of the boxed regions (white) in D1, D3 and D5, respectively. The LP and LM regions are indicated by brackets above D2, D4 and D6. (E) Overlap in localization of myosin IIA with the middle ring of F-actin at the IS in a representative cell stimulated on planar bilayer. (E1) Anti-myosin IIA antibody staining, (E3) phalloidin staining in the same cell, and (E5) merged image between E1 (green) and E3 (red). (E2, E4, E6) Magnified images of the boxed regions (white) in E1, E3 and E5, respectively. The LP and LM regions are indicated by brackets above E2, E4 and E6. (F) Phalloidin staining at the plane of contact with the bilayer (F1) and 1 μm above the plane of contact with the bilayer (F2) in a representative cell stimulated on a planar bilayer. (F3) Graph showing the relative intensities of phalloidin fluorescence across the IS for the green line in F1 (and the corresponding green intensity trace in F3) and the red line in F2 (and the corresponding red intensity trace in F3). The positions of the LP/dSMAC, LM/pSMAC and cSMAC regions are indicated by brackets above F3. (G) 3-D reconstructed views of phalloidin staining in a representative Jurkat cell stimulated on a planar bilayer. (G1) En-face view of phalloidin fluorescence at the plane of contact with the bilayer. (G2) Cross-section view of phalloidin fluorescence in the LP/dSMAC region (corresponding to the red line in G1). (G3) Cross-section view of phalloidin fluorescence in the LM/pSMAC region (corresponding to the green line in G1). (H) Cartoon of the LP/dSMAC, LM/pSMAC and cSMAC regions at the IS shown from an en-face view (H1) and a side view (H2). All scale bars = 5 μm.

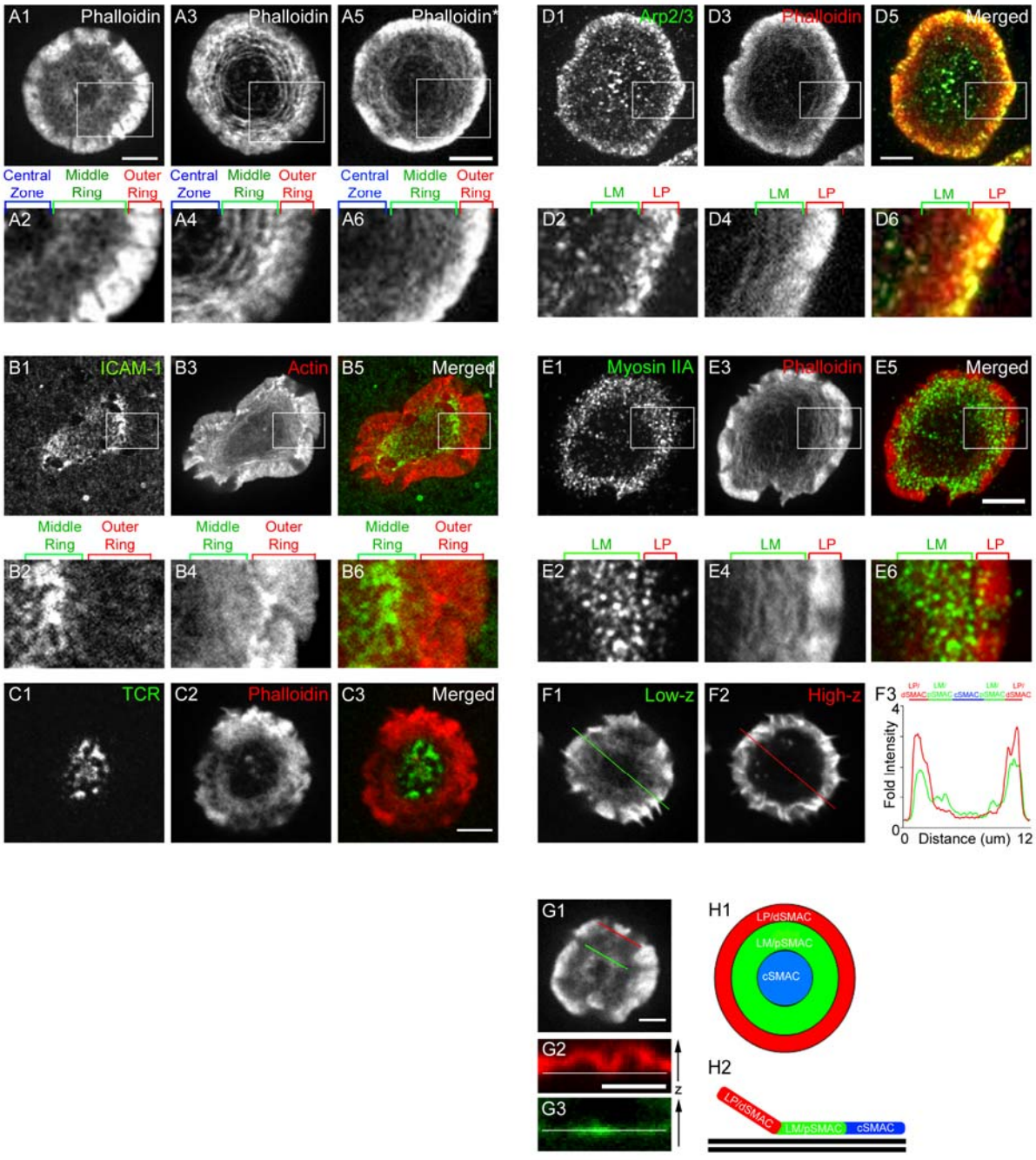
A1 Phalloidin
A3 Phalloidin
A5 Phalloidin*
Central Zone
Middle Ring
Outer Ring
A2
A4
A6
D1 Arp2/3
D3 Phalloidin
D5 Merged
LM
LP
D2
D4
D6
B1 ICAM-1
B3 Actin
B5 Merged
B2
B4
B6
E1 Myosin IIA
E3 Phalloidin
E5 Merged
E2
E4
E6
C1 TCR
C2 Phalloidin
C3 Merged
F1 Low-z
F2 High-z
F3
Fold intensity
Distance (um)
G1
G2
G3
z
H1
LP/dSMAC
LM/pSMAC
cSMAC
H2

dependent on TCR ligation, as bilayers containing only ICAM-1 molecules failed to form these two networks (Fig. 3 C). Importantly, Jurkat cells engaged on coverslips conjugated with immobilized anti-CD3ε antibody formed the two distinct F-actin networks (Fig. 4 A5 and A6), indicating that the dynamic organization of cortical F-actin at the plane of the IS does not require the rearrangement of integrins and TCR MCs that drives IS maturation (see also (Bunnell *et al.*, 2001).

We also found that phalloidin staining at the LP/dSMAC is usually most intense in confocal sections just above the lipid bilayer (Fig. 4 F1-F3; compare in F3 the intensity profiles of phalloidin staining across the cell at the plane of the bilayer [F1, Low Z, green line] versus 1 μm above the plane of the bilayer [F2, High Z, red line]). Conversely, phalloidin staining in the LM/pSMAC was always most intense at the plane of the lipid bilayer (Fig. 4 F3). These observations are consistent with dynamic ruffling activity at the LP/dSMAC and stable substrate adhesion at the LM/pSMAC. Further evidence for such ruffling activity in the LP/dSMAC was obtained from 3D-reconstructions of phalloidin-stained Jurkat cells engaged on bilayers (Fig. 4 G1-G3). Specifically, side views of F-actin in the LP/dSMAC region (Fig. 4 G1, red line) show that the F-actin network moves up and down relative to the bilayer (Fig. 4 G2, red signal; the white line marks the position of the bilayer). Conversely, side views of F-actin in the LM/pSMAC region (Fig. 4 G1, green line) show that the F-actin network here is always in close contact with the bilayer (Fig. 4 G3, green signal). We conclude from all of the results in Figure 4 that distinct LP and LM F-actin networks exist at the dSMAC and pSMAC regions of the IS, respectively, and that the LM/pSMAC is fully engaged at the plane of contact, consistent with its role as a zone of adhesion at the IS (Fig. 4 H1 and H2). Importantly, we show for the first time the presence of endogenous F-actin arcs in the LM/pSMAC. We also show for the first time that these arcs are rich in endogenous myosin IIA. These findings confirm and extend the idea that the dSMAC and

pSMAC regions of the T cell IS correspond spatially to LP and LM F-actin networks, respectively, as proposed by Dustin (Dustin, 2007)

b. **A prototype of F-Tractin, a novel reporter for F-actin, but not GFP-actin, localizes to both LP and LM actin networks at the IS**

We next sought to visualize the dynamics of F-actin in real time during the process of IS formation. Previous imaging studies utilizing GFP-tagged actin showed convincingly that the dSMAC corresponds to a region of dramatic actin polymerization at the leading edge and retrograde flow (Bunnell *et al.*, 2001; Kaizuka *et al.*, 2007). That said, problems have been encountered with the use of GFP-actin that include exclusion of GFP-actin from specific actin structures (Doyle and Botstein, 1996; Wu and Pollard, 2005; Wu *et al.*, 2006), as well as aberrations in cytoskeletal architecture and dynamics, especially when GFP-actin expression levels are high (Aizawa *et al.*, 1997; Westphal *et al.*, 1997). Consistent with such problems, when we fixed Jurkat cells expressing moderate levels of GFP-actin after engagement with bilayers and then stained them with Alexa-568-conjugated phalloidin, while the F-actin network at the LP/dSMAC was clearly visible in both channels as reported previously (Bunnell *et al.*, 2001; Kaizuka *et al.*, 2007), the actin arcs at the LM/pSMAC were visible only in the phalloidin channel (Fig. 5 A1-A6). This result, which we observed consistently, argues that GFP-actin does not incorporate to a significant extent into the actin arcs that are present as endogenous structures in the LM/pSMAC (Fig. 4). Consistent with our observations, no previous study of actin dynamics in T cells using GFP-actin reported the existence of actin arcs or rings in the LM/pSMAC.

In light of these observations, we decided to try an alternative to GFP-actin to visualize the dynamics of F-actin at the IS. Recently, the F-actin targeting domain of the enzyme inositol trisphosphate 3-kinase A (ITPKA), which phosphorylates Ins(1,4,5)P3 to Ins(1,3,4,5)P4 in the dendritic spines of hippocampal neurons, was reported to bind F-actin

both *in vitro* and *in vivo* (Johnson and Schell, 2009). Specifically, *in vitro* assays showed that peptides corresponding to residues 2-66 or 9-52 of ITPKA bind F-actin with modest affinity (~7 μM), and that they have little effect on the rate of depolymerization of preformed actin filaments (Johnson and Schell, 2009). Both of these properties are desirable for a dynamic F-actin reporter, as they should increase the chance that the reporter exhibits minimal effects on the organization and dynamics of the F-actin structures it seeks to report. Consistently, FRAP of F-actin structures in living cells that were labeled with a GFP-tagged version of IPTKA peptide 2-66 showed that the reporter turns over very rapidly (half time of recovery ~0.3 sec) (Johnson and Schell, 2009). While the F-actin binding domain of ITPKA has recently been further truncated to residues 9-40 and given the name F-Tractin (personal correspondence, Michael Schell, USUHS), the slightly longer 9-52 peptide has already been shown to be an excellent *in vivo* reporter for F-actin in two types of neurons (Johnson and Schell, 2009; Wagner *et al*., 2011). Since peptide 9-52 is in essence a prototype of F-Tractin, and since we used this slightly longer version throughout this study, we will refer to it throughout the text as F-Tractin-P.

To begin to validate the use of F-Tractin-P in Jurkat T cells, we fused it to mGFP, expressed it in cells, fixed the cells 5 min after they had contacted the bilayer, and stained them with Alexa-568-conjugated phalloidin. In striking contrast to the results described above using GFP-actin, the actin arcs in the LM/pSMAC were clearly visible in both the green and red channels in cells expressing mGFP-F-Tractin-P (Fig. 5 B1-B6). Given that any molecule or peptide that binds F-actin, even weakly like F-Tractin-P, should in principle shift the equilibrium from G-actin to F-actin to at least some extent, we performed a number of control experiments to exclude the possibility that the expression of F-Tractin-P in Jurkat cells induces non-physiological actin structures or significantly alters F-actin dynamics at the IS. First, mGFP-F-Tractin-P had no obvious effect on the total amount of F-actin in cells across a broad range of mGFP-F-Tractin-P expression levels (Fig. 6 A). Consistently, Fig. 6

Figure 5. Comparison of F-actin structures at the IS reported by GFP-actin and mGFP-F-Tractin-P.

(A) F-actin structures reported at the IS by GFP-actin and phalloidin in a representative Jurkat cell fixed after engagement on a planar bilayer. (A1) GFP-actin, (A2) phalloidin staining in the same cell, and (A3) merged image between A1 (green) and A2 (red). (A4-A6) Magnified images of the boxed regions (white) in A1-A3, respectively. (B) F-actin structures at the IS reported by GFP-F-Tractin-P and phalloidin in a representative Jurkat cell fixed after stimulation on a planar bilayer. (B1) GFP-F-Tractin-P, (B2) phalloidin staining in the same cell, and (B3) merged image between B1 (green) and B2 (red). (B4-B6) Magnified images of the boxed regions (white) in B1-B3, respectively. The positions of the LP/dSMAC and LM/pSMAC regions of the IS are indicated by the brackets above A4-A6 and B4-B6. All scale bars = 5 μm.

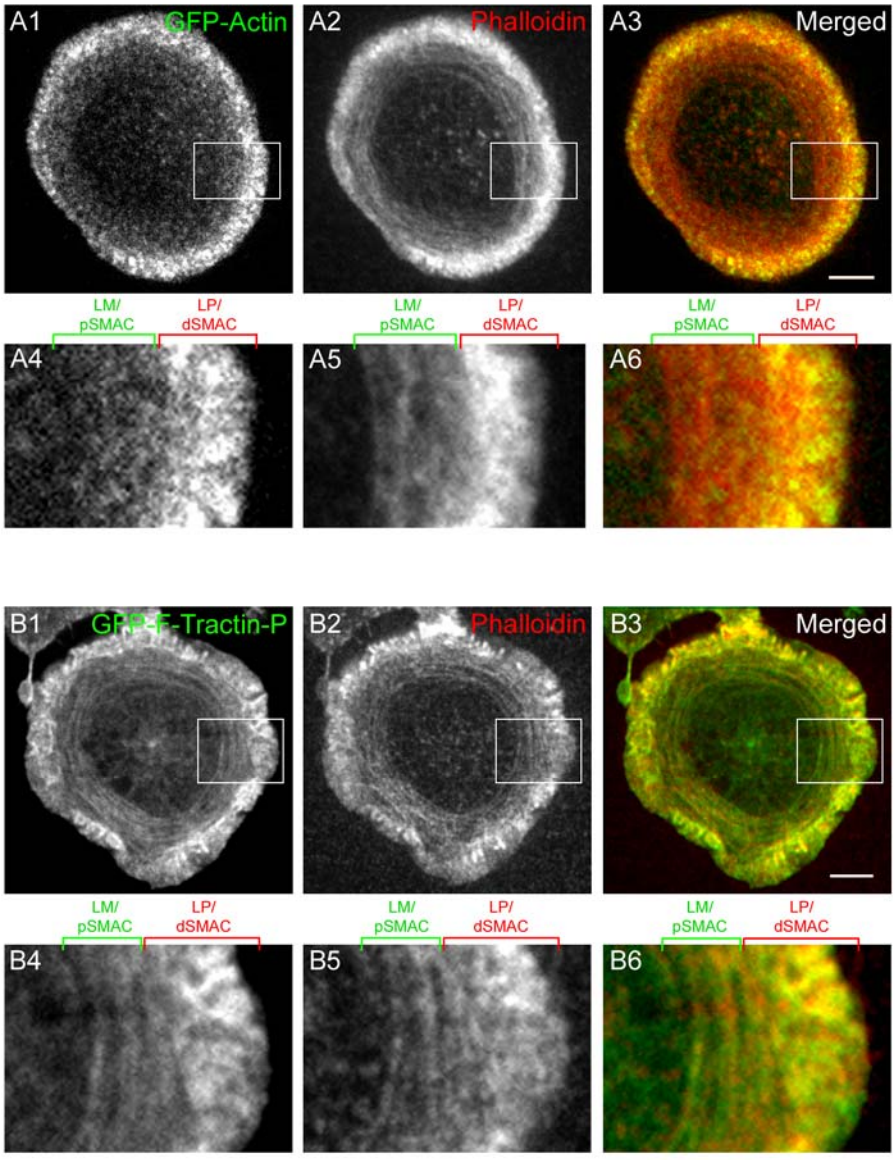

Figure 6. Lack of effect of mGFP-F-Tractin-P expression on cellular F-actin content and dynamics, and on TCR signaling.

(A) Graph showing the total fluorescence intensity per cell of Alexa-568-conjugated phalloidin for Jurkat cells bound to an anti-CD3ε-coated coverslip plotted against the total fluorescence intensity of mGFP-F-Tractin-P per cell. (B) Graph showing the average total fluorescence intensity of Alexa-568-conjugated phalloidin in coverslip-bound cells expressing control GFP, mGFP-F-Tractin-P, and GFP-actin (N=40). Note that the average intensity of cellular phalloidin staining in cells expressing a wide range of GFP-actin was significantly lower than in control cells ($p<0.001$), suggesting that the expression of GFP-actin shifts the equilibrium from F-actin to G-actin to some extent. (C) Time lapse images at the IS of a Jurkat cell expressing GFP-F-Tractin-P and bound to an anti-CD3ε-coated coverslip immediately following treatment with 10 μM Latrunculin A. (D) Rise in cytosolic calcium in an untransfected Jurkat cell induced upon contact with an anti-CD3ε-coated coverslip, assayed using Fluo-4 AM as the calcium sensor. (D1) Time lapse images of Fluo-4, (D2) corresponding time-lapse images of the same cell using transmitted light, and (D3) graph showing the relative fluorescence intensity of Fluo-4 in this cell as a function of time. (E) Rise in cytosolic calcium in a tdTomato-F-Tractin-P-expressing Jurkat cell induced upon contact with an anti-CD3ε-coated coverslip, assayed using Fluo-4 AM as the calcium sensor. (E1) Time lapse images of Fluo-4, (E2) corresponding time-lapse images of tdTomato-F-Tractin-P in the same cell, and (E3) graph showing the relative fluorescence intensity of Fluo-4 in this cell plotted over time. All scale bars = 5 μm.

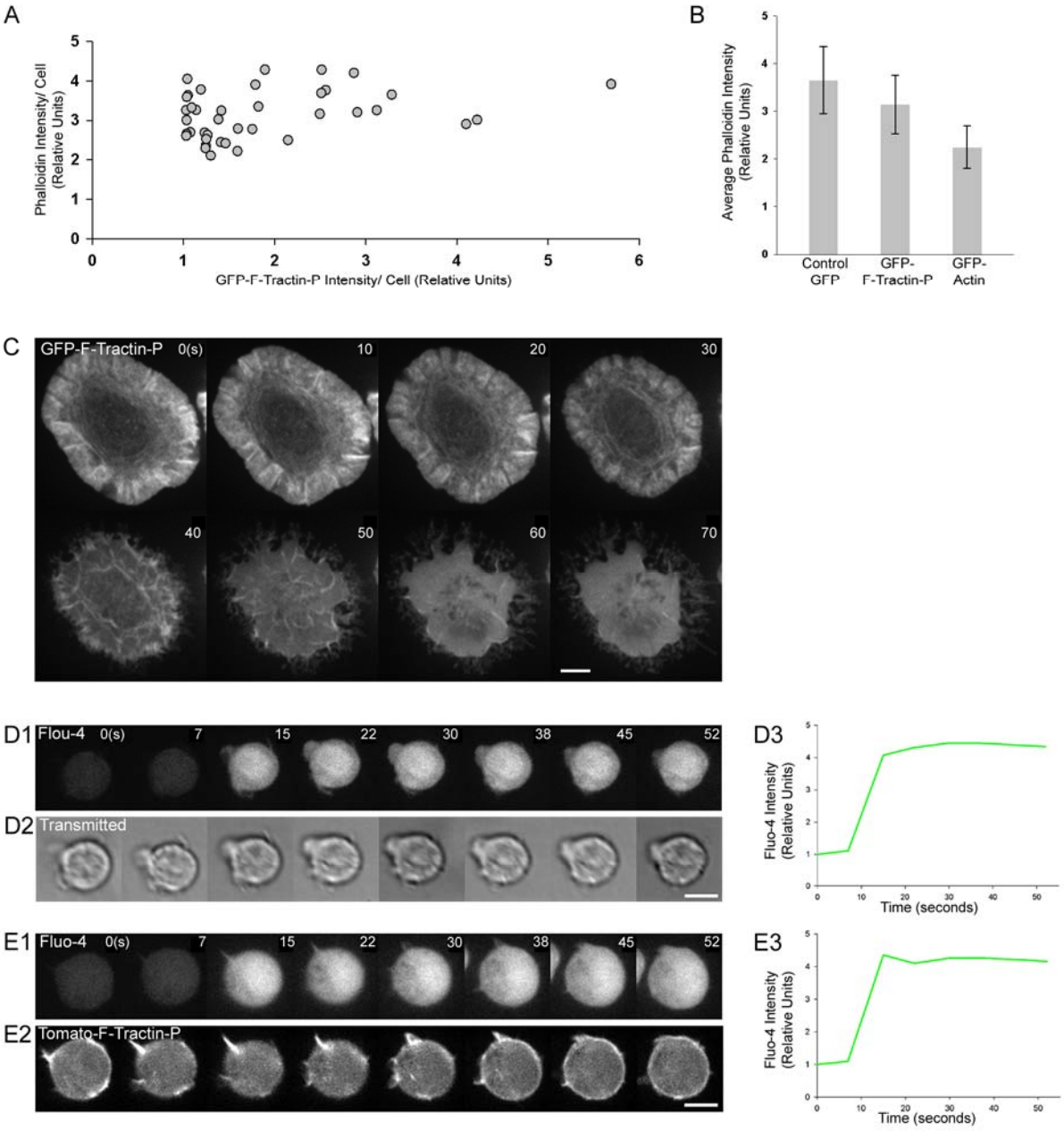
A
Phalloidin Intensity/ Cell (Relative Units)
GFP-F-Tractin-P Intensity/ Cell (Relative Units)
B
Average Phalloidin Intensity (Relative Units)
Control GFP
GFP-F-Tractin-P
GFP-Actin
C
GFP-F-Tractin-P
0(s)
10
20
30
40
50
60
70
D1
Flou-4
0(s)
7
15
22
30
38
45
52
D2
Transmitted
D3
Fluo-4 Intensity (Relative Units)
Time (seconds)
E1
Fluo-4
0(s)
7
15
22
30
38
45
52
E2
Tomato-F-Tractin-P
E3
Fluo-4 Intensity (Relative Units)
Time (seconds)

B shows that the average intensity of cellular phalloidin staining in all of the cells plotted in Fig. 6 A (mGFP-F-Tractin-P) was not significantly different from that of control cells expressing various levels of free mGFP (Control GFP) ($p>0.05$). These results argue that even relatively high levels of expression of mGFP-F-Tractin-P that are significantly beyond what is necessary to tract F-actin in living cells, and beyond the level of expression in cells we routinely imaged for data collection, do not significantly drive the formation of additional F-actin in cells. Second, expression of mGFP-F-Tractin-P does not appear to artificially stabilize actin filaments *in vivo*, as F-actin structures labeled by mGFP-F-Tractin-P were rapidly depolymerized by the addition of 10 μM Latrunculin-A (Fig. 6 C). Specifically, in cells expressing mGFP-F-Tractin-P, where depolymerization was gauged by watching in real time the disappearance of mGFP-F-Tractin-P-labeled structures (Fig. 6 C), as well as in untransfected cells and cells treated with just DMSO (the vehicle for latrunculin), where depolymerization was gauged by fixation and staining with phalloidin at various time points (DNS), the depolymerization of F-actin structures was very obvious at ~30 sec after latrunculin addition, and nearly complete at ~60 sec. Finally, Jurkat cells expressing F-Tractin-P tagged with tdTomato showed the same extent of calcium influx upon contact with the stimulatory lipid bilayer as control cells (Fig. 6 D and E; compare the control cell in S2 D1-D3 with the cell expressing tdTomato-F-Tractin-P in S2 E1-E3). This observation argues that downstream TCR signaling is not altered by the expression of F-Tractin-P. In summary, these controls, together with the crucial fact that mGFP-F-Tractin-P, but not GFP-actin, labels the actin arcs in the LM/pSMAC that are present as endogenous structures in phalloidin-stained, untransfected cells, leads us to conclude that F-Tractin-P is an ideal reporter for visualizing the dynamics of F-actin in both the LP and LM actin networks at the Jurkat IS.

c. Quantitation of F-actin dynamics using F-Tractin-P reveals a striking difference in centripetal flow rates between the LP/dSMAC and LM/pSMAC

Having established from fixed cell images that the LP/dSMAC and LM/pSMAC possess distinct organizations of F-actin, we next asked if the dynamics of F-actin in these two regions also differ. To address this question, we took time lapse images of Jurkat T cells expressing mGFP-F-Tractin-P after engagement on the planar bilayer (Fig. 7 A1-A3; unless indicated otherwise, all dynamic imaging was initiated 2 min after loading cells into the bilayer; see also Methods). In agreement with previous reports (Bunnell *et al.*, 2001; Kaizuka *et al.*, 2007), dramatic actin retrograde flow was observed in the LP/dSMAC region, as evidenced by kymograph images across this region (Fig. 7 A2, Low Contrast, LP/dSMAC). Moreover, the rate of retrograde flow across the LP/dSMAC appears both uniform and constant, as evidenced by the uniformity and linearity in the slopes that comprise the portion of kymographs corresponding to this zone.

Even more importantly, mGFP-F-Tractin-P revealed that the concentric actin arcs observed in the LM/pSMAC of untransfected cells stained with phalloidin (Fig. 4), and in still images of cells transfected with mGFP-F-Tractin-P (Fig. 5), are highly dynamic. Specifically, they form at the boundary between the LP/dSMAC and LM/pSMAC, move inward across the LM/pSMAC, as evidenced by kymograph images across this region (Fig. 7 A3, High Contrast, LM/pSMAC), and then disappear abruptly at the boundary between the LM/pSMAC and the cSMAC. Moreover, the rate of movement of these actin arcs across the pSMAC appears both uniform and constant, as evidenced by the uniformity and linearity in the slopes that comprise the portion of kymographs corresponding to this zone. Visual inspection of both kymographs and movies obtained from individual cells like the one shown in Fig. 7 A argue that the rates at which the distinct F-actin networks in the LP/dSMAC and LM/pSMAC move inward must be quite different. Consistently, measurements made using kymographs obtained from 8 cells yielded a value of 0.105 ± 0.006 μm/sec for the average rate of retrograde actin flow across the LP/dSMAC, and 0.037

Figure 7. Characterization of F-actin dynamics in the LP/dSMAC and LM/pSMAC regions of the IS.

(A) Centripetal actin flow in the LP/dSMAC and LM/pSMAC regions of the IS observed using GFP-F-Tractin-P in a representative Jurkat cell stimulated on a planar lipid bilayer. (A1) F-actin reported by GFP-F-Tractin-P at the IS. (A2, A3) Kymograph of GFP-F-Tractin-P in the region corresponding to the yellow line in A1, shown in low-contrast (A2) and high-contrast (A3). In this and all subsequent kymographs, the shallower the slope, he faster the speed, and the steeper the slope, the slower the speed. (B) Centripetal flow of F-actin and myosin IIA at the IS in a representative cell engaged on a bilayer. (B1) tdTomato-F-Tractin-P, (B2) GFP-myosin IIA HC in the same cell, and (B3) merged image between B1 (red) and B2 (green). (B4-B6) Magnified images of the boxed regions (orange) in B1-B3, respectively. White arrowheads indicate two arcs present in the LM/pSMAC that clearly possess both F-actin and myosin IIA. (B7) Low-contrast kymograph of tdTomato-F-Tractin-P in the region corresponding to the yellow line in B1. (B8) High-contrast kymograph of tdTomato-F-Tractin-P in the region corresponding to the yellow line in B1. (B9) Kymograph of GFP-Myosin IIA HC in the region corresponding to the yellow line in B2. The positions of the LP/dSMAC and LM/pSMAC regions of the IS are indicated by the brackets above A2, A3, B4-B6, and B7-B9. The time scales (in sec) for all of the kymographs shown are indicated on the left. Scale bars in A1 and B3 = 5 μm. Scale bars in A2, A3, B7 = 2 μm.

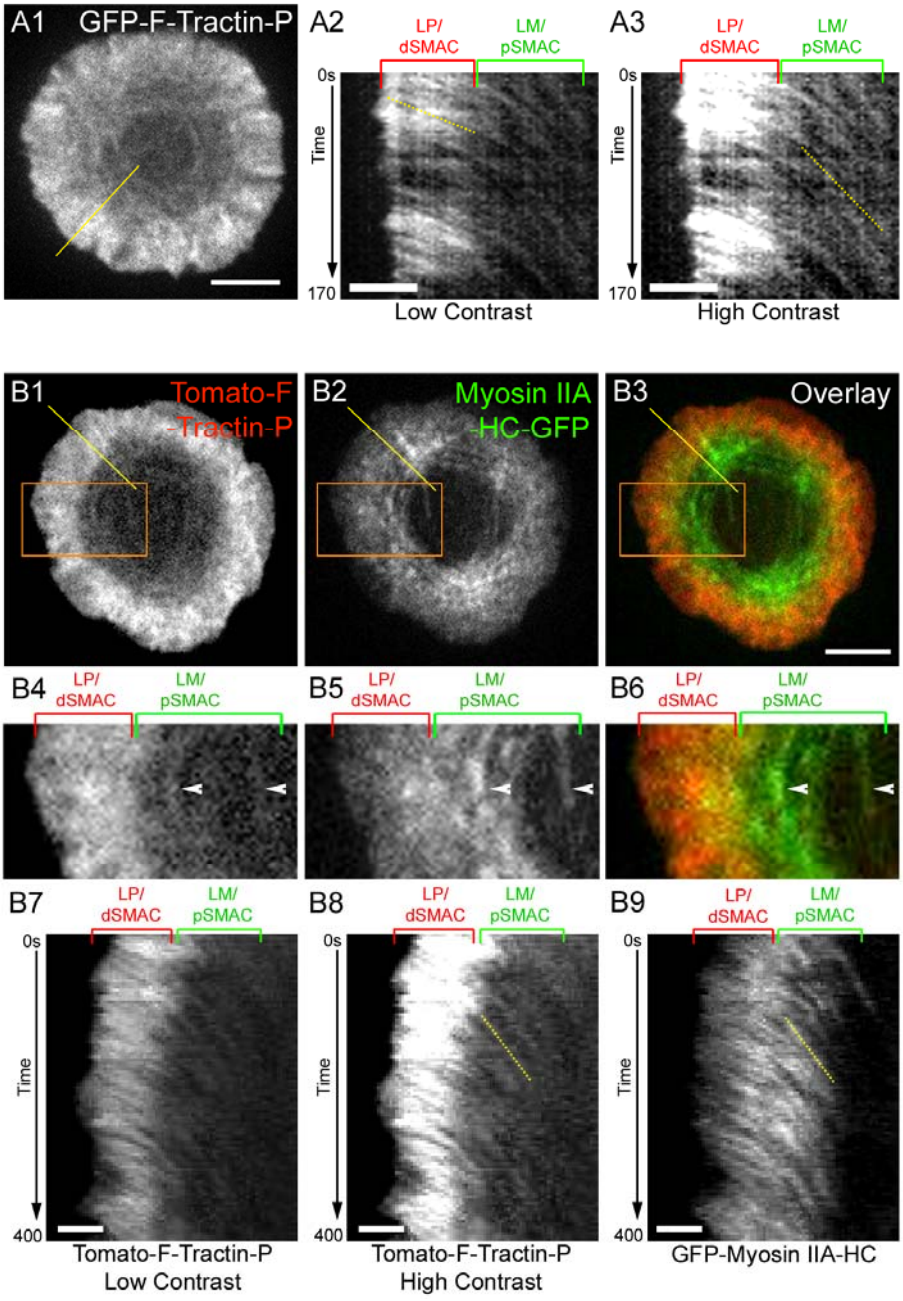
A1
GFP-F-Tractin-P
A2
LP/
dSMAC
LM/
pSMAC
0s
Time
170
Low Contrast
A3
LP/
dSMAC
LM/
pSMAC
0s
Time
170
High Contrast
B1
Tomato-F
-Tractin-P
B2
Myosin IIA
-HC-GFP
B3
Overlay
B4
LP/
dSMAC
LM/
pSMAC
B5
LP/
dSMAC
LM/
pSMAC
B6
LP/
dSMAC
LM/
pSMAC
B7
LP/
dSMAC
LM/
pSMAC
0s
Time
400
Tomato-F-Tractin-P
Low Contrast
B8
LP/
dSMAC
LM/
pSMAC
0s
Time
400
Tomato-F-Tractin-P
High Contrast
B9
LP/
dSMAC
LM/
pSMAC
0s
Time
400
GFP-Myosin IIA-HC

± 0.003 μm/sec for the average rate of centripetal actin arc movement across the LM/pSMAC (Fig. 10 A, compare LP/dSMAC Wild Type [WT] Actin to LM/pSMAC WT Actin; $p<0.001$). In addition to this ~3-fold difference in centripetal flow rate, we note that the transition between these two flow rates occurs quite abruptly at the boundary between the LP/dSMAC and LM/pSMAC (Fig. 7 A1-A3). Finally, we note that essentially identical rates of actin retrograde flow and centripetal actin arc movement were observed when Jurkat cells expressing mGFP-F-Tractin-P were engaged on coverslips coated with immobilized anti-CD3ε antibody (Fig. 8 A). This result indicates that the dynamics of the two distinct actin networks in the LP and LM, as well as their formation (see Fig. 4), does not require the rearrangement of integrin and TCR clusters that drives IS maturation (see also (Bunnell *et al.*, 2001)). Together, these data indicate that the LP/dSMAC and LM/pSMAC regions possess organizations of F-actin that are kinetically as well as structurally distinct.

d. Myosin IIA moves inward with the actin arcs in the LM/pSMAC

Given that the mGFP-F-Tractin-P-labeled actin arcs in the LM/pSMAC undergo apparent contraction, as observed for myosin II-containing actin arcs in the LM of migrating cells (Gupton and Waterman-Storer, 2006; Medeiros *et al.*, 2006), and that the LM/pSMAC stains extensively for endogenous myosin IIA (Fig. 4 E), we next asked if these actin arcs co- localize with myosin IIA in living cells. To accomplish this, we co-transfected Jurkat cells with tdTomato-F-Tractin-P and the heavy chain of myosin IIA fused at its N-terminus to GFP (GFP-myosin IIA HC), and we imaged the cells after engagement on bilayers. As in the previous figure using mGFP-F-Tractin-P, tdTomato-F-Tractin-P reported the two structurally (Fig. 7 B1 and the inset in B4) and kinetically (Fig. 7 B7 and B8, see Low Contrast for the LP/dSMAC and High Contrast for the LM/pSMAC) distinct zones of F-actin in the LP/dSMAC and LM/pSMAC. With regard to the signal for myosin IIA, in addition to weak fluorescence in the LP/dSMAC, an intense signal was observed in the LM/pSMAC (Fig. 7 B2 and the

Figure 8. Rates of actin retrograde flow and acto-myosin II arc contraction in DMSO-treated Jurkat cells engaged on coverslip and planar bilayer substrates, and imaging of actin arcs in the LM/pSMAC using only dynamic probes for myosin IIA.

(A) Graph showing the rates (in μm/sec) of centripetal, GFP-F-Tractin-P-labeled actin flow and TCR MC movement in the LP/dSMAC and LM/pSMAC regions of DMSO-treated Jurkat cells stimulated on a planar bilayer, GFP-F-Tractin-P-labeled actin flow in the LP/dSMAC and LM/pSMAC regions of DMSO-treated Jurkat cells stimulated on a coverslip substrate, and GFP-myosin IIA HC- or GFP-myosin II RLC-labeled actin arc flow in the LM/pSMAC of DMSO-treated Jurkat cells stimulated on either a planar bilayer or a coverslip substrate. The number of cells used per measurement are indicated inside the bars. (B1) Dynamics of myosin IIA-containing actin arcs in the LM/pSMAC region of a Jurkat cell expressing GFP-myosin IIA HC after engagement on a planar bilayer. (B2) Kymograph of the region corresponding to the yellow line in B1. (C1) Dynamics of myosin IIA-containing actin arcs in the LM/pSMAC region of a Jurkat cell expressing GFP-myosin II RLC after engagement on a planar bilayer. (C2) Kymograph of the region corresponding to the yellow line in C1. (D1) Dynamics of myosin IIA-containing actin arcs in the LM/pSMAC region of a Jurkat cell expressing GFP-myosin IIA HC after engagement on a planar bilayer. (D2) Time lapse images of the region corresponding to the white box in D1. Elapsed time (in sec) is indicated above D2. Bright discontinuities in GFP-myosin II fluorescence within the arcs are indicated by yellow arrowheads in D2. The time scales (in sec) are indicated to the left of the kymographs. Scale bars in B1, C1, D1 = 5 μm. Scale bars in B2, C2, = 2 μm. Scale bar in D2 = 1 μm.

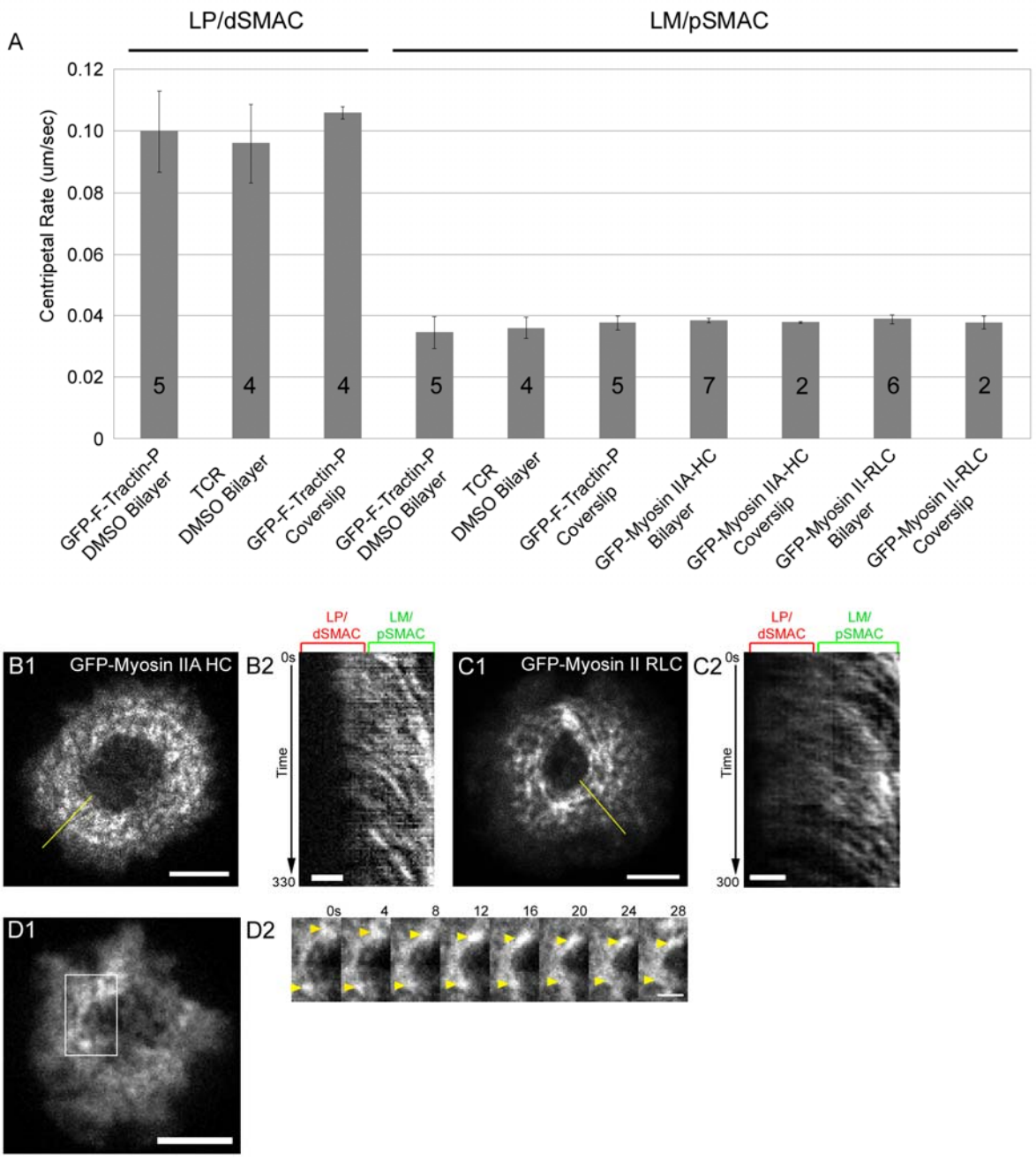
A
LP/dSMAC
LM/pSMAC
Centripetal Rate (um/sec)
0.12
0.10
0.08
0.06
0.04
0.02
0
5
4
4
5
4
5
7
2
6
2
GFP-F-Tractin-P DMSO Bilayer
TCR DMSO Bilayer
GFP-F-Tractin-P Coverslip
GFP-F-Tractin-P DMSO Bilayer
TCR DMSO Bilayer
GFP-F-Tractin-P Coverslip
GFP-Myosin IIA-HC Bilayer
GFP-Myosin IIA-HC Coverslip
GFP-Myosin II-RLC Bilayer
GFP-Myosin II-RLC Coverslip
B1
GFP-Myosin IIA HC
B2
LP/ dSMAC
LM/ pSMAC
0s
Time
330
C1
GFP-Myosin II RLC
C2
LP/ dSMAC
LM/ pSMAC
0s
Time
300
D1
D2
0s
4
8
12
16
20
24
28

inset in B5; see also the overlaid images in B3 and B6). Moreover, kymographs revealed that this intense signal for myosin IIA, which often has the appearance of rings or arcs, also moves centripetally in the LM/pSMAC zone (Fig. 7 B9). Importantly, measurements made using kymographs obtained from 7 cells yielded a value of 0.038 ± 0.001 μm/sec for the average rate of centripetal movement of these myosin IIA-rich structures across the LM/pSMAC (Fig. 8 A). This value is not different from the average rate of centripetal movement of actin arcs in the LM/pSMAC (Fig. 10 A; $p>0.05$). We note that the expression of GFP-tagged myosin IIA HC alone (i.e. without F-Tractin-P) also reports these translocating myosin IIA-rich structures in the LM/pSMAC (Fig. 8 A, B1, B2). This result argues that these myosin IIA-rich, arc-like structures are not induced by our F-actin reporter. Finally, we obtained very similar images and rate values when we visualized myosin IIA by tagging its regulatory light chain with GFP (GFP-myosin II RLC) instead of its heavy chain (Fig. 8 A, C1, C2).

The fact that the region of the Jurkat cell cortex that contains the actin arcs, i.e. the LM/pSMAC, is also the region that has the highest concentration of myosin IIA (both endogenous (Fig. 4 E1-E6) and exogenous (Fig. 7 B1-B6) suggests that what we are actually seeing in this zone are circularized, contracting acto-myosin IIA bundles. Consistent with this idea, the rates at which the actin arcs and the myosin IIA-rich structures move inward in the LM/pSMAC are indistinguishable (see above). Moreover, close inspection of the signals for actin and myosin IIA in the LM/pSMAC shows that in many cases the two signals completely overlap in the form of concentric bands or arcs (Fig. 7 B4-B6; see arrowheads). Finally, time-lapse images of arcs exhibiting variations in GFP-myosin IIA HC intensity within the arc show that small regions of increased fluorescence intensity get closer together over time, consistent with arc contraction (Fig. 8 D1 and D2). We conclude, therefore, that the pSMAC is rich in contracting acto-myosin IIA bundles, much

like the LM of a crawling cell (Medeiros *et al.*, 2006). To our knowledge, this is the first observation of contracting acto-myosin II arcs at the IS in T cells.

e. TCR microclusters move inward at the speed of actin retrograde flow in the LP/dSMAC and at the speed of acto-myosin IIA arc contraction in the LM/pSMAC

TCR MC transport at the IS requires F-actin (Varma *et al.*, 2006; Nguyen *et al.*, 2008). Moreover, numerous studies have pointed to actin polymerization and subsequent retrograde flow as the principal if not sole mechanism driving the centripetal movement of these MCs (Kaizuka *et al.*, 2007; DeMond *et al.*, 2008; Yu *et al.*, 2010). That said, none of these studies took into account the existence of the contracting acto-myosin IIA arcs in the LM/pSMAC described above. Therefore, we next sought to correlate the rates of TCR MC movement across the entire IS with the rates of centripetal actin movement in the two structurally and kinetically distinct zones of F-actin at the IS described here. To accomplish this, Jurkat cells expressing mGFP-F-Tractin-P were imaged on bilayers containing anti-CD3ε antibody labeled with rhodamine-X to report the position of bound TCR MCs in the Jurkat plasma membrane. Imaging initiated immediately after the T cell had contacted the bilayer show that TCR MCs first appear at the distal edge of the cell, at which point they then move inward at a near constant speed and in a relatively linear path across the entire LP/dSMAC (Fig. 9 A, frames 0-40 sec, see arrowheads). Moreover, comparison of the kymographs for actin retrograde flow and the movement of individual MCs across the LP/dSMAC (Fig. 9 B1-B3, LP/dSMAC) show that these two rates closely match throughout this zone. Even more strikingly, upon entering the LM/pSMAC zone, the movement of TCR MCs slows abruptly (Fig. 9 A, frames 40-90 sec, see arrowheads). In other words, upon entering the LM/pSMAC, the centripetal movement of TCR MCs appears to decrease abruptly to match that of the slower contracting acto-myosin IIA arcs in this zone. Consistent with this conclusion, comparison of kymographs for actin arc contraction and the

Figure 9. Characterization of TCR MC dynamics at the LP/dSMAC and LM/pSMAC regions of the IS.

(A) Time-lapse images showing TCR MC movements in the LP/dSMAC and LM/pSMAC regions of the IS in a representative Jurkat cell stimulated on a planar bilayer. TCR MCs (pseudo-colored green) reported by Rhodamine X-labeled anti-CD3ε antibody in the bilayer. F-actin (pseudo-colored red) reported by GFP-F-Tractin-P. White arrowheads point to a TCR MC undergoing inward movement. The frame at 40s that is boxed in orange indicates the moment when this TCR MC moved from the LP/dSMAC into the LM/pSMAC during its centripetal movement. (B1) Kymograph of GFP-F-Tractin-P in the region corresponding to the yellow line in A (0s), (B2) kymograph of a TCR MC in the region corresponding to the yellow line in A (0s), and (B3) merged image between B1 (red) and B2 (green). The positions of the LP/dSMAC and LM/pSMAC regions of the IS are indicated by the brackets above B1-B3. The boundary between the LP/dSMAC and LM/pSMAC is indicated by the orange line in B1-B3. The time scale of the kymographs in B1-B3 is indicated to the left of B1. (C) Paths of all visible TCR MCs in a representative Jurkat cell stimulated on a planar bilayer. TCR MC paths in the LP/dSMAC are shown in red, while TCR MC paths in the LM/pSMAC are shown in green. The paths are discontinuous because we purposely avoided making measurements at the dSMAC/pSMAC boundary. (D) Spatial and kinetic relationship between a TCR MC and surrounding acto-myosin II arcs in the LM/pSMAC region of the IS. (D1) eGFP-Myosin IIA HC (pseudo-colored red) and TCR MCs (pseudo-colored green) at the IS of a Jurkat cell stimulated on a planar bilayer. (D2) Magnified image of the boxed region (white) in D1. (D3) Relative intensities for myosin IIA (red) and a TCR MC (green) across the yellow line in D2. (D4) Kymograph of two prominent myosin IIA-containing arcs in the region corresponding to the yellow line in D1, (D5) kymograph of a TCR MC in the region corresponding to the yellow line in D1, and (D6) merged image between D4 (red) and D5 (green). The time scale of the kymographs in D4-D6 is indicated to the right of D6. Scale bars in A, B3, D6 = 2 μm. Scale bar in D1 = 5 μm.

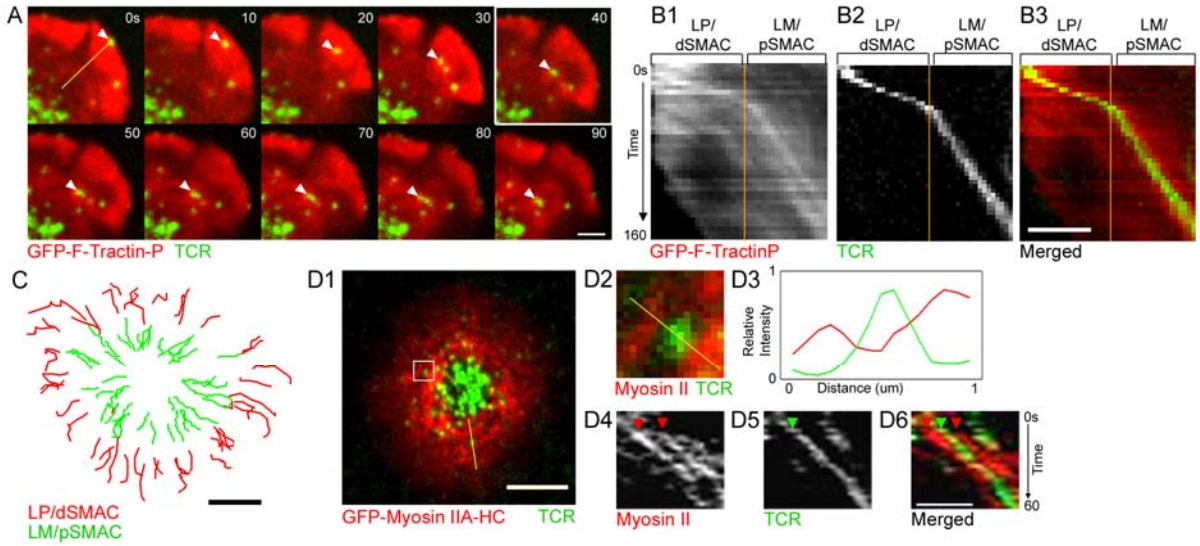

movement of individual TCR MCs across the LM/pSMAC (Fig. 9 B1-B3, LM/pSMAC) show that these two rates closely match throughout this zone. These results suggest, therefore, that there is fairly precise spatial and kinetic coupling between the centripetal movements of TCR MCs and F-actin in both the LP/dSMAC and LM/pSMAC. This in turn argues that TCR MCs are tightly coupled to the rapid retrograde actin flow in the LP/dSMAC and to the slower, contracting, acto-myosin IIA arcs in the LM/pSMAC.

To provide quantitative support for the above conclusions, we next measured the rates of centripetal TCR MC movement and centripetal actin flow across both the LP/dSMAC and LM/pSMAC in 15 Jurkat cells engaged on bilayers and imaged every 4 sec. Fig. 9 C shows the paths of all of the TCR MCs in a representative cell, where tracks across the LP/dSMAC and LM/pSMAC have been color coded red and green, respectively. To determine the rates of TCR MC transport, we manually tracked MCs and calculated their instantaneous, frame-to-frame velocities (see Methods for details). To determine the rates of retrograde actin flow and actin arc contraction, we measured the slopes in kymographs of the mGFP-F-Tractin-P signal. Consistent with the conclusions drawn above, the average instantaneous velocity of centripetal TCR MC movement across the LP/dSMAC (0.094 ± 0.016 μm/sec) was not statistically different from that of actin retrograde flow in this zone (0.105 ± 0.006 μm/sec) (Fig. 10 A, compare LP/dSMAC WT Actin to LP/dSMAC WT TCR; $p>0.05$). Likewise, the average instantaneous velocity of centripetal TCR MC movement across the LM/pSMAC (0.038 ± 0.006 μm/sec) was not statistically different from that of actin arc contraction in this zone (0.037 ± 0.003 μm/sec) (Fig. 10 A, compare LM/pSMAC WT Actin to LM/pSMAC WT TCR; $p>0.05$). Together, these results argue strongly that the centripetal movements of TCR MCs at the IS are driven sequentially by rapid retrograde actin flow in the LP/dSMAC and slower, contracting, acto-myosin IIA arcs in the LM/pSMAC. These results also argue that the coupling between the centripetal movement of TCR MCs

and the retrograde movement of F-actin is much less dissipative then previously reported (Kaizuka *et al.*, 2007) (see Discussion).

To further investigate the precise spatial relationship within the LM/pSMAC between the centripetal movement of TCR MCs and the inward movement of the contracting acto-myosin IIA arcs, we imaged TCR MCs movements in Jurkat cells expressing GFP-myosin IIA HC (Fig. 9 D1). Two-color line scans (Fig. 9 D3) across individual, green TCR MCs in the LM/pSMAC (Fig. 9 D2) of a typical cell (Fig. 9 D1) show that the peak of fluorescence intensity for the MC usually falls in between two peaks of fluorescence intensity for myosin IIA arcs. Moreover, two-color kymographs show that MCs continue to localize over time in between the successive, contracting, acto-myosin IIA arcs (Fig. 9 D4-D6, see arrowheads). Of 100 TCR MCs picked at random, 71 fell in between myosin IIA arcs based on both visual inspection and line scans, arguing that this phenomenon is common. These observations, together with the fact that TCR MCs move in tandem with the contracting acto-myosin IIA arcs in the LM/pSMAC (Fig. 10 A), raise the possibility that MC transport across this zone is driven by a "sweeping" motion generated by the acto-myosin IIA arcs, although this does not preclude either direct or indirect physical interactions between the MCs and the arcs.

f. Inhibition of myosin IIA with blebbistatin slows TCR MC movement in the LP/dSMAC and disrupts both the organization of actin arcs and the directed transport TCR MCs in the LM/pSMAC

Given the tight coupling within the LM/pSMAC between the centripetal movement of TCR MCs and the apparent contraction of acto-myosin IIA arcs, we next sought to measure the contribution made by myosin IIA to the organization of F-actin and the transport of MCs in this region of the IS. More specifically, we sought to examine in detail the effects of conditionally inhibiting myosin IIA on the rates of centripetal actin flow and TCR MC movement in both the LP/dSMAC and LM/pSMAC using bilayer-engaged Jurkat cells expressing tdTomato-F-Tractin-P. To inhibit myosin IIA rapidly and selectively, we used 50

Figure 10. Effect of Blebbistatin on the dynamics of F-actin and TCR MCs in the LP/dSMAC and LM/pSMAC regions of the IS.

(A) Graph showing the rates of centripetal movement (in μm/sec) of actin (red) and TCR MCs (green) in the LP/dSMAC and LM/pSMAC regions of WT (in this study, WT is used to indicate untreated cells), BB-, CD-Jas-, and CD-Jas-BB-treated Jurkat cells stimulated on planar bilayers. The bars indicate the mean and standard deviation (SD) for the centripetal rate. The number of cells that was analyzed for each measurement is indicated inside (or above) the bar (~50 TCR MCs were measured per cell). (B) Graph showing the meandering index (net displacement/ total distance traveled) of TCR MCs measured in the LP/dSMAC and LM/pSMAC region of WT, BB-, and CD-Jas-treated cells. Each bar shows the mean and SD for the meandering index. The number of cells that were analyzed for each measurement is indicated inside the bar. (C) Graph showing the percentage of TCR MCs that moved one or more pixels (black) or zero pixels (gray) per frame in the LP/dSMAC and LM/pSMAC regions of WT, BB-, CD-Jas-, and CD-Jas-BB-treated cells. The bars show the percentages of all measurements that fall in these two categories. (D) The effect of BB on the dynamics of actin arcs and the movements of TCR MCs in the LM/pSMAC region of the IS. (D1) tdTomato-F-Tractin-P at the IS in a BB-treated cell stimulated on a planar bilayer. (D2) Time-lapse images of the boxed region (white) in D1. The yellow arrowheads point to a buckling actin arc in the LM/pSMAC. (D3) Kymograph of Tomato-F-Tractin-P in the region corresponding to the yellow line in D1, (D4) kymograph of TCR MCs in the region corresponding to the yellow line in D1, and (D5) merged image between D3 (red) and D4 (green). The positions of the LP/dSMAC and LM/pSMAC regions of the IS are indicated by the brackets above D3-D5. The time scale of the kymographs in D3-D5 is indicated to the right of D5. Scale bar in D1 = 5 μm. Scale bar in D4 = 2 μm.

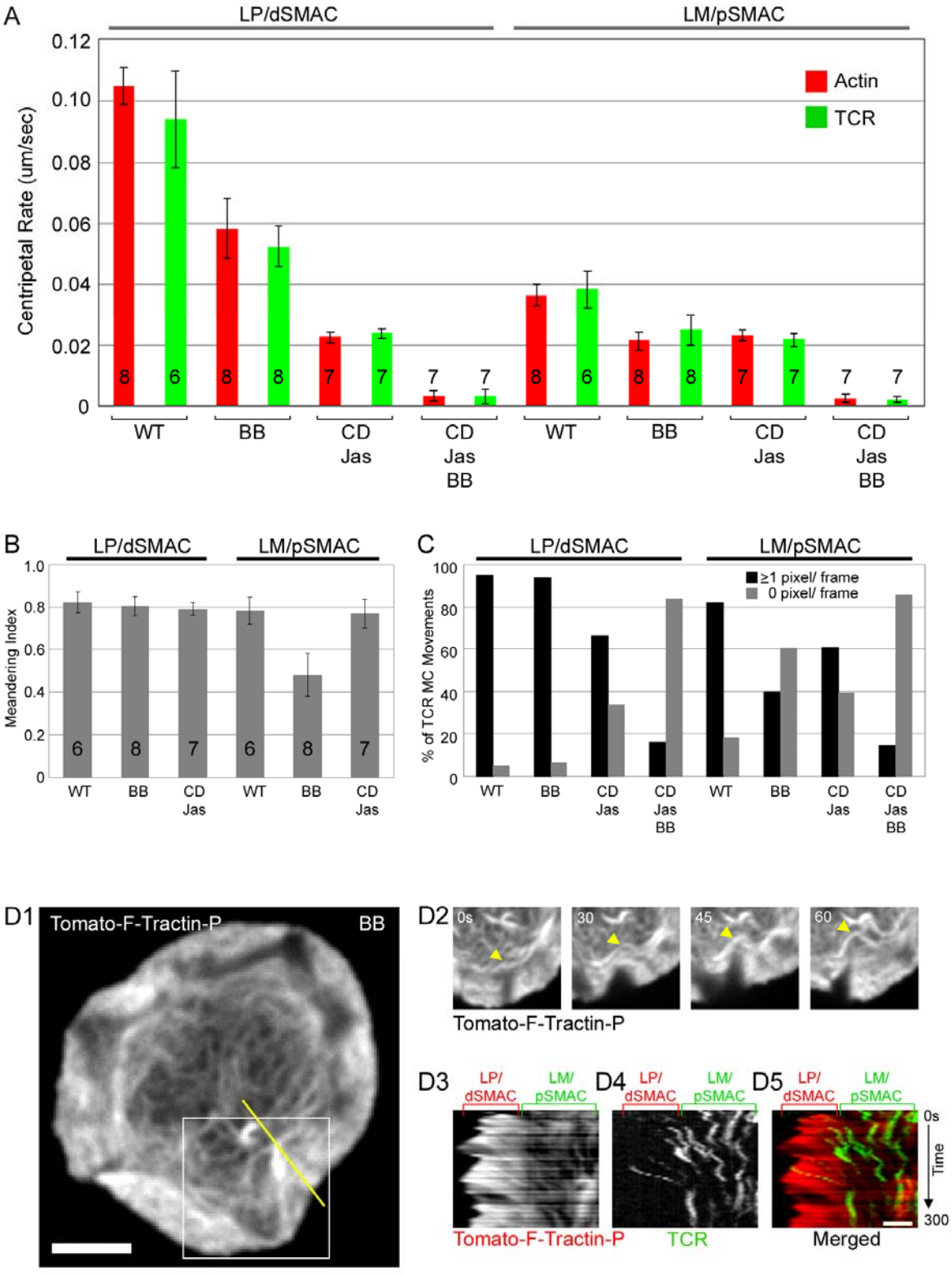
A
LP/dSMAC
LM/pSMAC
Actin
TCR
Centripetal Rate (um/sec)
0.12
0.10
0.08
0.06
0.04
0.02
0
8 6 8 8 7 7 7 7 8 6 8 8 7 7 7 7
WT
BB
CD Jas
CD Jas BB
WT
BB
CD Jas
CD Jas BB
B
LP/dSMAC
LM/pSMAC
Meandering Index
1.0
0.8
0.6
0.4
0.2
0
6 8 7 6 8 7
WT
BB
CD Jas
WT
BB
CD Jas
C
LP/dSMAC
LM/pSMAC
≥1 pixel/ frame
0 pixel/ frame
% of TCR MIC Movements
100
80
60
40
20
0
WT
BB
CD Jas
CD Jas BB
WT
BB
CD Jas
CD Jas BB
D1
Tomato-F-Tractin-P
BB
D2
0s
30
45
60
Tomato-F-Tractin-P
D3
LP/ dSMAC
LM/ pSMAC
D4
LP/ dSMAC
LM/ pSMAC
D5
LP/ dSMAC
LM/ pSMAC
0s
Time
300
Tomato-F-Tractin-P
TCR
Merged

μM blebbistatin (BB), a cell-permeable and highly-specific inhibitor of myosin IIA's ATPase activity (Allingham *et al.*, 2005) that locks the myosin in a weakly-bound, ADP-Pi state, causing it to dissociate from F-actin. In all experiments, Jurkat cells were engaged with the bilayer following a 30 min pre-incubation with BB at 37ºC. We took special care to avoid the use of blue light, which rapidly inactivates BB (Sakamoto *et al.*, 2005).

For Jurkat cells treated for 30 min with DMSO (the vehicle for BB), the rates of centripetal actin flow and TCR MC movement in both the LP/dSMAC and LM/pSMAC were not statistically different from the rates in untreated cells (Fig. 8 A; $p>0.05$). In contrast, BB treatment led to a 44.4% reduction in the average speed of actin retrograde flow across the LP/dSMAC region, from 0.105 ± 0.006 μm/sec to 0.058 ± 0.010 μm/sec (Fig. 10 A, compare LP/dSMAC WT Actin to LP/dSMAC BB Actin; $p<0.001$). This result is consistent with the effect of BB on the rate of actin retrograde flow in the LP of other cell types (Medeiros *et al.*, 2006; Wilson *et al.*, 2010), and is presumably due to a BB-induced reduction in the pulling force within the LM (see below). In parallel with this reduction in the rate of actin retrograde flow, the average rate of centripetal TCR MC movement in the LP/dSMAC was reduced by 44.2% following BB treatment, from 0.094 ± 0.016 μm/sec to 0.052 ± 0.006 μm/sec (Fig. 10 A, compare LP/dSMAC WT TCR to LP/dSMAC BB TCR; $p<0.001$). The directionality of TCR MC movements in the LP/dSMAC of BB-treated cells, as measured using the "meandering index" (total distance /net displacement; see Methods) were not, however, significantly different from WT (Fig. 10 B, compare LP/dSMAC WT to LP/dSMAC BB; $p>0.05$). Together, these results argue that while myosin IIA contributes to efficient actin retrograde flow and TCR MC movement in the LP/dSMAC, presumably as a consequence of its crucial role in generating via actin arc contraction a pulling force within the LM/pSMAC ((Vicente-Manzanares *et al.*, 2009) and see below), it is not essential for the directed/persistent movement of TCR MCs in the LP/dSMAC. We also note that the rates of actin retrograde flow and inward TCR MC movement across the LP/dSMAC of BB-treated

cells remain tightly coupled, as these two rates are not statistically different (compare LP/dSMAC BB Actin to LP/dSMAC BB TCR in Figure 10 A; $p>0.05$).

With regard to the effects of BB treatment on the rates of actin arc contraction and centripetal TCR MC movement in the LM/pSMAC, the initial and most striking observation was that BB disrupted the organization of the concentric actin arcs found in this zone (Fig. 10 D1-D5). Specifically, BB treatment changed the organization of these actin arcs from the fairly ordered pattern of concentric rings seen in WT (Figs. 4,5,7) and DMSO-treated control cells (DNS), to one in which the arcs appear loose, disorganized, and not strongly concentric (Fig 10 D1). Moreover, time lapse imaging shows that the actin arcs in BB-treated cells tend to buckle and deform due to the pushing force exerted by continued actin retrograde flow in the LP/dSMAC region (Fig. 10 D2; see arrowheads). These defects in arc behavior are also evident in kymographs of centripetal actin flow in BB-treated cells (Fig. 10 D3, LM/pSMAC), where individual slopes that span the LM/pSMAC are not uniform across this zone, as compared to actin arcs in untreated cells (compare the LM/pSMAC actin kymograph for the BB-treated cell in Fig. 10 D3 to the LM/pSMAC actin kymograph for the WT cell in Fig. 7 A3). These defects in actin arc organization and dynamics are very evident when one compares movies of untreated and BB-treated cells side by side, where the disorganized and non-uniform inward movement of arcs in the LM/pSMAC of BB-treated cells contrasts sharply with the relatively uniform inward progression of actin arcs in the LM/pSMAC of untreated cells (DNS).

With regard to the quantitative effect of BB treatment on the rate of actin arc contraction in the LM/pSMAC, the drug reduced this rate by 43.2%, from 0.037 ± 0.003 μm/sec to 0.021 ± 0.003 μm/sec (Fig. 10 A, compare LM/pSMAC WT Actin to LM/pSMAC BB Actin; $p<0.001$; note that this measurement used only the centripetal and non-vertical [i.e. moving] portions of individual slopes in the kymographs; see Methods for more details). In parallel with this reduction in the rate of actin arc contraction in the LM/pSMAC, the

average rate of centripetal TCR MC movement in this zone was reduced following BB treatment by 34.2%, from 0.038 ± 0.006 μm/sec to 0.025 ± 0.005 μm/sec (Fig. 10 A, compare LM/pSMAC WT TCR to LM/pSMAC BB TCR; $p<0.002$). Moreover, the percentage of total TCR MC frames recorded where individual MCs did not advance by at least one pixel per frame is much higher in the LM/pSMAC region of BB-treated cells (60%) than in the LM/pSMAC region of control cells (6%) (Fig. 10 C). This observation reveals a pronounced increase in the frequency of very slow displacements or pauses in the inward transport of TCR MCs across the LM/pSMAC with BB treatment. Since these "pauses" were not included in the analysis of TCR MC rates, the data in Fig. 10 A underestimates to some extent the magnitude of the decrease in inward TCR MC movement across the LM/pSMAC of BB-treated cells. The directionality of TCR MC movements in the LM/pSMAC of BB-treated cells was also significantly degraded relative to that in WT cells (Fig. 10 B, compare LM/pSMAC BB to LM/pSMAC WT; $p<0.001$). Finally, two-color kymographs (Fig. 10 D3-D5) show that the paths of TCR MCs in the LM/pSMAC of BB-treated cells follow in zigzag fashion the convoluted paths of the inwardly moving actin arcs. Together, these results argue that while myosin IIA is not absolutely essential for the inward movement of actin arcs and TCR MCs across the LM/pSMAC, the myosin does make a major contribution to the overall organization and inward movement of the actin arcs, and consequently to the speed and directional persistence of centripetal TCR MC movements across the LM/pSMAC. Moreover, just as the robustness of retrograde actin flow and coupled MC movement in the LP/dSMAC is dependent on the pulling force provided by acto-myosin II-driven contraction in the LM/pSMAC (see above), we think the persistence of some inward actin arc movement and coupled MC movement in the LM/pSMAC in the absence of myosin II-driven contraction is due to the persistence of the actin retrograde flow-driven pushing force in the LP/dSMAC. Indeed, this pushing force, and the degree to which it pushes the flaccid actin arcs in the LM/pSMAC of a BB-treated cells inward, is very clear in time lapse movies of tdTomato-F-

Tractin-P (DNS). We note that the rates of actin retrograde flow and inward TCR MC movement across the LM/pSMAC of BB-treated cells remain coupled, as these two rates are not statistically different (compare LM/pSMAC BB Actin to LM/pSMAC BB TCR in Figure 10 A; $p>0.05$). We also note that myosin IIA, as visualized using its RLC tagged with mRFP, does not co-localize with the disorganized actin arcs present in BB-treated cells, consistent with the mode of action of this inhibitor (DNS).

Interestingly, the region in the center of the IS that is normally largely devoid of F-actin, and that corresponds to the cSMAC, was no longer visible in BB-treated cells (Fig 10 D1). This observation is consistent with the proposed role for myosin II in the severing of LM actin bundles and the subsequent disassembly of the LM actin network (Medeiros *et al.*, 2006; Wilson *et al.*, 2010).

g. Inhibition of actin retrograde flow causes the F-actin network and associated TCR MCs in the LP/dSMAC to retract at a speed that corresponds to slowed acto-myosin II arc contraction in the LM/pSMAC

To gauge the relative contribution of actin polymerization-driven retrograde flow to TCR MC transport across the IS, we sought to selectively inhibit the polymerization of F-actin at the distal edge of the LP/dSMAC using cytochalasin D (CD), a membrane permeable molecule that tightly caps (K_d = 0.5 nM) the fast-growing, free barbed end of the actin filament, preventing further filament elongation (Carlier *et al.*, 1986). In previous studies, 1-5 μM CD was shown to cause the rapid and complete retraction of the LP actin network in numerous cell types (Forscher and Smith, 1988; Henson *et al.*, 1999). Moreover, in newt lung cells, low-dose CD (0.1-0.5 μM) was shown to selectively disrupt actin retrograde flow in the LP while having no obvious effect on the rate of acto-myosin II-driven flow in the LM (Ponti *et al.*, 2004). In an effort to replicate these effects in Jurkat T cells, we initially tested different concentrations of CD on cells expressing mGFP-F-Tractin-P and engaged on coverslips coated with anti-CD3ε antibody. Concentrations of CD above 0.5 μM

Figure 11. Testing the effects of CD, Jas, and CD-Jas treatments on actin retrograde flow in cells engaged on coverslips.

(A) Effect of low-dose CD on the organization and dynamics of F-actin at the IS in a Jurkat cell stimulated on a coverslip substrate. (A1) GFP-F-Tractin-P at the IS before addition of low-dose CD. (A2) GFP-F-Tractin-P at the IS of this same cell 4 min after addition of low-dose CD. (A3) Kymograph of GFP-F-Tractin-P in the region corresponding to the yellow line in A2. (A4) Kymograph of GFP-F-Tractin-P in the region corresponding to the red line in A2. The black and orange arrowheads in these two kymographs, as well as those in B4 and C4, mark the time when CD and/or Jas was added and when the LP network began to retract, respectively. (B) Effect of Jas on the organization and dynamics of F-actin at the IS in a Jurkat cell stimulated on a coverslip substrate. (B1) GFP-F-Tractin-P at the IS before addition of Jas. (B2) GFP-F-Tractin-P at the IS in this same cell 4 min after addition of Jas. (B3) GFP-F-Tractin-P at the IS in this same cell 6 min after addition of Jas. The pronounced rings of F-actin that accumulate following Jas addition at the boundary between LP/dSMAC and LM/pSMAC, and at the boundary between the LM/pSMAC and cSMAC, are indicated by the red and green arrowheads, respectively. (B4) Kymograph of GFP-F-Tractin-P in the region corresponding to the yellow line in B2. (C) Effect of CD-Jas on the organization and dynamics of F-actin at the IS in a Jurkat cell stimulated on a coverslip substrate. (C1) GFP-F-Tractin-P at the IS before addition of CD-Jas. (C2) GFP-F-Tractin-P at the IS in this same cell 4 min after addition of CD-Jas. (C3) Merged image between C2 (green) and farnesylated-RFP (red), which marks the plasma membrane. (C4) Kymograph of GFP-F-Tractin-P in the region corresponding to the yellow line in C2. The positions of the LP/dSMAC and LM/pSMAC regions of the IS are indicated by the brackets above A3, A4, B4, and C5. The time scales (in sec) for all of the kymographs shown are indicated on the right. Scale bars in A1, B1, C1 = 5 μm. Scale bars in A3, A4, B3, C4 = 2 μm.

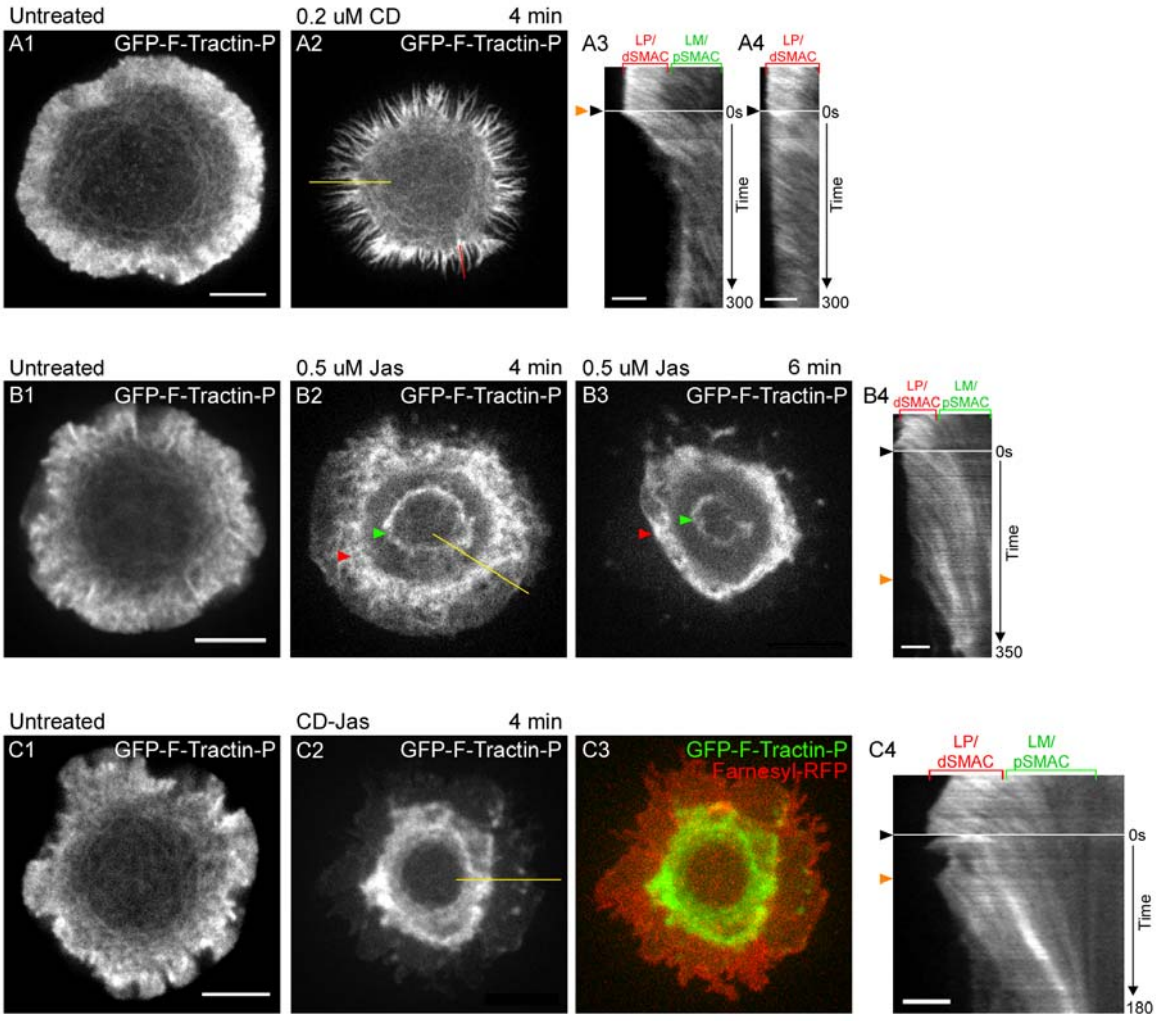
Untreated
A1
GFP-F-Tractin-P
0.2 uM CD
4 min
A2
GFP-F-Tractin-P
A3
LP/ dSMAC
LM/ pSMAC
0s
Time
300
A4
LP/ dSMAC
0s
Time
300
Untreated
B1
GFP-F-Tractin-P
0.5 uM Jas
4 min
B2
GFP-F-Tractin-P
0.5 uM Jas
6 min
B3
GFP-F-Tractin-P
B4
LP/ dSMAC
LM/ pSMAC
0s
Time
350
Untreated
C1
GFP-F-Tractin-P
CD-Jas
4 min
C2
GFP-F-Tractin-P
C3
GFP-F-Tractin-P
Farnesyl-RFP
C4
LP/ dSMAC
LM/ pSMAC
0s
Time
180

caused cells to rapidly round up, making imaging impossible (DNS). Conversely, CD concentrations at or below 0.1 μM had little immediate effect on the cells. At a CD concentration of 0.2 μM, however, a significant fraction of the F-actin network in the LP/dSMAC retracted within 4 min (compare the signals for GFP-F-Tractin-P before treatment with CD [Fig. 11 A1] to that 4 min after CD addition [Fig. 6 A2]). The time course of this effect was rapid, as retraction of actin in the LP/dSMAC began almost immediately after CD addition. This is shown by the kymograph in Fig. 11 A3, which was taken from the region of the LP/dSMAC highlighted by the yellow line in A2 (the time when CD was added Is marked by the black arrowhead, while the time when retraction began is marked by the orange arrowhead). Moreover, the contraction of acto-myosin II arcs in the LM/pSMAC continued uninterrupted for up to 5 min after addition of low-dose CD (see the LM/pSMAC region in the kymograph in Fig. 11 A3). While these observations are reminiscent of the effect of CD on newt lung cells (Ponti *et al.*, 2004), the inhibition of actin retrograde flow in the LP/dSMAC of these CD-treated Jurkat cells was far from complete. Specifically, as portions of the actin network comprising the LP/dSMAC began to retract, a large number of spike-like F-actin-rich structures were left behind (Fig. 11 A2). In addition, the actin in these spikes continued to undergo actin treadmilling, as evidenced by the slopes in the kymograph in Fig. 11 A4, which was taken from the region of the LP/dSMAC highlighted by the red line in A2 that spans one of these F-actin spikes.

We next sought an alternative to CD to inhibit actin retrograde flow in the LP/dSMAC more completely. In the previous study by Ponti *et al*. (Ponti *et al.*, 2004), the addition of 1 μM jasplakinolide (Jas), a cell permeable molecule that stabilizes actin filaments, was shown to block actin retrograde flow in the LP without significantly disrupting myosin II-driven actin flow in the LM. Jas is thought to inhibit actin retrograde flow in the LP by blocking the depolymerization of F-actin on the back side of the LP, leading to the rapid depletion of a pool of G-actin used preferentially to support polymerization at the leading edge (Cramer,

1999; Ponti *et al.*, 2004). As with CD, we initially tested different concentrations of Jas on Jurkat cells expressing mGFP-F-Tractin-P and engaged on coverslips coated with anti-CD3ε antibody. Concentrations of Jas of 1 μM or above caused cells to rapidly round up, making imaging difficult (DNS). The addition of 0.5 μM Jas, however, caused the complete retraction of the actin network in the LP/dSMAC within 6 min (compare the signals for GFP-F-Tractin-P before treatment with Jas [Fig. 11 B1] to that 4 min [Fig. 11 B2] and 6 min [Fig. 11 B3] after addition of Jas). Moreover, the actin arcs in the LM/pSMAC continued to contract inwardly, as evidenced by the slopes in the LM/pSMAC region of the kymograph in Fig. 11 B4, which was taken from the region of the LM/pSMAC highlighted by the yellow line in B2. Additionally, these arcs appeared to accumulate over time in the form of a dense ring of actin at the border between the LM/pSMAC and cSMAC (Fig 11 B2 and B3; see green arrowheads). The appearance of this actin ring presumably reflects the Jas-dependent inhibition in the disassembly of the acto-myosin II arcs at the inner aspect of the LM (Medeiros *et al.*, 2006; Wilson *et al.*, 2010). We note that Jas addition caused the retracting actin network in the LP/dSMAC to also accumulate over time in the form of a broad actin ring at the border between LP/dSMAC and LM/pSMAC (Fig. 11 B2 and B3; see red arrowheads). The appearance of this ring presumably reflects the Jas-dependent inhibition in the large scale depolymerization of LP F-actin that probably occurs at the inner aspect of the LP (Ponti *et al.*, 2004).

While treatment with 0.5 μM Jas was successful in that, given enough time, it resulted in the near complete retraction of the LP actin network, i.e. it did not leave behind the F-actin spikes observed with CD treatment, the time course of the effect was relatively slow. Specifically, while the accumulation of actin arcs near the cSMAC border was nearly complete after 4 min of Jas treatment (see the green arrowhead in Fig. 11 B2), retraction of the actin network in the LP/dSMAC was just beginning at this point in time. This is evident in the kymograph in Fig. 11 B4, where the time of Jas addition and the time when the

retraction of the LP/dSMAC began are marked by black and orange arrowheads, respectively. This delay in the retraction of actin at the leading edge is presumably due to the fact that the mechanism by which Jas inhibits polymerization (monomer starvation) takes time to develop.

Given the results above, we sought to block actin retrograde flow in the LP/dSMAC both rapidly and completely by simultaneously blocking both actin polymerization at the leading edge using 0.2 μM CD and actin depolymerization at the rear of the LP using 0.5 μM Jas (CD-Jas). In Jurkat cells expressing GFP-F-Tractin-P and farnesylated-RFP and engaged on coverslips, addition of CD-Jas caused the entire actin network in the LP/dSMAC to retract within 4 min (compare the signal for GFP-F-Tractin-P before treatment with CD-Jas [Fig. 11 C1] to that 4 min after CD-Jas addition [Fig. 11 C2]). Moreover, this inhibitory effect was rapid, as the actin network in the LP/dSMAC began to retract within 1 min after addition of CD-Jas (compare the time of CD-Jas addition [black arrowhead] to the time when the retraction of the LP/dSMAC began [orange arrowhead] in the kymograph in Fig. 11 C4, which was taken from the region of the LP/dSMAC highlighted by the yellow line in C2). Finally, the inhibitory effect of combined CD-Jas treatment was complete, as residual actin spikes were not observed (Fig. 11 C2). Importantly, using farnesylated-RFP to mark the T cell plasma membrane, we confirmed that CD-Jas treatment caused the LP actin network to pull away from the leading edge membrane (see the spatial separation between the signals for farnesylated-RFP and GFP-F-Tractin-P in Fig. 11 C3). Therefore, the effect of combined CD-Jas treatment in Jurkat cells engaged on coverslips mirrors the classic result seen in giant Aplysia growth cones treated with cytochalasin B, where the actin meshwork in the LP separates and retreats from the leading edge plasma membrane (Forscher and Smith, 1988).

Having established a method to inhibit actin polymerization both rapidly and completely for cells engaged on a coverslip substrate, we next transitioned to engaging cells

on bilayers in order to test the effect of CD-Jas treatment on the inward movement of TCR MCs. As with coverslip-engaged cells, the addition of CD-Jas to bilayer-engaged cells expressing GFP-F-Tractin-P and farnesylated mRFP caused the retraction of the actin network in the LP/dSMAC within 4 min (compare the signals for GFP-F-Tractin-P before treatment with CD-Jas [Fig. 12 A1] to that 4 min after CD-Jas addition [Fig. 12 A2]). This inhibitory effect was rapid, as retraction of the actin network in the LP/dSMAC began within 1 min after addition of CD-Jas (compare the time of Jas addition [black arrowhead] to the time when the retraction of the LP/dSMAC began [orange arrowhead] in the kymograph in Fig. 12 A4, which was taken from the region of the LP/dSMAC highlighted by the yellow line in A2). This inhibitory effect was also complete, as residual actin spikes were not observed after treatment (Fig. 12 A2). In striking contrast to coverslip-engaged cells, however, in bilayer-engaged cells much of their leading edge plasma membrane marked with farnesylated RFP retracted together with the actin network in the LP/dSMAC (Fig. 12 A3). This is presumably due to the lack of opposing friction in the planar bilayer substrate.

Despite the lack of complete separation between the retracting actin network and the leading edge plasma membrane, we proceeded to test the effect of CD-Jas treatment on the dynamics of both actin and TCR MCs within each region of the IS. In the LM/pSMAC, the rate of actin arc contraction was reduced following the addition of CD-Jas by 37%, from 0.037 ± 0.003 μm/sec to 0.023 ± 0.002 μm/sec (Fig. 10 A, compare LM/pSMAC WT Actin to LM/pSMAC CD-Jas Actin; $p < 0.001$). Moreover, the rate of inward TCR MC movement across the LM/pSMAC slowed by 44%, from 0.039 ± 0.006 μm/sec to 0.022 ± 0.002 μm/sec (Fig. 10 A, compare LM/pSMAC WT TCR to LM/pSMAC CD-Jas TCR; $p < 0.001$), matching the reduced rate of actin arc contraction in the LM/pSMAC. The directionality of TCR MC movements in the LM/pSMAC were not affected by Jas-CD treatment, however (Fig. 10 B; $p > 0.05$). We do note that a modest level of “pauses” in TCR MC movements was observed in the LM/pSMAC (Fig. 10 C). This pausing may be due to the large accumulation of F-actin

Figure 12. Inhibition of actin retrograde flow and acto-myosin II arc contraction using combinations of CD, Jas, and BB.

(A) Effect of CD-Jas treatment on the dynamics and distribution of F-actin at the IS of a Jurkat cell stimulated on a planar bilayer. (A1) GFP-F-Tractin-P at the IS of a cell before addition of CD-Jas. (A2) GFP-F-Tractin at the IS of this same cell 4 min after addition of CD-Jas. (A3) Merged image between A2 (green) and farnesylated-RFP (red), which marks the plasma membrane. (A4) Kymograph of the region corresponding to the yellow line in A1 and A2. The black arrowhead indicates the time of CD-Jas addition, while the blue arrowhead indicates the start of actin retraction in the LP/dSMAC. (B) Effect of CD-Jas treatment on F-actin dynamics and distribution and on TCR MC movement at the IS of a Jurkat cell stimulated on a planar bilayer. (B1) GFP-F-Tractin-P at the IS of a cell 4 min after addition of CD-Jas. (B2) TCR MCs at the IS of this same cell 4 min after addition of CD-Jas. The red arrowhead marks the position of a marooned TCR MC. The green arrowhead marks a TCR MC that moved with the retracting actin network. (B3) Merged image between B1 (red) and B2 (green). (B4) Kymograph of GFP-F-Tractin-P in the region corresponding to the yellow line in B3, (B5) kymograph of TCR MCs in the region corresponding to the yellow line in B3, and (B6) merged image between B4 (red) and B5 (green). The red arrowhead in B5 indicates the immobile, marooned TCR MC marked in B2 that was left behind at the IS periphery, while the green arrowhead in B5 indicates the TCR MC marked in B2 that moved with the retracting actin network (see B6 for the overlay). (C) The effect of combined CD-Jas-BB treatment on F-actin dynamics and distribution at the IS of a Jurkat cell stimulated on a planar bilayer. (C1) tdTomato-F-Tractin-P at the IS of a BB-pretreated cell before addition of CD-Jas-BB. (C2) tdTomato-F-Tractin-P at the IS of this same cell 30 sec after addition of CD-Jas-BB. (C3) Kymograph of the region corresponding to the yellow line in C1 and C2. The black arrowhead in C3 indicates the time of CD-Jas-BB addition. The positions of the LP/dSMAC and LM/pSMAC regions of the IS are indicated by the brackets above A4 and C3. The time scales of the kymographs in A3, B4-B6 and C3 are indicated to the right of A4, B6 and C3, respectively. Scale Bars in A1, B1, C1 = 5 μm. Scale bars in A4, B3, C3 = 2 μm.

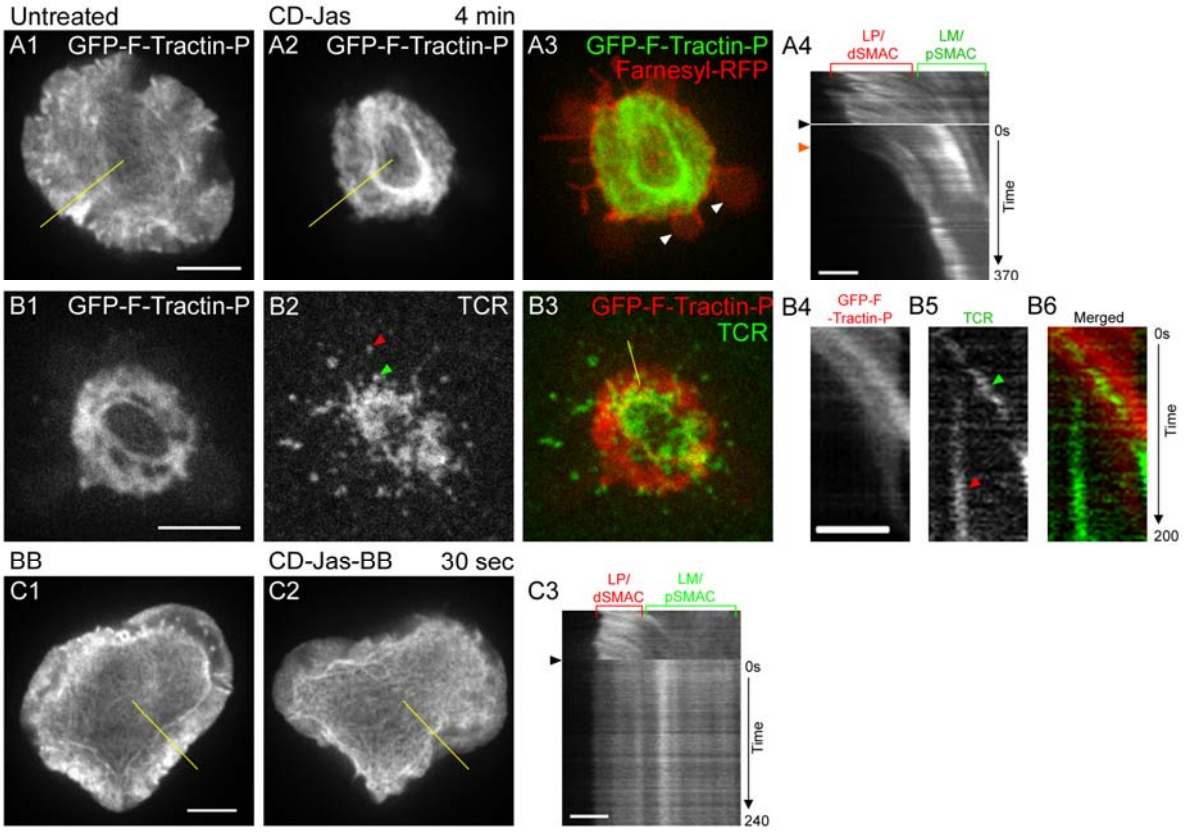
Untreated
CD-Jas
4 min
A1 GFP-F-Tractin-P
A2 GFP-F-Tractin-P
A3 GFP-F-Tractin-P
Farnesyl-RFP
A4
LP/
dSMAC
LM/
pSMAC
0s
Time
370
B1 GFP-F-Tractin-P
B2 TCR
B3 GFP-F-Tractin-P
TCR
B4
GFP-F
-Tractin-P
B5
TCR
B6
Merged
0s
Time
200
BB
CD-Jas-BB
30 sec
C1
C2
C3
LP/
dSMAC
LM/
pSMAC
0s
Time
240

at the boundary between the LM/pSMAC and cSMAC seen with Jas addition, which could create a logjam for TCR MCs passing into the cSMAC.

With regard to the LP/dSMAC following CD-Jas treatment, quantification showed that the rate at which the actin network in this zone retracted (0.023 ± 0.002 μm/sec) corresponds exactly to the reduced speed of acto-myosin II arc contraction in the LM/pSMAC (0.023 ± 0.002 μm/sec) (Fig. 10 A, compare LP/dSMAC CD-Jas Actin to LM/pSMAC CD-Jas Actin: $p > 0.05$). This result is completely consistent with previous results in Aplysia neuron growth cones and sea urchin coelomocytes, where acto-myosin II contraction in the LM was shown to drive the retraction of the LP actin network following the addition of cytochalasin to inhibit actin polymerization at the leading edge (Henson *et al.*, 1999; Medeiros *et al.*, 2006). Most importantly, the speed at which TCR MCs move inward across the LP/dSMAC of CD-Jas treated cells (0.024 ± 0.002 μm/sec) matches precisely the speed of actin network retraction (0.023 ± 0.002 μm/sec) (Fig. 10 A, compare LP/dSMAC CD-Jas TCR to LP/dSMAC CD-Jas Actin and LM/pSMAC CD-Jas Actin; $p > 0.05$). This result is also evident in the kymographs in Fig. 12 B4-B6, which were taken from the region of the LP/dSMAC highlighted by the yellow line in B3. Specifically, the green arrowhead in B5 indicates that the TCR MC marked by the green arrowhead in B2 moved inward in concert with the retracting actin. These results indicate that TCR MCs are tightly coupled to the underlying cortical F-actin network during the retraction process. Moreover, these results argue that the contraction of the acto-myosin II arcs in the LM/pSMAC drives these slow inward movements of TCR MCs when actin polymerization is abrogated. While the directionality of TCR MC movements in the LP/dSMAC were not affected by Jas-CD treatment (Fig. 10 B), a modest increase in “pauses” relative to control cells was observed (Fig. 10 C). These pauses may be due to the accumulation of F-actin at the border between the LP/dSMAC and LM/pSMAC seen with Jas addition, which may create a logjam for TCR MCs passing into the pSMAC.

Finally, while most of the leading edge plasma membrane of bilayer-engaged cells retracted together with the actin network following the addition of CD and Jas (Fig. 12 A3), in a few instances portions of the plasma membrane remained in place as the actin network retreated (see white arrowheads in Fig. 12 A3). In these cases, we observed small populations of marooned TCR MCs that were left behind by the retracting actin network in the LP/dSMAC (Fig. 12 B2; see red arrowhead). These TCR MCs, which appear totally disengaged from the actin network, were completely non-motile, as evidenced by kymographs (Fig. 12 B4-B6; see the red arrowhead). These observations are consistent with previous reports showing that the centripetal transport of TCR MCs is completely blocked by the depolymerization of F-actin using latrunculin (Varma *et al.*, 2006; Kaizuka *et al.*, 2007). Together, the results above are consistent with actin retrograde flow driving the fast (~0.1 μm/sec) movement of TCR MCs in the LP/dSMAC, and myosin II-dependent actin arc contraction driving the slow (~0.03 μm/sec) movement of TCR MCs in the LM/pSMAC.

h. Simultaneous inhibition of both actin retrograde flow and acto-myosin II arc contraction blocks the vast majority of centripetal TCR MC movements at the IS

To confirm that TCR MC movements at the IS are driven largely if not entirely by a combination of two forces- the pushing force of actin polymerization-driven retrograde flow and the pulling force of myosin II-driven actin arc contraction- we sought to inhibit both of these forces simultaneously using combined treatment with 50 μM BB, 0.2 μM CD, and 0.5 μM Jas (BB-CD-Jas). Using bilayer-engaged Jurkat cells expressing tdTomato-F-Tractin-P that had been pre-incubated with BB for 30 min, we found that addition of CD and Jas in the continued presence of BB resulted in the nearly immediate and complete inhibition of actin retrograde flow and actin arc contraction. This overall freezing of F-actin movement throughout the cell is evident in the kymograph of tdTomato-F-Tractin-P in Fig. 12 C3, which was taken from the region of the IS highlighted by the yellow line across the cell in Fig. 12

C1 [Tomato-F-Tractin-P in a BB-pretreated cell before addition of BB-CD-Jas] and Fig. 12 C2 [Tomato-F-Tractin-P in this same BB-pre-treated cell 30 sec after addition of BB-CD-Jas] (the time of addition of BB-CD-Jas is marked by the black arrowhead in C3). Indeed, the rate of retrograde actin flow across the LP/dSMAC in these cells was reduced by 97%, from 0.105 ± 0.006 μm/sec to 0.003 ± 0.002 μm/sec (Fig. 10 A, compare LP/dSMAC WT Actin to LP/dSMAC BB-CD-Jas Actin: $p<0.001$). Similarly, the rate of actin arc contraction across the LM/pSMAC in these cells was reduced by 93%, from 0.037 ± 0.003 μm/sec to 0.003 ± 0.001 μm/sec (Fig. 10 A, compare LM/pSMAC WT Actin to LM/pSMAC BB-CD-Jas Actin; $p< 0.001$). Of note, these effects on actin flow were reversible, as actin polymerization and retrograde flow resumed almost immediately when the three drugs were washed out 5 min after their addition (DNS). Most importantly, consistent with our two-force model for the inward movement of TCR MCs, TCR MC movement across the LP/dSMAC was reduced in BB-CD-Jas treated cells by 97%, from 0.094 ± 0.016 μm/sec to 0.003 ± 0.002 μm/sec (Fig. 10 A, compare LP/dSMAC WT TCR to LP/dSMAC BB-CD-Jas TCR; $p<0.001$), while the inward movement of TCR MCs across the LM/pSMAC was reduced by 94%, from 0.038 ± 0.006 μm/sec to 0.002 ± 0.001 μm/sec (Fig. 10 A, compare LM/pSMAC WT TCR to LM/pSMAC BB-CD-Jas TCR; $p<0.001$). Taken together, these results argue that actin retrograde flow and acto-myosin II arc contraction cooperate to drive the vast majority of centripetal TCR MC transport at the IS.

i. **Acto-myosin II contraction is required for the accumulation of LFA-1 clusters at the inner aspect of the LM/pSMAC**

Finally, we investigated the relationship between the F-actin network and the distribution of LFA-1 clusters at the IS by characterizing in greater detail the apparent spatial overlap (Fig. 4 B1-B6, E1-E6) between these clusters and the acto-myosin II arcs that populate the LM/pSMAC. To report the localization of ligand-bound LFA-1 clusters in the

plasma membrane, Jurkat cells were engaged on planar bilayers containing ICAM-1 tagged with Alexa-546. One min after bilayer engagement, LFA-1 clusters were distributed largely evenly across the LM/pSMAC (Fig. 13 A1 and the corresponding line scan in A2). Separate control experiments performed using Jurkat cells expressing the HC of myosin IIA tagged with GFP confirmed that this distribution of LFA-1 clusters largely overlaps that of the acto-myosin II arcs in the LM/pSMAC (DNS). After 3 min, however, LFA-1 clusters had begun to accumulate near the border between the LM/pSMAC and cSMAC, leading to the formation of a gradient of LFA-1 clusters across the LM/pSMAC (Fig. 13 A3). This gradient is evident in line scans across the IS, which show a progressive increase in the fluorescence intensity of ICAM-1 as one approaches the pSMAC/cSMAC border (Fig. 13 A4). Moreover, after 5 min (Fig. 13 A5), the peak intensity of ICAM-1 signal at the inner aspect of the LM/pSMAC, defined as the innermost 1 μm-wide region of the LM/pSMAC, was ~3-fold higher than the peak intensity of ICAM-1 in this same region after only 1 min of engagement (compare the ICAM-1 signal at the inner aspect of the LM/pSMAC in Fig. 13 A2 [1 min; red arrowheads] with that in Fig. 13 A6 [5 min; green arrowheads]). This is, to our knowledge, the first description of LFA-1 cluster accumulation at the inner aspect of the LM/pSMAC, and it may represent a distinct maturation step in the formation of the adhesion zone between the T cell and the APC.

Finally, we used BB to test the role of acto-myosin II arc contraction in driving the two distinct phases of LFA-1 cluster localization at the IS, i.e. evenly distributed LFA-1 clusters in the LM/pSMAC after 1 min, and accumulation of LFA-1 clusters at the inner aspect of the LM/pSMAC after 5 min. In bilayer-engaged, BB-treated cells, LFA-1 clusters appeared evenly distributed across the LM/pSMAC after 1 min of engagement, similar to WT and DMSO-treated cells (Fig. 13 B1, C1, D1). This result indicates that the early phase of LFA-1 cluster distribution across the LM/pSMAC is independent of myosin II contraction. In contrast, while LFA-1 clusters accumulated at the inner aspect of the LM/pSMAC after 5 min

Figure 13. The effect of myosin II inhibition on the accumulation of LFA-1 clusters at the inner aspect of the LM/pSMAC.

(A) Accumulation of LFA-1 clusters at the inner aspect of the LM/pSMAC in Jurkat cells stimulated on planar bilayers. (A1) Distribution of LFA-1clusters, reported by Alexa-546-labeled ICAM-1 in the bilayer, at the IS of a Jurkat cell 1 min after engagement on a planar bilayer. (A3) LFA-1 clusters in the same cell 3 min after engagement. (A5) LFA-1 clusters in the same cell 5 min after engagement. (A2, A4, A6) Relative intensities of ICAM-1 fluorescence in the line scans (yellow lines) in A1, A3, and A5, respectively. Arrowheads indicate peaks of ICAM-1 fluorescence intensity in A2 (red) and A6 (green). (B-D) Distributions of LFA-1 clusters at the IS of WT, DMSO-, and BB -treated Jurkat cells stimulated on planar bilayers. (B) LFA-1 clusters at the IS of a WT Jurkat cell 1 min (B1) and 5 min (B2) after engagement. (C) LFA-1 clusters at the IS of a DMSO-treated Jurkat cell 1 min (C1) and 5 min (C2) after engagement. (D) LFA-1 clusters at the IS of a BB-treated Jurkat cell 1 min (D1) and 5 min (D2) after engagement. (E) Percent increase in the accumulation of ICAM-1 fluorescence at the inner aspect of the pSMAC (i.e. within the yellow boxed regions in B1-D2) 5 min after bilayer engagement in WT, DMSO-, and BB-treated cells. The numbers of cells used per measurement are indicated inside (or above) the bar. Scale bar in A5 = 5 μm. Scale Bars in B2, C2, D2 = 2 μm.

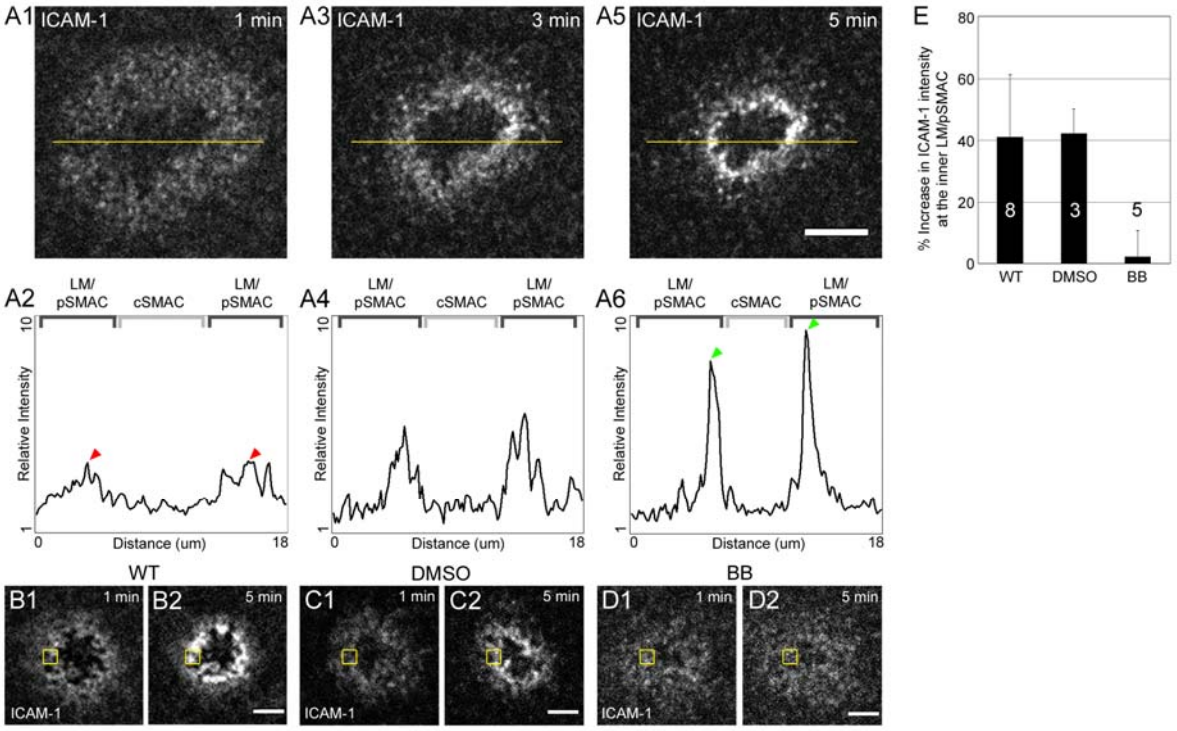

in WT and DMSO-treated cells (Fig. 13 B2 and C2), they did not accumulate at this region in BB-treated cells (Fig. 13 D2). Quantitation of the increase in intensity of ICAM-1 signals within a 1 μm square area at the inner aspect of the pSMAC (boxed regions in Fig. 13 B1, B2, C1, C2, D1, and D2) showed that the average total intensity of ICAM-1 in this region increased from 1 min of engagement to 5 min of engagement by 41 ± 20% in WT cells and by 42 ± 8% in DMSO-treated cells, but by only 2 ± 9% in BB-treated cells (Figure 13 E). Indeed, LFA-1 clusters appeared evenly distributed across the LM/pSMAC of BB-treated cells even after 10 min of engagement (DNS). We conclude, therefore, that while myosin II activity is not required for the early phase of LFA-1 cluster distribution in the LM/pSMAC, it does play an important role in the subsequent accumulation of these clusters at the inner aspect of the LM/pSMAC.

IV. Discussion

Previous studies established that the dSMAC region of the IS corresponds to an actin network characterized by robust actin polymerization-driven retrograde flow, i.e. to a LP. Using F-Tractin-P, a novel reporter for F-actin, we defined for the first time in a clear way the organization of F-actin in the pSMAC region of the IS. Importantly, the actin arcs that populate the pSMAC are endogenous structures, and they undergo myosin II-driven contraction that drives their inward movement. These and other observations clearly define the pSMAC as a LM actin network, as hypothesized by Dustin (Dustin, 2007). Moreover, as in typical crawling cells, we found that the dynamics of F-actin in the LP/dSMAC and LM/pSMAC are both distinct and interdependent. Specifically, the fast (~0.1 μm/sec) pushing force of retrograde actin flow in the LP/dSMAC depends in part on the slower (~0.03 μm/sec) pulling force provided by the contracting acto-myosin II arcs in the LM/pSMAC, and vice versa. Most importantly, we showed that the speeds with which TCR MCs move from the perimeter of the cell inwards to the cSMAC follow very closely the

speeds of actin flow in the LP/dSMAC and LM/pSMAC regions of the IS. Moreover, inhibition of actin flow in these latter two zones individually and in combination showed that the flow of actin in these two zones drives most if not all inward TCR MC movement. Finally, we showed that the normal accumulation of integrin clusters at the inner aspect of the LM/pSMAC requires myosin II-driven actin arc contraction.

a. Correspondence between LP and LM actin networks and the SMAC regions of the IS

Our demonstration that the dSMAC, pSMAC, and cSMAC coincides spatially with the LP, LM, and actin-depleted central zone in bilayer-engaged cells provides strong support for the model proposed by Dustin (Dustin, 2007). Moreover, our observations indicate that the actin cytoskeleton at the IS conforms to the classical model of spatially-distinct, non-overlapping LP and LM actin networks at the leading edge of cells (Henson *et al.*, 1999; Zhang *et al.*, 2003; Medeiros *et al.*, 2006), as opposed to the two-layered model of Sheetz and colleagues (Giannone *et al.*, 2007), where the LP actin network is proposed to overlap with and exist on top of the LM network. Specifically, both endogenous staining and dynamic imaging of actin and myosin II show that the LP and LM actin networks at the Jurkat IS are completely distinct spatially. Moreover, kinetic data shows that the inward movement of TCR MCs in the LP/dSMAC corresponds to the rate of actin retrograde flow and not to a mixture of rates corresponding to actin retrograde flow and acto-myosin II contraction, as would be expected from a two-layered organization of actin in the LP/dSMAC.

Our results using coverslip substrates coated with immobilized anti-CD3ε antibodies also show that the LP and LM actin networks form independently of receptor cluster reorganization at the IS membrane. These and other observations argue strongly that the formation of LP and LM networks is upstream of SMAC formation, and that, once established, actin dynamics in these two networks drive the reorganization of receptors into

the concentric SMAC domains. Indeed, the normal accumulation of LFA-1 clusters near the pSMAC-cSMAC border signifies that the pSMAC is but a snapshot of receptors at the dynamically changing IS membrane whose distribution is driven by a distinct cortical LM network containing contracting acto-myosin II arcs.

b. Novel observation of contracting acto-myosin II arcs in the LM/pSMAC

We imaged for the first time acto-myosin II arcs in the LM/pSMAC region of the IS. These arcs were observed as both endogenous structures and as dynamic structures using tdTomato-F-Tractin-P together with GFP-tagged myosin II constructs. Previous imaging of endogenous F-actin at the IS was not of sufficient resolution to identify specific actin structures within the LM/pSMAC (Sims *et al.*, 2007). Even more importantly, essentially all previous efforts to image F-actin dynamics at the IS utilized GFP-actin (Bunnell *et al.*, 2001; Kaizuka *et al.*, 2007; Yu *et al.*, 2010), which we show here localizes very poorly to these actin arcs. Not surprisingly, therefore, the existence of these actin arcs in the LM/pSMAC was not reported in any previous live-imaging study. That said, close inspection of previously published movies made using GFP-actin (see, for example, SI Movie 2 in (Kaizuka *et al.*, 2007) hint at the endogenous actin arcs described here. Moreover, Yu *et al.* reported that the speed with which GFP-actin speckles move inward slows as the speckles move further from the cell perimeter, consistent with our observations that actin flow is fast in the LP/dSMAC and slow in the LM/pSMAC (Yu *et al.*, 2010). The key advantage here was our use of F-Tractin (Johnson and Schell, 2009), which we think is clearly superior to GFP-actin for imaging actin structures/dynamics in Jurkat T cells. Why GFP-actin does not incorporate efficiently into actin arcs is unclear, but may have to do with the likelihood that formins, which may play an important role in forming the arcs (Tojkander *et al.*, 2011), do not use GFP-actin efficiently (if at all) as a substrate (Wu *et al.*, 2006). Finally, consistent with numerous studies demonstrating that myosin II contraction is the major driving force behind

cortical actin flow in the LM (Lin *et al.*, 1996; Henson *et al.*, 1999; Ponti *et al.*, 2004; Medeiros *et al.*, 2006), we provided multiple lines of evidence that the acto-myosin II arcs reported here are undergoing myosin II-driven contraction. Most importantly, discontinuities in GFP-myosin II fluorescence within arcs get closer together with time, consistent with arc contraction, and BB treatment results in flaccid arcs that move inward in a slow and haphazard fashion due solely to the continued pushing force of actin retrograde flow in the LP.

c. Kinetic coupling between TCR MC movement and cortical actin network flow at the IS

We observed a very strong correspondence between the rates of centripetal actin flow and inward TCR MC movement across both the LP/dSMAC and LM/pSMAC regions of the IS. Moreover, this strong kinetic coupling between cortical actin flow and inward TCR MC movement was maintained after each drug treatment. This strong coupling is in contrast to a previous report using bilayer-engaged Jurkat T cells (Kaizuka *et al.*, 2007), where the rate of inward TCR MC movement at the periphery of the IS was reported to be ~40% the rate of centripetal actin flow. As described in more detail in the Introduction, this and other studies, especially those that have characterized the effects of physical barriers within the bilayer on the rates of TCR MC movement (Hartman and Groves, 2011), have led to a dissipative or frictional coupling model of TCR MC-actin cytoskeleton interaction that allows slippage between the MC and actin flow. While we certainly believe that such slippage would occur if we had employed physical barriers, we think that in the absence of such barriers the coupling between TCR MCs and actin flow is probably quite tight. That said, at least part of the difference between our study and that of Kaizuka and colleagues as regards the kinetic coupling between actin flow and TCR MC movement could be due to possible differences in bilayer conditions between the two studies (e.g. densities of ICAM-1 and anti-

CD3ε antibody, lipid mobility). It is also possible that, in the study by Kaizuka *et al*., the quantitation of actin flow rate was restricted largely to the LP/dSMAC (due to the usage of GFP-tagged actin), while the quantitation of TCR MC movements was made predominately in the LM/pSMAC, leading to the discrepancy between their respective centripetal rates. Obviously, much remains to be learned regarding the components and physical properties of the mechanisms that couple TCR MCs and integrin clusters to cortical actin flow during IS formation.

Our demonstration that TCR MCs exhibit two distinct rates of centripetal movement across the IS can actually be reconciled with a large number of rates reported previously. First, the fast rate (~0.1 μm/sec) across the LP/dSMAC reported here corresponds relatively well with rates at the periphery of the IS reported by several groups (~0.14 μm/sec, (Kaizuka *et al.*, 2007); ~0.15 μm/sec, (Ilani *et al.*, 2009); ~0.09 μm/sec, (Yokosuka *et al.*, 2005)). Moreover, the slow rate (~0.03 μm/sec) across the LM/pSMAC reported here corresponds quite well with rates reported for regions of the IS that are almost certainly inside the LP/dSMAC i.e. to the LM/pSMAC (~0.02 μm/sec, (DeMond *et al.*, 2008); ~0.03 μm/sec, (Varma *et al.*, 2006); ~0.04 μm/sec, (Yokosuka *et al.*, 2005)). Thus, our finding that TCR MCs move at different speeds depending on the region of movement, i.e. the LP/dSMAC versus the LM/pSMAC, helps to reconcile the wide range of speeds reported previously for TCR MC movements at the IS.

d. The role of myosin IIA at the IS

As discussed in the Introduction, the role of myosin IIA in IS formation has been somewhat controversial. Specifically, an earlier study using BB argued that myosin IIA is not required for IS formation (Jacobelli *et al.*, 2004), while a more recent report employing BB and RNAi-mediated knockdown of myosin II argued that the myosin is required for significant TCR MC transport, cSMAC formation, and IS stability (Ilani *et al.*, 2009). Our

study offers a possible bridge between these divergent reports in that myosin II was found to play an important, but not essential, role in IS formation. Specifically, our data shows that actin retrograde flow and acto-myosin II-based flow coordinately drive receptor cluster movements at the IS. Moreover, in the absence of myosin IIA activity, the pushing force of actin retrograde flow in the LP/dSMAC can drive residual cortical actin flow and TCR MC movement across the LM/pSMAC, albeit slowly and with greatly reduced directional persistence. Thus, although the quality and speed of TCR MC movements across the LM/pSMAC are dramatically disrupted in BB-treated cells, the overall bull's eye-patterned IS can still form over time in a significant fraction of myosin II-inhibited T cells. Finally, our demonstration of the dramatic effect that BB has on the organization and dynamics of the actin arcs that populate the LM/pSMAC, as well as the distortion and slow inward displacement of these disorganized, flaccid arcs that occurs as a result of continued actin retrograde flow in the LP/dSMAC of BB-treated cells, provide a mechanistic framework to understand the effects of myosin II inhibition on the motion of TCR MCs during IS formation.

e. Regulation and dynamics of F-actin networks at the IS

Our functional inhibition experiments revealed several important aspects of actin network regulation at the IS. For example, inhibition of acto-myosin II arc contraction slowed actin retrograde flow in the LP/dSMAC, while inhibition of actin retrograde flow slowed acto-myosin II arc contraction in the LM/pSMAC. Such interdependence between pushing and pulling forces in the LP/dSMAC and LM/pSMAC, respectively, have been observed in the LP and LM of numerous cells types (Lin *et al.*, 1996; Henson *et al.*, 1999; Ponti *et al.*, 2004), arguing for a conserved mechanism of cortical F-actin regulation in T cells. Also of note, the appearance of two prominent F-actin rings following the addition of Jas suggests that robust actin depolymerization is occurring at the borders between the LP/dSMAC-LM/pSMAC and the LM/pSMAC-cSMAC. This conclusion is consistent with studies in other cell types

showing that ~90% of LP F-actin depolymerizes at the rear of the LP (Ponti *et al.*, 2004), and that myosin II-dependent contraction leads to actin bundle disassembly at the rear of the LM (Medeiros *et al.*, 2006; Wilson *et al.*, 2010). Finally, we note that the rate of actin retrograde flow at the IS (~0.10 μm/sec) is much faster than in other model cell systems (e.g. ~0.01 μm/sec in PTK1 cells (Ponti *et al.*, 2004)) and ~0.06 μm/sec in neuronal growth cones (Medeiros *et al.*, 2006)). This fact, together with the clear presence of organized, dynamic actin arcs in the LM/pSMAC, suggest that Jurkat T cells, which are easily transfected and amenable to RNAi knockdown, could serve as a robust model system for studying the regulation and dynamics of the actin cytoskeleton, similar to what has been done using *Drosophila* S2 cells (Rogers *et al.*, 2003).

f. Role of microtubules and dynein-based TCR MC transport at the IS

Recently, Saito and colleagues reported that while actin retrograde flow drives the inward movement of TCR MCs at the periphery of the IS (approximately the LP/dSMAC), the minus-end directed microtubule motor dynein drives the inward movement of TCR MCs along microtubules at the inner regions of the IS (approximately the LM/pSMAC and cSMAC) (Hashimoto-Tane *et al.*, 2011). Furthermore, complementary work by the Batista lab showed that dynein associates with the B cell receptor (BCR), and that dynein likewise drives the centripetal movement of BCR MCs at the B cell synapse (Schnyder *et al.*, 2011). These observations are a distinct departure from the widely-held view that the inward flow of cortical F-actin drives the centripetal transport of TCR MCs (Babich and Burkhardt, 2011). Indeed, like previous data using latrunculin to disassemble the actin cytoskeleton (Varma *et al.*, 2006; Kaizuka *et al.*, 2007), our data using combined treatment with CD, Jas and BB to freeze the actin cytoskeleton argues that most if not all inward TCR MC movement is driven by the cortical flow of F-actin. How to reconcile these studies, and how microtubule-dependent TCR MC transport might be coordinated with actin-based transport, particularly

in the LM/pSMAC region of the IS, is at present unclear. For example, given that the inhibition of dynein or microtubule assembly inhibited only those extremely rapid (> 0.4 μm/sec) TCR MC movements that occur during the first 30 sec of TCR MC movement (Hashimoto-Tane *et al.*, 2011), we may have missed many of them. Alternatively, the centripetal movement of TCR MCs in the actin-depleted cSMAC region may be largely dynein-driven, while TCR MC movement in the dSMAC and pSMAC may be driven largely by actin retrograde flow and acto-myosin II arc contraction, respectively. The possibility also exists that dynein-dependent MC movements only occur in the presence of an intact, functioning actin cytoskeleton, although we never witnessed the very rapid movements of MCs described by Saito and colleagues even in untreated cells. More experiments are needed to resolve these complex issues.

g. Conclusion

Overall, our study provides an integrated model of actin-based receptor cluster transport at the IS. Specifically, our results show that coordination between the pushing force of actin retrograde flow in the LP/dSMAC and the pulling force of acto-myosin II arc contraction in the LM/pSMAC drives the centripetal transport of TCR MCs at the IS. Thus, as predicted by Dustin (Dustin, 2007) and confirmed here, the actin cytoskeleton at the IS represents a symmetric version of a migrating cell, where retrograde forces within LP and LM actin networks that serve to move the cell forward are converted into centripetal forces at the IS to move receptor complexes toward the center of the IS. This conservation in cytoskeletal mechanism may be further reflected in our observation that the accumulation of LFA-1 clusters at the inner LM/pSMAC requires acto-myosin II arc contraction, as the contractile force of myosin II links integrin receptors to the extracellular matrix within the LM of migrating cells (Pasapera *et al.*, 2010). Indeed, we think that LFA-1 receptor clusters are probably intimately linked to the acto-myosin II arcs identified here within the LM/pSMAC,

the region where myosin II-driven receptor transport and substrate adhesion are integrated at the IS. The details of these interactions, which occur within the region of active TCR signaling and tightest apposition between the T cell and APC, represent important areas for further investigation.

V. Materials and methods

Cell culture and transfection

E6.1 Jurkat T cells (gift from L. Samelson, NCI, NIH), which were used for all experiments, were maintained at 37^{o}C in IMDM media (Invitrogen, #12440) supplemented with fetal bovine serum (Sigma-Aldrich, #F0392), sodium pyruvate (Invitrogen, #11360), L-glutamine (Invitrogen, #25030), Penicillin-Streptomycin (Invitrogen, #15140), and MEM non-essential amino acids solution (Invitrogen, #11140). Cells were replated every 48 hrs at a concentration of 2.0 x 10^5 cells/ml. Transfections were performed by nucleofection using cells at a concentration of 1.0 x 10^6 cells/ml, 1-3 μg of plasmid DNA, Amaxa Kit V (Lonza-Amaxa), and the electroporation protocol for Jurkat T cells.

Plasmids and reagents

F-Tractin-P (ITPKA-9-52) tagged with mGFP or tdTomato were gifts from M. Schell (Uniformed Services University). The mouse myosin IIA heavy chain and mouse myosin II regulatory light chain constructs tagged with mGFP and mRFP, respectively, as well as the polyclonal antibody against human platelet myosin IIA heavy chain, were gifts from R. S. Adelstein (NHLBI, NIH). The anti-p34-arc antibody was purchased from Upstate Cell Signaling Solutions (#07-227). Alexa-568-conjugated phalloidin, Alexa-488 and Alexa-568-conjugated goat anti-rabbit secondary antibodies, Jasplakinolide (# J7473), and Fluo-4 AM (# F14217) were purchased from Molecular Probes/Invitrogen. Cytochalasin D was purchased from Calbiochem (# 250255). Blebbistatin was purchased from Toronto

Research Chemicals (# B592500). DMSO used to reconstitute inhibitors and as a vehicle control was purchased from Sigma (#472301).

Fixation and staining

Jurkat cells were allowed to adhere to the substrate for 5 min at 37^{o}C and then fixed for 15 min in a solution containing 4% (w/v) paraformaldehyde (Polysciences, Inc., #00380), 1x PBS (pH 7.4) (Quality Biological, Inc., #119-069-101). Samples were then incubated in a blocking solution consisting of 10% fetal bovine serum (Sigma-Aldrich, #F0392), 0.01% sodium azide (Sigma, #S8032), 1x PBS, and 0.2% Saponin (Sigma, #S-7900) for 15 min at room temperature (RT). Following three 5 min washes in 1x PBS, the cells were stained with primary antibody (1:200-500 fold dilution in 1x PBS) for 60 min at RT, followed by secondary antibody (1:1000 fold dilution in 1x PBS) or phalloidin (1: 200 dilution) for 60 min at RT. Following three 5 min washes in PBS, the cells were stored in PBS and imaged immediately.

Planar lipid bilayers and immobilized coverslip substrates

Liposomes were prepared and glass-supported planar lipid bilayers were formed essentially as described previously (Dustin *et al*., 2007). Liposomes were created using a mixture of DOPC (Avanti Polar Lipids, #850375C), biotin-CAP-PE (1% molar ratio) (Avanti Polar Lipids, #180061C), and DOGS-NTA (1% molar ratio) (Avanti Polar Lipids, #790528C) lipids. The anti-CD3ε antibody (Biovest International, # OKT3) was mono-biotinylated and labeled with fluorescent dyes following the protocol of Carrasco *et al*. (Carrasco *et al*,, 2004). A flow chamber was assembled by initially attaching two layers of double-sided tape to the sides of a glass slide. To create a bilayer within the flow cell, a 1.5 µl drop of liposomes was deposited on the glass slide in between the strips of double-stick tape, and then a glass coverslip that has been washed in Piranha solution (70% [v/v] sulfuric acid [Fisher, #A300]

and 30% [v/v] hydrogen peroxide [Fisher, #H325]) was placed on top of the glass slide across the double-stick tape, simultaneously allowing a single planar bilayer to form on the coverslip surface and creating a flow chamber. 200 µl of HEPES buffer saline was then flowed through the chamber to wash away remaining liposomes, followed by 100 µl of a blocking solution containing 5% (w/v) casein (Sigma, #C5890) to block non specific sites. Next, a 1:2 ratio of mono-biotinylated anti-CD3ε antibody labeled with either Alexa-647 or rhodamine-X (10 µg/ml) and streptavidin (Sigma, #85878) were added to the flow chamber to conjugate the anti-CD3ε antibody with the biotin-CAP-PE lipids in the bilayer. Similarly, His-tagged ICAM-1, either unlabeled or labeled with Alexa-647 (0.5 µg/ml), was added to the flow chamber to conjugate with the DOGS-NTA lipids in the bilayer. The uniformity and lateral mobility of lipids in the bilayers was accessed by imaging the diffusion of His-tagged ICAM-1 molecules labeled with Alexa-647 on the surface of the bilayer. Coverslip substrates coated with immobilized antibodies were prepared following the protocol of Bunnell *et al*. (Bunnell *et al*., 2003). Specifically, 8-well cover-glass chamber slides (Labtek, #155411) were washed in a cleaning solution consisting of 1M hydrogen chloride (Mallinckrodt, #H613) and 70% (v/v) ethanol (Warner-Graham Company, #64-175) diluted in ddH_2O. Following three 5 min washes in 1x PBS, each well was then incubated for 30 min at RT in 500 µl of a solution containing 0.01% poly-L-Lysine (Sigma, P8920). After a washing step, each well was then incubated for 30 min at RT in 500 µl of a solution containing 20 µg/µl of anti-CD3ε antibody and 20 µg/µl of anti-CD28 antibody (BD Pharmingen, #555725) diluted in 1x PBS. Wells were used following a washing step.

Image acquisition

Images were acquired using either a 100x (1.40 NA) or 150x (1.45 NA) objective on an Olympus IX81 microscope fitted with a Yokogawa CSU-X1 spinning disk confocal unit and a QuantEM: 512SC camera (Photometrix). Images were analyzed using MetaMorph software.

For dynamic imaging, we loaded cells into a flow chamber containing the planar bilayer, placed the chamber on the microscope stage, identified cells which were well engaged and spread, then began imaging immediately. In general this process took 2 min. All time lapse images were acquired at 4 sec/frame over a duration of 5 min, unless indicated otherwise. For simultaneous imaging of fluorescent molecules in the bilayer and in the cortex of the Jurkat cell, imaging was performed at the plane of the bilayer. For the z-stack imaging of endogenous F-actin structures at the IS, a Prior NanoScan Z stage controller system was used to acquire 2 μm-thick z-sections of phalloidin-stained Jurkat cells engaged on bilayers. Linescans (through z-x axis) across the LP/dSMAC and LM/pSMAC were obtained from the acquired z-stack images using MetaMorph software. For dynamic imaging, the temperature of the stage was maintained at 37^{o}C using a Nevtek stage heater. For imaging of calcium fluxes, Jurkat cells were loaded with Fluo-4 AM as described in the Molecular Probes product information sheet, and stimulated using coverslip substrates. The Prior NanoScan Z stage controller was used to take 4D time-lapse images of these cells before and after contact with stimulatory coverslip substrates. The relative intensities of Fluo-4 fluorescence over time were calculated using the region measurement tool in MetaMorph software. For inhibitor studies using CD and/or Jas, mGFP-F-Tractin-P expressing cells were imaged for 2 min after engagement with the substrate. When 8-well coverslip chambers were used, 0.2 μM CD and/or 0.5 μM Jas were added directly without removal of the chamber from the stage, allowing continuous imaging of the cells. When planar bilayer substrates were used, the flow chamber was removed from the microscope stage and 0.2 μM CD and/or 0.5 μM Jas was rapidly flowed into the chamber. The chamber was then returned to the previous x-y position on the stage to allow imaging of the same cells. These procedures took ~30 sec to complete. For BB studies using bilayer-engaged T cells, 50 μM BB was added to the flow chambers as just described. For these experiments, we did not use the 488 nm laser line, as blue light rapidly inactivates BB, and the inactivation reaction generates harmful free

radicals (Allingham *et al*., 2005). Moreover, to ensure the efficacy of BB, we reconstituted it in the dark, froze it in aliquots at 10 µl, and used only freshly-thawed aliquots once. Jurkat cells were pre-incubated for 30 min in 50 µM BB before imaging. In experiments using BB, CD, and Jas, tdTomato-F-Tractin-P-expressing Jurkat cells were incubated for 30 min in 50 µM BB, added to the planar bilayer flow chamber, and imaged for 2 min on the microscope. The chamber was then removed, 50 µM BB, 0.2 µM CD, and 0.5 µM Jas were flowed into the chamber, and the chamber was returned to the previous x-y position on the stage to allow continuous imaging of the same cells. For imaging of ICAM-1 clusters, we utilized a planar bilayer containing His-ICAM-1 labeled with X-Rhodamine and mono-biotinylated anti-CD3ε antibody labeled with Alexa-647. For measurements of the total intensity levels of Alexa-568-Phalloidin and mGFP-F-Tractin-P in the entire cell volume of Jurkat cells engaged on coverslip substrates, we imaged a 20 µm z-section of the cell using the NanoScan Z stage controller and measured the total integrated intensity through the entire z-stack per acquisition channel per cell using the region measurement tool in MetaMorph software.

Analyses of actin flow and TCR MC movements

The dynamics of cortical F-actin and TCR MCs were measured after engaging Jurkat T cells with the planar bilayer by simultaneous imaging of mGFP-F-Tractin-P and the anti-CD3ε antibody OKT3 labeled with X-rhodamine, using spinning disk confocal microscopy. For experiments with BB, we used mono-biotinylated anti-CD3ε antibody conjugated to Alexa-647 and Jurkat cells expressing tdTomato-F-Tractin-P to avoid imaging using blue light. For kymograph analyses of centripetal F-actin flow, the IS was separated into four quadrants and a line was drawn from the distal edge to the cell center in each quadrant using MetaMorph software. Each kymograph was made using a 2x2 line width (pixels). Four measurements of F-actin flow rate, each generated by measuring the steepness of the

slopes using the kymograph analysis tool in MetaMorph, were made in the LP/dSMAC and LM/pSMAC regions within all four quadrants of the kymograph. The LP/dSMAC and LM/pSMAC regions were demarcated by the abrupt change in the slope of F-actin flow that was invariably observed between these two regions. In low-dose CD- and Jas-treated cell, where the slopes of F-actin flow in the LP/dSMAC and LM/pSMAC regions were indistinguishable, the movement of F-actin before the addition of drugs was tracked in time-lapse images to define the LP/dSMAC and LM/pSMAC regions so as to mark their positions after drug addition. In BB-treated cells, where the kymograph of F-actin flow in the LM/pSMAC often contained positive, negative and vertical slopes (signifying inward, backward, and paused movements, respectively), only the positive slopes in the kymograph were included in the measurements. In all experiments, the rates of centripetal F-actin flow determined in all four quadrants of the cell were then averaged for the LP/dSMAC region and for the LM/pSMAC region to give a single value of centripetal F-actin flow rate for each region within a single cell. The means and standard deviations of F-actin flow rate per region were then calculated by averaging the single-cell values of all cells measured using Microsoft Excel software. For analysis of TCR MC dynamics, the frame-to-frame movement of every visible TCR MC in each cell was tracked using the particle tracking application in MetaMorph software. The acquired images of TCR MCs and F-Tractin-P were merged to allow identification of TCR MC movements relative to the LP/dSMAC and LM/pSMAC regions of the IS. The instantaneous speeds of all TCR MCs were averaged per region to calculate the rate of TCR MC movement within the LP/dSMAC and LM/pSMAC regions in a single cell. Instantaneous values of 0 were excluded from the calculation of TCR MC rates. The means and standard deviations of TCR MC movements per region were calculated by averaging the single-cell values of all cells measured using Excel software. The particle tracking data was also used to calculate the meandering index (net displacement/ total

distance traveled) of TCR MC paths per region. The net displacement of each TCR MC path was calculated using the following formula:

$$\textit{Net displacement} = \textit{square root } [(X \textit{ initial} - X \textit{ final})^2 + (Y \textit{ initial} - Y \textit{ final})^2]$$

The total distance traveled was calculated by summing the distance between the frame-to-frame movements of all movements in each TCR MC path per IS region. Net displacement was divided by the total distance traveled to give the meandering index per TCR MC path, and the meandering index values of all TCR MC paths per region were averaged to give the meandering index values of TCR MC paths within the LP/dSMAC and LM/pSMAC regions in a single cell. The means and standard deviations of meandering index values per region were calculated by averaging the single-cell values of all cells measured using Excel software. For the analysis of TCR MC pausing data, the instantaneous speeds of all TCR MC movements in all cells were collected per region. We then binned the instantaneous speed values into two categories, 0 and greater than 0, and counted the number of values in each bin. Each bin count was divided by the total number of instantaneous speed values to give the percent of TCR MC movements at 0 or greater than 0 per region. For the visualization TCR MC paths, we used the x-y position information from the particle tracking data to graph the TCR MC paths per region using SigmaPlot 11.0. For all statistical analyses, P values above 0.05 were considered to be not significantly different.

VI. Acknowledgments

We would like to thank Michael Schell for F-Tractin-P plasmids and input regarding actin reporters, Robert Adelstein and Mary Anne Conti for myosin IIA constructs and antibodies, Jose Martina for help with cell culture and transfection protocols, Rajat Varma for generous help with bilayers, advice on T cells, and comments on the manuscript, Jim Sellers for advice on the proper use and handling of BB, and Lawrence Samelson for the E6.1 Jurkat cell line. We also wish to thank Alison Zajac, Jack Chen, and Estaban Toro, who

performed several preliminary experiments related to this study during the 2009 Physiology course at the Marine Biological Laboratory in Woods Hole, MA.

VII. References

Aizawa, H., Sameshima, M., and Yahara, I. (1997). A green fluorescent protein-actin fusion protein dominantly inhibits cytokinesis, cell spreading, and locomotion in Dictyostelium. Cell Struct Funct *22*, 335-345.

Allingham, J.S., Smith, R., and Rayment, I. (2005). The structural basis of blebbistatin inhibition and specificity for myosin II. Nat Struct Mol Biol *12*, 378-379.

Babich, A., and Burkhardt, J.K. (2011). Lymphocyte signaling converges on microtubules. Immunity *34*, 825-827.

Billadeau, D.D., Nolz, J.C., and Gomez, T.S. (2007). Regulation of T-cell activation by the cytoskeleton. Nat Rev Immunol *7*, 131-143.

Bunnell, S.C., Kapoor, V., Trible, R.P., Zhang, W., and Samelson, L.E. (2001). Dynamic actin polymerization drives T cell receptor-induced spreading: a role for the signal transduction adaptor LAT. Immunity *14*, 315-329.

Campi, G., Varma, R., and Dustin, M.L. (2005). Actin and agonist MHC-peptide complex-dependent T cell receptor microclusters as scaffolds for signaling. J Exp Med *202*, 1031-1036.

Carlier, M.F., Criquet, P., Pantaloni, D., and Korn, E.D. (1986). Interaction of cytochalasin D with actin filaments in the presence of ADP and ATP. J Biol Chem *261*, 2041-2050.

Cramer, L.P. (1999). Role of actin-filament disassembly in lamellipodium protrusion in motile cells revealed using the drug jasplakinolide. Curr Biol *9*, 1095-1105.

DeMond, A.L., Mossman, K.D., Starr, T., Dustin, M.L., and Groves, J.T. (2008). T cell receptor microcluster transport through molecular mazes reveals mechanism of translocation. Biophys J *94*, 3286-3292.

Doyle, T., and Botstein, D. (1996). Movement of yeast cortical actin cytoskeleton visualized in vivo. Proc Natl Acad Sci U S A *93*, 3886-3891.

Dustin, M.L. (2007). Cell adhesion molecules and actin cytoskeleton at immune synapses and kinapses. Curr Opin Cell Biol *19*, 529-533.

Dustin, M.L. (2009). Supported bilayers at the vanguard of immune cell activation studies. J Struct Biol *168*, 152-160.

Fooksman, D.R., Vardhana, S., Vasiliver-Shamis, G., Liese, J., Blair, D.A., Waite, J., Sacristan, C., Victora, G.D., Zanin-Zhorov, A., and Dustin, M.L. (2010). Functional anatomy of T cell activation and synapse formation. Annu Rev Immunol *28*, 79-105.

Forscher, P., and Smith, S.J. (1988). Actions of cytochalasins on the organization of actin filaments and microtubules in a neuronal growth cone. J Cell Biol *107*, 1505-1516.

Freiberg, B.A., Kupfer, H., Maslanik, W., Delli, J., Kappler, J., Zaller, D.M., and Kupfer, A. (2002). Staging and resetting T cell activation in SMACs. Nat Immunol *3*, 911-917.

Gardel, M.L., Schneider, I.C., Aratyn-Schaus, Y., and Waterman, C.M. (2010). Mechanical integration of actin and adhesion dynamics in cell migration. Annu Rev Cell Dev Biol *26*, 315-333.

Giannone, G., Dubin-Thaler, B.J., Rossier, O., Cai, Y., Chaga, O., Jiang, G., Beaver, W., Dobereiner, H.G., Freund, Y., Borisy, G., and Sheetz, M.P. (2007). Lamellipodial actin mechanically links myosin activity with adhesion-site formation. Cell *128*, 561-575.

Grakoui, A., Bromley, S.K., Sumen, C., Davis, M.M., Shaw, A.S., Allen, P.M., and Dustin, M.L. (1999). The immunological synapse: a molecular machine controlling T cell activation. Science *285*, 221-227.

Gupton, S.L., and Waterman-Storer, C.M. (2006). Spatiotemporal feedback between actomyosin and focal-adhesion systems optimizes rapid cell migration. Cell *125*, 1361-1374.

Hartman, N.C., and Groves, J.T. (2011). Signaling clusters in the cell membrane. Curr Opin Cell Biol *23*, 370-376.

Hartman, N.C., Nye, J.A., and Groves, J.T. (2009). Cluster size regulates protein sorting in the immunological synapse. Proc Natl Acad Sci U S A *106*, 12729-12734.

Hashimoto-Tane, A., Yokosuka, T., Sakata-Sogawa, K., Sakuma, M., Ishihara, C., Tokunaga, M., and Saito, T. (2011). Dynein-driven transport of T cell receptor microclusters regulates immune synapse formation and T cell activation. Immunity *34*, 919-931.

Henson, J.H., Svitkina, T.M., Burns, A.R., Hughes, H.E., MacPartland, K.J., Nazarian, R., and Borisy, G.G. (1999). Two components of actin-based retrograde flow in sea urchin coelomocytes. Mol Biol Cell *10*, 4075-4090.

Ilani, T., Vasiliver-Shamis, G., Vardhana, S., Bretscher, A., and Dustin, M.L. (2009). T cell antigen receptor signaling and immunological synapse stability require myosin IIA. Nat Immunol *10*, 531-539.

Jacobelli, J., Chmura, S.A., Buxton, D.B., Davis, M.M., and Krummel, M.F. (2004). A single class II myosin modulates T cell motility and stopping, but not synapse formation. Nat Immunol *5*, 531-538.

Johnson, H.W., and Schell, M.J. (2009). Neuronal IP3 3-kinase is an F-actin-bundling protein: role in dendritic targeting and regulation of spine morphology. Mol Biol Cell *20*, 5166-5180.

Kaizuka, Y., Douglass, A.D., Varma, R., Dustin, M.L., and Vale, R.D. (2007). Mechanisms for segregating T cell receptor and adhesion molecules during immunological synapse formation in Jurkat T cells. Proc Natl Acad Sci U S A *104*, 20296-20301.

Lin, C.H., Espreafico, E.M., Mooseker, M.S., and Forscher, P. (1996). Myosin drives retrograde F-actin flow in neuronal growth cones. Neuron *16*, 769-782.

Medeiros, N.A., Burnette, D.T., and Forscher, P. (2006). Myosin II functions in actin-bundle turnover in neuronal growth cones. Nat Cell Biol *8*, 215-226.

Monks, C.R., Freiberg, B.A., Kupfer, H., Sciaky, N., and Kupfer, A. (1998). Three-dimensional segregation of supramolecular activation clusters in T cells. Nature *395*, 82-86.

Nguyen, K., Sylvain, N.R., and Bunnell, S.C. (2008). T cell costimulation via the integrin VLA-4 inhibits the actin-dependent centralization of signaling microclusters containing the adaptor SLP-76. Immunity *28*, 810-821.

Pasapera, A.M., Schneider, I.C., Rericha, E., Schlaepfer, D.D., and Waterman, C.M. (2010). Myosin II activity regulates vinculin recruitment to focal adhesions through FAK-mediated paxillin phosphorylation. J Cell Biol *188*, 877-890.

Pollard, T.D., and Borisy, G.G. (2003). Cellular motility driven by assembly and disassembly of actin filaments. Cell *112*, 453-465.

Ponti, A., Machacek, M., Gupton, S.L., Waterman-Storer, C.M., and Danuser, G. (2004). Two distinct actin networks drive the protrusion of migrating cells. Science *305*, 1782-1786.

Rogers, S.L., Wiedemann, U., Stuurman, N., and Vale, R.D. (2003). Molecular requirements for actin-based lamella formation in Drosophila S2 cells. J Cell Biol *162*, 1079-1088.

Sakamoto, T., Limouze, J., Combs, C.A., Straight, A.F., and Sellers, J.R. (2005). Blebbistatin, a myosin II inhibitor, is photoinactivated by blue light. Biochemistry *44*, 584-588.

Schnyder, T., Castello, A., Feest, C., Harwood, N.E., Oellerich, T., Urlaub, H., Engelke, M., Wienands, J., Bruckbauer, A., and Batista, F.D. (2011). B cell receptor-mediated antigen gathering requires ubiquitin ligase Cbl and adaptors Grb2 and Dok-3 to recruit dynein to the signaling microcluster. Immunity *34*, 905-918.

Sims, T.N., Soos, T.J., Xenias, H.S., Dubin-Thaler, B., Hofman, J.M., Waite, J.C., Cameron, T.O., Thomas, V.K., Varma, R., Wiggins, C.H., Sheetz, M.P., Littman, D.R., and Dustin, M.L. (2007). Opposing effects of PKCtheta and WASp on symmetry breaking and relocation of the immunological synapse. Cell *129*, 773-785.

Tojkander, S., Gateva, G., Schevzov, G., Hotulainen, P., Naumanen, P., Martin, C., Gunning, P.W., and Lappalainen, P. (2011). A molecular pathway for myosin II recruitment to stress fibers. Curr Biol *21*, 539-550.

Vardhana, S., Choudhuri, K., Varma, R., and Dustin, M.L. (2010). Essential role of ubiquitin and TSG101 protein in formation and function of the central supramolecular activation cluster. Immunity *32*, 531-540.

Varma, R., Campi, G., Yokosuka, T., Saito, T., and Dustin, M.L. (2006). T cell receptor-proximal signals are sustained in peripheral microclusters and terminated in the central supramolecular activation cluster. Immunity *25*, 117-127.

Vicente-Manzanares, M., Ma, X., Adelstein, R.S., and Horwitz, A.R. (2009). Non-muscle myosin II takes centre stage in cell adhesion and migration. Nat Rev Mol Cell Biol *10*, 778-790.

Wagner, W., Brenowitz, S.D., and Hammer, J.A., 3rd. (2011). Myosin-Va transports the endoplasmic reticulum into the dendritic spines of Purkinje neurons. Nat Cell Biol *13*, 40-48.

Westphal, M., Jungbluth, A., Heidecker, M., Muhlbauer, B., Heizer, C., Schwartz, J.M., Marriott, G., and Gerisch, G. (1997). Microfilament dynamics during cell movement and chemotaxis monitored using a GFP-actin fusion protein. Curr Biol *7*, 176-183.

Wilson, C.A., Tsuchida, M.A., Allen, G.M., Barnhart, E.L., Applegate, K.T., Yam, P.T., Ji, L., Keren, K., Danuser, G., and Theriot, J.A. (2010). Myosin II contributes to cell-scale actin network treadmilling through network disassembly. Nature *465*, 373-377.

Wu, J.Q., and Pollard, T.D. (2005). Counting cytokinesis proteins globally and locally in fission yeast. Science *310*, 310-314.

Wu, J.Q., Sirotkin, V., Kovar, D.R., Lord, M., Beltzner, C.C., Kuhn, J.R., and Pollard, T.D. (2006). Assembly of the cytokinetic contractile ring from a broad band of nodes in fission yeast. J Cell Biol *174*, 391-402.

Yokosuka, T., Sakata-Sogawa, K., Kobayashi, W., Hiroshima, M., Hashimoto-Tane, A., Tokunaga, M., Dustin, M.L., and Saito, T. (2005). Newly generated T cell receptor microclusters initiate and sustain T cell activation by recruitment of Zap70 and SLP-76. Nat Immunol *6*, 1253-1262.

Yu, C.H., Wu, H.J., Kaizuka, Y., Vale, R.D., and Groves, J.T. (2010). Altered actin centripetal retrograde flow in physically restricted immunological synapses. PLoS One *5*, e11878.

Zhang, X.F., Schaefer, A.W., Burnette, D.T., Schoonderwoert, V.T., and Forscher, P. (2003). Rho-dependent contractile responses in the neuronal growth cone are independent of classical peripheral retrograde actin flow. Neuron *40*, 931-944.

CHAPTER 3

CORTICAL FORCE GENERATION BY DYNEIN AND LIS1 DRIVES THE BI-PHASIC REPOSITIONING OF THE MTOC IN T CELLS

I. Abstract

Upon engagement of APCs, T cells undergo rapid MTOC polarization to position their secretory apparatus at the immunological synapse for directed effector function. Due to the lack of spatial and temporal control in most previous studies, the kinetics of MTOC repositioning have not been well characterized in T cells. In addition, the specific roles of dynein and dynein regulatory proteins during T cell activation have not been defined. In this study, we show using a novel laser trap-controlled T cell activation method that TCR and LFA-1 signaling are both required for robust MTOC repositioning. This repositioning process is bi-phasic, characterized by fast MTOC movement during the first polarization phase, and slow MTOC movement during the second docking phase. Moreover, we report evidence of apparent strong cortical force generation at the immunological synapse when the MTOC movement is impeded, as the synaptic membranes of both the T cell and the APC become dramatically invaginated toward the MTOC. Lastly, inhibition experiments using dominant negative constructs show that dynein and LIS1 are required for rapid and persistent MTOC movement during the polarization phase, and for initiation and maintenance of the docking phase of MTOC repositioning. In conclusion, cortical force generation by dynein and LIS1 drives the bi-phasic repositioning of the MTOC during T cell activation.

II. Introduction

T cell recognition of stimulatory antigen occurs in densely populated lymphoid regions of the body, requiring directed secretion of effector molecules to specified APCs. In the case of targeted cell killing by CTLs, an organized structure called the IS forms at the contact site between the CTL and target cell, to mediate directed secretion of lytic components (Stinchcombe *et al.*, 2006). Specifically, the centrosome repositions toward and makes contact with the membrane of the IS, allowing localized delivery of lytic granules to the site of contact with the target cell (Stinchcombe and Griffiths, 2007). These granules undergo minus-end directed movement toward the centrosome and fuse with the IS membrane to release their lytic contents for targeted cell killing (Stinchcombe and Griffiths, 2007). In addition to directed secretion, centrosome repositioning is required for sustained TCR signaling, maturation of the IS, and asymmetric cell division after T cell activation (Chang *et al.*, 2007; Martin-Cofreces *et al.*, 2008), indicating that the regulation of MT cytoskeleton polarization is important for multiple aspects of T cell function.

While MTOC repositioning is known to be dependent on TCR engagement, the downstream signaling pathways leading to repositioning are poorly understood. Molecules involved in early TCR signaling, including Lck, ZAP70, LAT, SLP76, and VAV1, are required for MTOC polarization in T cells (Sancho *et al.*, 2002; Kuhne *et al.*, 2003). Studies also show that TCR-proximal events, including calcium flux, are involved in MTOC repositioning (Kuhne *et al.*, 2003). However, the cascade of TCR-proximal events leading to MTOC repositioning is unclear, as M. Huse and colleagues reported using a photoactivateable pMHC ligand system that DAG, but not calcium flux, is required for MTOC repositioning in T cells (Quann *et al.*, 2009). In their signaling model, PLCγ1-directed cleavage of PIP_2 produces DAG, which then signals through atypical PKCs to recruit the cortical force generator to the IS (Quann *et al.*, 2011).

Studies have also pointed to the involvement of cytoplasmic dynein in the MTOC repositioning process. Dynein is localized to the IS after TCR engagement, and inhibition studies using siRNA knockdown and overexpression of dominant negative (DN) constructs show that dynein is required for MTOC repositioning in T cells (Combs *et al.*, 2006; Martin-Cofreces *et al.*, 2008). Moreover, the important role of cytoplasmic dynein in centrosome repositioning has been established in other cell systems, as inhibition of dynein causes displacement of the centrosome from the cell center in interphase cells and wounded fibroblasts (Burakov *et al.*, 2003; Gomes *et al.*, 2005), and from the leading process in migrating neural progenitor cells (Tsai *et al.*, 2007). Additionally, minus end-directed MT pulling by cortically-bound dynein is known to drive spindle movements during asymmetric cell division in *C. Elegans* and budding yeast (Adames and Cooper, 2000; Gundersen, 2002). In light of these results, dynein has been implicated as the cortical force generator in T cells (Kuhn and Poenie, 2002; Combs *et al.*, 2006). Specifically, cortically anchored dynein, localized at an outer SMAC region, has been proposed to capture and pull MTs, causing MT sliding and net MTOC polarization to the IS (Combs *et al.*, 2006). However, the precise localization of dynein at the IS, the regulation of dynein activity, and the dynamics of MTOC repositioning are not yet known in T cells.

The lack of information regarding MTOC repositioning in T cells is due to the difficulty of imaging the activation process in T cell-APC conjugates. Polarization of the MTOC is rapid, as it becomes positioned at the contact site within 2-3 min after APC engagement (Kuhn and Poenie, 2002). Moreover, without temporal and spatial control over the engagement of T cells and APCs, it is difficult to image full MTOC repositioning events consistently and dynamically. In this study we developed an optical trap system for T cell activation, by using the optical trap to guide APCs to a position opposite the location of the centrosome in T cells. Utilizing this approach, we were able to consistently induce MTOC repositioning in APC-engaged T cells, and define the relative contributions of TCR and

LFA-1 signaling to MTOC repositioning. Also, our imaging studies showed that the MTOC repositioning event is biphasic, and that the transition between the two phases occurs consistently when the MTOC gets ~2 μm from the IS. Moreover, striking evidence of apparent strong cortical force generation was observed when MTOC movements were impeded, as the T cell and APC synaptic membranes became dramatically invaginated toward the T cell's centrosome in these conjugates. Using the planar bilayer engagement of T cells to image the IS, we observed spots of dynein recruited to and transiently bound at the IS, without preferential localization to a specific SMAC region. Lastly, inhibition studies, using DN constructs in T cell-APC conjugates, showed that both dynein and LIS1 were required for the rapid and persistent movement of the centrosome during the first polarization phase, and for initiation and maintenance of the second docking phase of MTOC repositioning. Overall, our results show that the MTOC repositioning process occurs in distinct kinetic steps, and that dynein and LIS1 mediate the cortical force generation required for MTOC repositioning in T cells.

III. Results

a. Optical trap-controlled activation induces robust MTOC repositioning in Jurkat T cells

A number of experiments have assayed MTOC repositioning in T cells. The general strategy has been to mix T cells with stimulatory agents, either anti-TCR antibody-coated latex beads or antigen presenting cells, forming activated T cell conjugates (Stowers *et al.*, 1995; Sedwick *et al.*, 1999; Kuhn and Poenie, 2002; Combs *et al.*, 2006; Gomez *et al.*, 2007). These conjugates are then plated, fixed, and stained for the centrosome. However, without spatial and temporal control, these studies lacked dynamic information about the MTOC repositioning process in T cells. Also, due to the random point of contact between the T cell and the stimulatory agent, their data suffered from a high level of "background"

Figure 14. T cell activation and MTOC repositioning induced by the optical trap system of T cell engagement.

(A) Illustration of the optical trap system. (A1) Optical trap (yellow cones) is focused on the SEE-coated Raji B cell (light gray) to engage the Jurkat T cell (dark gray). (A2) Conjugation of the SEE-coated Raji B cell opposite the position of the MTOC (green dots) induces MTOC repositioning to the contact site. (B1) Time lapse images of Flou-4 AM in a Jurkat cell engaged by SEE-coated Raji B cell using the optical trap system. (B2) Transmitted time lapse images of a Jurkat cell engaged by SEE-coated Raji B cell using the optical trap system. (C1) Time lapse images of Flou-4 AM in a Jurkat cell engaged by an uncoated Raji B cell using the optical trap system. (C2) Time lapse images of Flou-4 AM in a Jurkat cell engaged by an uncoated Raji B cell using the optical trap system. (B3, C3) Graphs showing Flou-4 relative intensity levels over time. (D) Merged time lapse images of a GFP-Cen-2 expressing Jurkat cell engaged by a SEE-coated Raji B cell using the optical trap system. All scale bars = 10 μm.

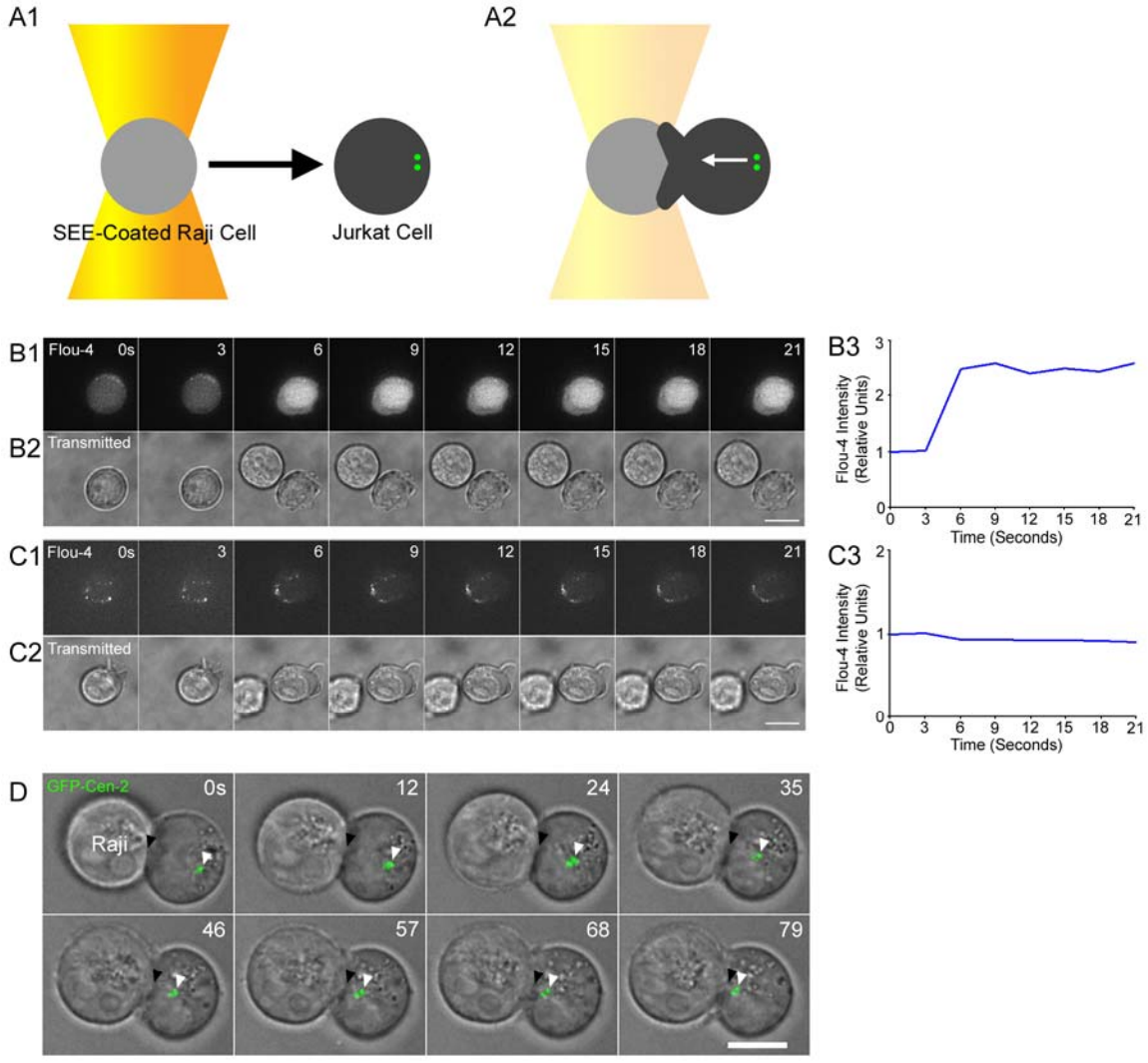

MTOC polarization ("background" polarization referring to ~30% MTOC repositioning levels reported in negative control experiments due to the MTOC being positioned near the site of contact before TCR engagement), and were not useful for detecting partial defects in MTOC repositioning. While a photoactivation system has recently been developed by M. Huse and colleagues to overcome these issues, and has provided important information about the signaling pathways leading to dynein accumulation and MTOC repositioning, it utilized a coverslip substrate coated with immobilized pMHC which does not allow rearrangement of membrane receptors to form a mature IS (Huse *et al.*, 2007; Quann *et al.*, 2009; Quann *et al.*, 2011). Therefore, we sought to study MTOC repositioning in T cell-APC conjugates by using an optical trap to guide an APC to a coverslip-bound T cell, allowing imaging directly after APC engagement, and precise conjugation of the APC opposite the position of the centrosome (Fig. 14 A1 and A2). Staphylococcal Enterotoxin E (SEE)-coated Raji B cells were used to stimulate the Jurkat T cells, and transient expression of GFP- or RFP-tagged centrin-2 (cen-2) was used to dynamically image the MTOC.

The optical trap-controlled method proved to be effective at triggering activation of TCR signaling and MTOC repositioning in engaged Jurkat T cells. Calcium flux, imaged using the Flou-4AM probe, was observed in the Jurkat T cell after contact with the optical trap-controlled Raji cell coated with SEE (+SEE Raji), showing that TCR signaling is induced by the optical trap method of T cell engagement (Fig. 14 B). On the other hand, calcium flux was not observed after contact with uncoated Raji cells (-SEE Raji), showing that T cell activation requires SEE stimulation in our system (Fig. 14 C). Importantly, rapid MTOC repositioning was induced in the Jurkat cell after conjugation to a +SEE Raji cell, as we observed the centrosome (marked by GFP-Cen-2) translocating across the entire diameter of the cell (~6 μm) within 2 min (Fig. 1 D). This induced MTOC repositioning was robust, as ~75% of Jurkat cells fully repositioned their MTOC after +SEE Raji engagement (see 'WT +SEE' in Fig. 15 B). In addition, "background" MTOC repositioning was avoided, as very

few MTOC repositioning events were observed in LAT signaling-deficient Jurkat T cells (JCAM2.5) (5% “Full” repositioning; see ‘JCAM2.5 +SEE’ in Fig. 15 B). We note that the optical trap itself did not induce T cell activation, as calcium flux and MTOC polarization were not observed in Jurkat T cells irradiated with the infrared laser alone (data not shown [DNS]). Overall, these results show that the optical trap system provides a robust method for inducing MTOC repositioning in T cells.

b. TCR and LFA-1 signaling are both required for robust MTOC repositioning

Having established a method for inducing MTOC repositioning with high spatial and temporal control in Jurkat T cells, we sought to test the contribution of TCR and LFA-1 signaling pathways to MTOC repositioning. While it is known that key TCR signaling components are required for MTOC repositioning, conflicting results have been reported regarding the role of LFA-1. An early study using fixed T cell-APC conjugates showed a partial defect in MTOC repositioning in LFA-1α-deficient Jurkat cells (JB2.7) (Kuhn *et al.*, 2001). Furthermore, immunostaining experiments by Kuhn *et al*. suggested that LFA-1 clusters may be involved in the anchoring of the cortical force generator and MTs at the IS (Kuhn and Poenie, 2002). In contrast, a later study also using the JB2.1 Jurkat cell line reported no defects in MTOC repositioning (Combs *et al.*, 2006). We suspected that high “background” levels of MTOC repositioning made it difficult to distinguish partial defects in these studies, and therefore, we decided to assay MTOC repositioning in wild type (WT; E6.1) and JB2.1 cells using the optical trap system.

First, we sought to categorize repositioning events after engagement of Jurkat cells with optical trap-controlled Raji B cells. For the purpose of the MTOC repositioning assay, translocation of the MTOC to a position < 2 um distance from the plane of contact was scored as ‘Full Repositioning’, between 2 – 4 um distance from the plane of contact was scored as ‘Partial Repositioning’, and > 4 um distance from the plane of contact was scored

Figure 15. Contribution of TCR and LFA-1 signaling pathways to MTOC repositioning.

(A) Illustration of the scoring system used to assay repositioning events in conjugates formed between a Jurkat T cell (blue) and a SEE-coated Raji B cell (light brown) using the optical trap system. (B) Percentage of repositioning events in WT, JCAM2.5 and JB2.7 Jurkat cells conjugated to Raji B cells coated with or without SEE using the optical trap system.

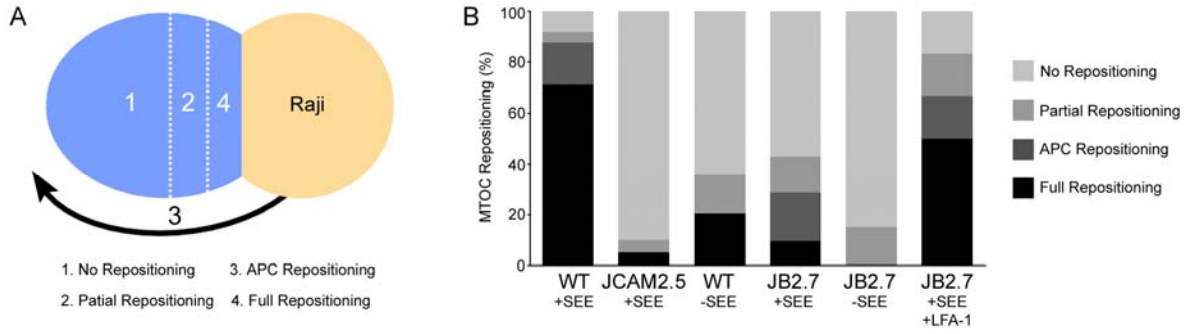

as ‘No Repositioning’ (Fig. 15 A). In addition to these MTOC repositioning events, we sometimes observed repositioning of the Raji B cell to the location of the MTOC, which we scored as ‘APC Repositioning’ (Fig. 15 A). Since the molecular machinery generating the pulling forces are anchored at the synapse, obstruction of MTOC movement can lead to a tug-of-war between the MTOC and the synaptic interface, at times resulting in APC movement toward the centrosome. In this regard, ‘APC Repositioning’ can be considered equivalent to ‘Full Repositioning.’

To confirm the role of TCR signaling in MTOC repositioning, we engaged WT Jurkat cells with +SEE and -SEE Raji B cells. When WT Jurkat T cells were conjugated to +SEE Raji cells (i.e. with TCR engagement), ‘APC/Full MTOC Repositioning’ events were robust, occurring in 87.6% of conjugates (n=73; see ‘WT +SEE’ in Fig. 15 B). After conjugation to -SEE Raji cells (i.e. without TCR engagement), WT Jurkat cells exhibited 20.5% ‘Full Repositioning’ (n=39; see ‘WT –SEE’ in Fig. 15 B), showing that while TCR engagement is needed for robust MTOC repositioning, engagement of LFA-1 and other co-stimulatory receptors can also lead to MTOC translocation. We note here that detection of such residual MTOC repositioning activity has not been possible using traditional static assays because of the ~30% “background” repositioning inherent in such assays, and demonstrates the superior resolution afforded by the optical trap system.

To test the role of LFA-1 signaling in MTOC repositioning, we engaged JB2.1 Jurkat cells with +SEE and -SEE Raji cells. When JB2.1 cells were conjugated to +SEE Raji cells (i.e. no LFA-1 signaling), ~30% ‘APC/Full Repositioning’ events were observed, showing that LFA-1 co-stimulation contributes significantly to the MTOC polarization process (n=21; see ‘JB2.1 +SEE’ in Fig. 15 B). Moreover, conjugation of JB2.1 Jurkat cells with -SEE Raji cells (i.e. no TCR or LFA-1 signaling) resulted in complete inhibition of ‘APC/Full repositioning’ (n=20, see ‘JB2.1 –SEE’ in Fig. 15 B). Lastly, reconstitution of the JB2.7 cell line with GFP-LFA-1α rescued the MTOC polarization defect, as 66.7% ‘Full/APC

Repositioning' events were observed (n=12; see 'JB2.7 +SEE +LFA-1' in Fig. 15 B). Together, these results show that LFA-1 plays an important role in MTOC repositioning, and that both LFA1 and TCR signaling are required for robust polarization of the MTOC toward the IS. Furthermore, these results validate the ability of our optical trap system to avoid "background" repositioning, and highlight the importance of temporal and spatial control when assaying MTOC repositioning events in T cells.

c. MTOC repositioning in T cells is bi-phasic

Next, we proceeded to study the kinetics of the MTOC repositioning process in Jurkat T cells. Expression of GFP-Cen2 and Farnesyl-RFP was utilized to label the centrosome and plasma membrane, respectively. Close examination of the MTOC translocation event revealed that the repositioning occurs in two distinct phases: a fast movement toward the contact site during the first phase (referred from here on as the 'polarization phase'), followed by a slow movement toward the center of the IS during the second phase (referred from here on as the 'docking phase'), leading to the close approximation of the centrosome near the IS membrane reported previously (Stinchcombe *et al.*, 2006) (Fig. 16 A and D). Moreover, the transition between the polarization and docking phases occurred as the centrosome reach a distance of ~2 um from the synaptic membrane (see yellow arrowheads in Fig. 16 A and B). Stack overlay of the time lapse images showed that, in addition to the distinct kinetics of the two phases, the direction of MTOC movement changes during the transition into the docking phase (Fig. 16 B). This is likely due to the fact that the MTOC must navigate around the large nucleus (estimated to be ~80% cell volume) during the polarization phase, while the MTOC movement is relatively unhindered during the docking phase

We then analyzed the kinetics of this bi-phasic movement by measuring the relative distance between the centrosome and the synaptic membrane, frame by frame.

Figure 16. Two kinetic phases of MTOC movement and invagination of the synaptic interface during T cell activation.

(A) Merged time lapse images of GFP-Cen-2 and RFP-Farnesyl in a Jurkat cell engaged by a +SEE Raji cell using the optical trap system. (B) Stack overlap of GFP-Cen-2 time lapse images (left) and transmitted image of Jurkat-Raji cell conjugate (right) shown in A and B. Yellow arrowheads in A and B denote transition between the polarization and docking phases of MTOC movement. (C) Graph showing the frame-to-frame instantaneous speeds of MTOC movement plotted against the distance between the MTOC and the IS during the respective frame of movement. n = 9 cells (D) Illustration of the bi-phasic MTOC movement in the T cell (blue) during conjugation with +SEE Raji B cell (light brown). MTOC = yellow dots. Phase movement = black arrows. (E) Merged time lapse images of GFP-Cen-2 and PKH26 (top row) and transmitted time lapse images (bottom row) showing membrane invagination in a Jurkat cell engaged by a +SEE Raji cell using the optical trap system. (F) Merged time lapse images of GFP-Cen-2 and RFP-Farnesyl (top row) and transmitted time lapse images (bottom row) showing membrane invagination in a Jurkat cell engaged by a +SEE Raji cell using the optical trap system. Scale bar in A = 5 μm. All other scale bars = 10 μm.

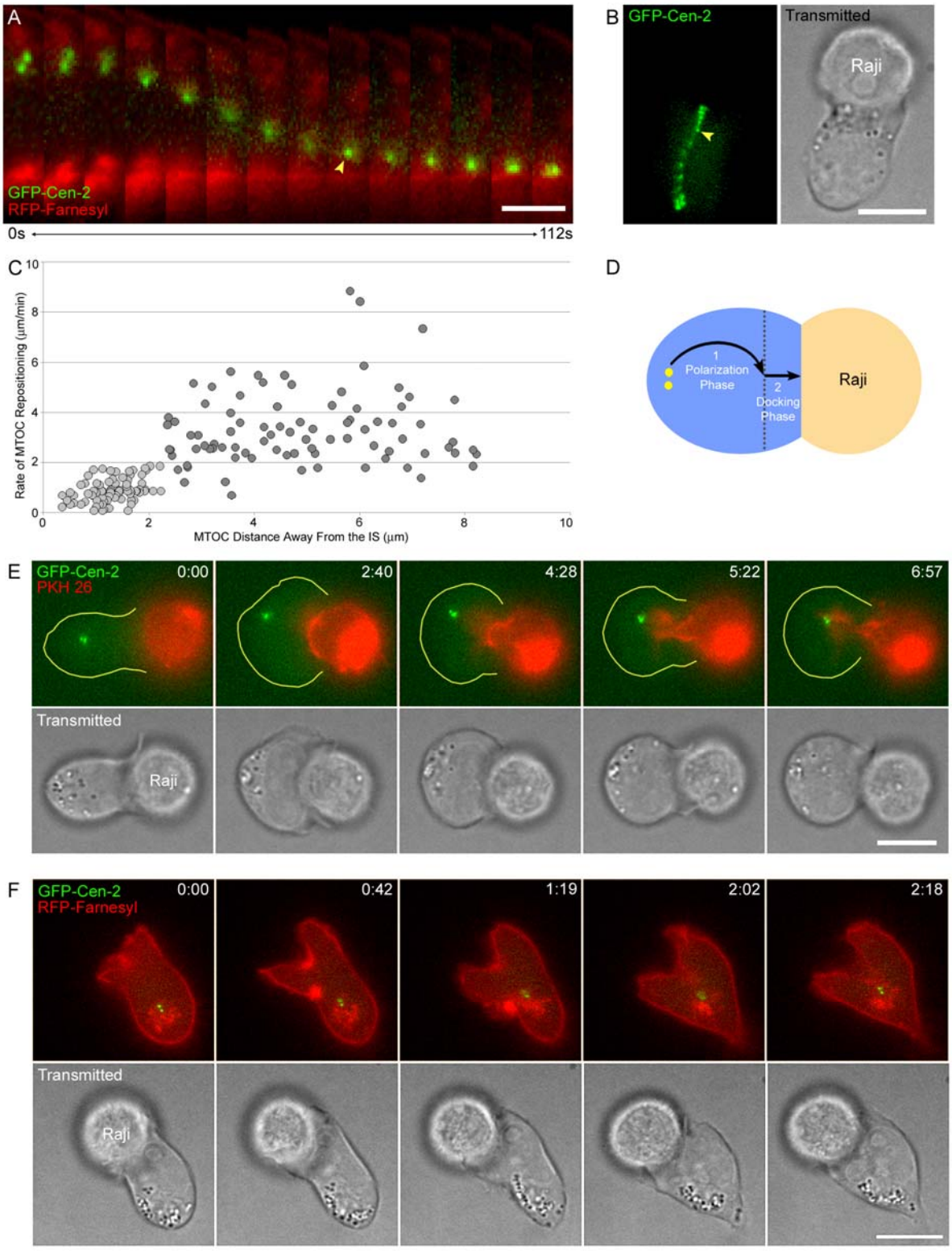
A
GFP-Cen-2
RFP-Farnesyl
0s
112s
B
GFP-Cen-2
Transmitted
Raji
C
Rate of MTOC Repositioning (μm/min)
MTOC Distance Away From the IS (μm)
D
1
Polarization
Phase
2
Docking
Phase
Raji
E
GFP-Cen-2
PKH 26
0:00
2:40
4:28
5:22
6:57
Transmitted
Raji
F
GFP-Cen-2
RFP-Farnesyl
0:00
0:42
1:19
2:02
2:18
Transmitted
Raji

Instantaneous speeds of MTOC movement in 9 Jurkat cells showed that the average rate of MTOC movement during the initial repositioning phase (3.26 ± 0.77 μm/min; see 'WT' under 'Repositioning Phase' in Fig. 18 B) is significantly faster than the rate during the final docking phase (0.90 ± 0.16 μm/min; see 'WT' under 'Docking Phase' in Fig. 18 B; $p<0.001$). Furthermore, the range of instantaneous MTOC speeds were bound in a relatively linear range across different MTOC distances from the synapse (see 8.25 - 2.25 μm MTOC distance away from the synapse for 'polarization phase' speeds, and 2.25 - 0.00 μm MTOC distance away from the synapse for 'docking phase' speeds in Fig. 16 C), and strongly linear slopes were observed at each phase in the time-lapse montage (Fig. 16 A), indicating a uniform speed and arguing that significant acceleration or deceleration did not occur during each phase of MTOC movement. Additionally, there was a steep drop-off in the instantaneous speeds of MTOC movement at the transition point between the two phases (see 2.25 μm MTOC distance away from the synapse in Fig. 16 C), suggesting that the MTOC may encounter an unknown resistance force at this distance from the synaptic membrane. Together, these results show for the first time that MTOC repositioning occurs in two distinct kinetic steps during T cell activation, and that a critical transition between the steps occurs at the MTOC approaches a distance of 2.25 μm from the IS. Moreover, these results are consistent with the idea proposed by G. Griffiths and colleagues that MTOC repositioning during CTL cell killing is a multi-step process (Jenkins *et al.*, 2009; Tsun *et al.*, 2011), and suggest that the transition from the polarization phase to the docking phase is a possible regulatory checkpoint for T cell effector function.

d. Large invagination of the synaptic interface is observed when MTOC movement is impeded

In further trials, the Raji B cell was marked with the membrane dye, PHK67, to allow alternative imaging of the synapse interface. As the MTOC must navigate around the large

nucleus during repositioning, there are rare instances when the MTOC movement becomes obstructed by the nucleus, presumably because the pulling forces on MTs at opposite sides of the nucleus are symmetric. A striking observation was made in these instances; as the centrosome movement was impeded, the attached Raji cell membrane became invaginated into the Jurkat T cell (see 4:23 time frame in Fig. 16 E). This invagination proceeded until the APC membrane reached the centrosome of the Jurkat cell, marked by GFP-cen-2 (see 6:57 time frame in Fig. 16 E). Similar deformation of the synaptic interface was observed when the T cell membrane was labeled using RFP-Farnesyl (Fig. 16 F), indicating that the APC and T cell membranes both become invaginated in these instances, as expected. In all, we observed invagination of the synaptic membrane in 75% of cells that did not fully reposition their MTOC to the IS. Since these cases of synaptic membrane invaginations can be considered to be another form of MTOC repositioning, the 87.6% value of combined 'APC/ Full Repositioning' events observed in our MTOC repositioning assay (see 'WT + SEE' in Fig. 15 B) is likely an underestimate. Together, these results indicate that strong cortical forces are generated at the synaptic membrane during T cell activation, and provide support for the idea that a cortical force generator is recruited to the IS to drive MTOC repositioning in T cells, as proposed by M. Poenie and colleagues (Kuhn and Poenie, 2002).

e. Cortical dynein spots are uniformly distributed and transiently bound at the IS

Having observed evidence of a strong pulling force at the IS, we sought to investigate the role of dynein in cortical force generation during the MTOC repositioning process. First, we sought to image cortical dynein at the IS by utilizing a planar bilayer substrate containing anti-CD3ε antibody and ICAM-1 to engage Jurkat cells expressing GFP-tagged dynein intermediate chain 2C (GFP-DIC). Consistent with previous reports (Combs *et al.*, 2006; Martin-Cofreces *et al.*, 2008), dynein accumulated at the IS in Jurkat cells bound to the stimulatory planar bilayer substrate (Fig. 17 A). Moreover, this

recruitment of dynein was dependent on TCR engagement as dynein did not accumulate at the contact plane in cells bound to the planar bilayer substrate containing only ICAM-1 (DNS). Contrary to the previous report of dynein localization at the dSMAC ring (Combs *et al.*, 2006), we observed a mostly uniform pattern of localization for dynein spots at the IS, without preferential localization to a SMAC region or other defined structures at the IS, including TCR MCs (see below) (Fig. 17 B). A noticeable exception, however, was a strong accumulation of dynein seen near the centrosome, and more specifically, in a region between the two centrioles (red arrowheads point to the two centrioles and green arrowhead points to the strong dynein accumulation in Fig. 17 B), that is consistent with the localization of dynein observed in other cell systems (Gonczy *et al.*, 1999; Quintyne *et al.*, 1999; King *et al.*, 2003; Splinter *et al.*, 2010).

Next, we sought to test whether these spots of dynein co-localize with TCR MCs at the IS, as recently published by Hashimoto-Tane *et al.* (Hashimoto-Tane *et al.*, 2011). During the early maturation stage of IS formation (3 min after engagement to planar bilayer substrate), both TCR MCs and dynein spots were uniformly distributed at the IS (Fig. 17 C). However, in contrast to the near-perfect co-localization between TCR MCs and dynein reported by Saito and colleagues (Hashimoto-Tane *et al.*, 2011), we observed very little co-localization between the dynein spots and TCR MCs at the IS (15.3% co-localization, 4 cells; also see Fig. 17 C). Moreover, at the mature stage of IS formation (8 min after engagement to planar bilayer substrate), TCR MCs localized at the cSMAC region of the IS (see Fig. 17 D [left]), whereas the localization of dynein spots remained uniform (see Fig. 17 D [middle and right]). These results show that, in our system, dynein does not strongly co-localize with TCR MCs, and suggest that TCR MCs are not the preferential anchoring site for cortical dynein at the IS.

To observe the dynamics of these dynein spots at the IS, Jurkat cells were imaged on a planar bilayer substrate at a rapid acquisition rate (0.25 sec/frame). While the strong

Figure 17. Localization of cortical dynein at the IS.

(A) Side view (x-z) images of RFP-Cen-2 (top), GFP-DIC (middle), and RFP-Cen-2 and GFP-DIC merged (bottom) in a Jurkat cell bound to a planar bilayer substrate. (B) En face view (x-y) images of RFP-Cen-2 (left), GFP-DIC (middle), and RFP-Cen-2 and GFP-DIC merged (right) at the IS in a Jurkat cell bound to a planar bilayer substrate. (C) En face view images of TCR (labeled using anti-CD3ε antibodies in the planar bilayer) (left), GFP-DIC (middle), and TCR and GFP-DIC merged (right) at the IS in a Jurkat cell bound to a planar bilayer substrate for 3 min. (D) En face view images of TCR (labeled using anti-CD3ε antibodies in the planar bilayer) (left), GFP-DIC (middle), and TCR and GFP-DIC merged (right) at the IS in a Jurkat cell bound to a planar bilayer substrate for 8 min. (E) En face view images of mCherry-Tubulin (left), GFP-DIC (middle), and mCherry-Tubulin and GFP-DIC merged (right) at the IS in a Jurkat cell bound to a planar bilayer substrate for 8 min. (F) Zoomed time lapse images of GFP-DIC (right) selected from the area outlined by the white box on the left single time frame image. Scale bar in A = 2 μm. Scale bar in F = 1 μm. All other scale bars = 5 μm.

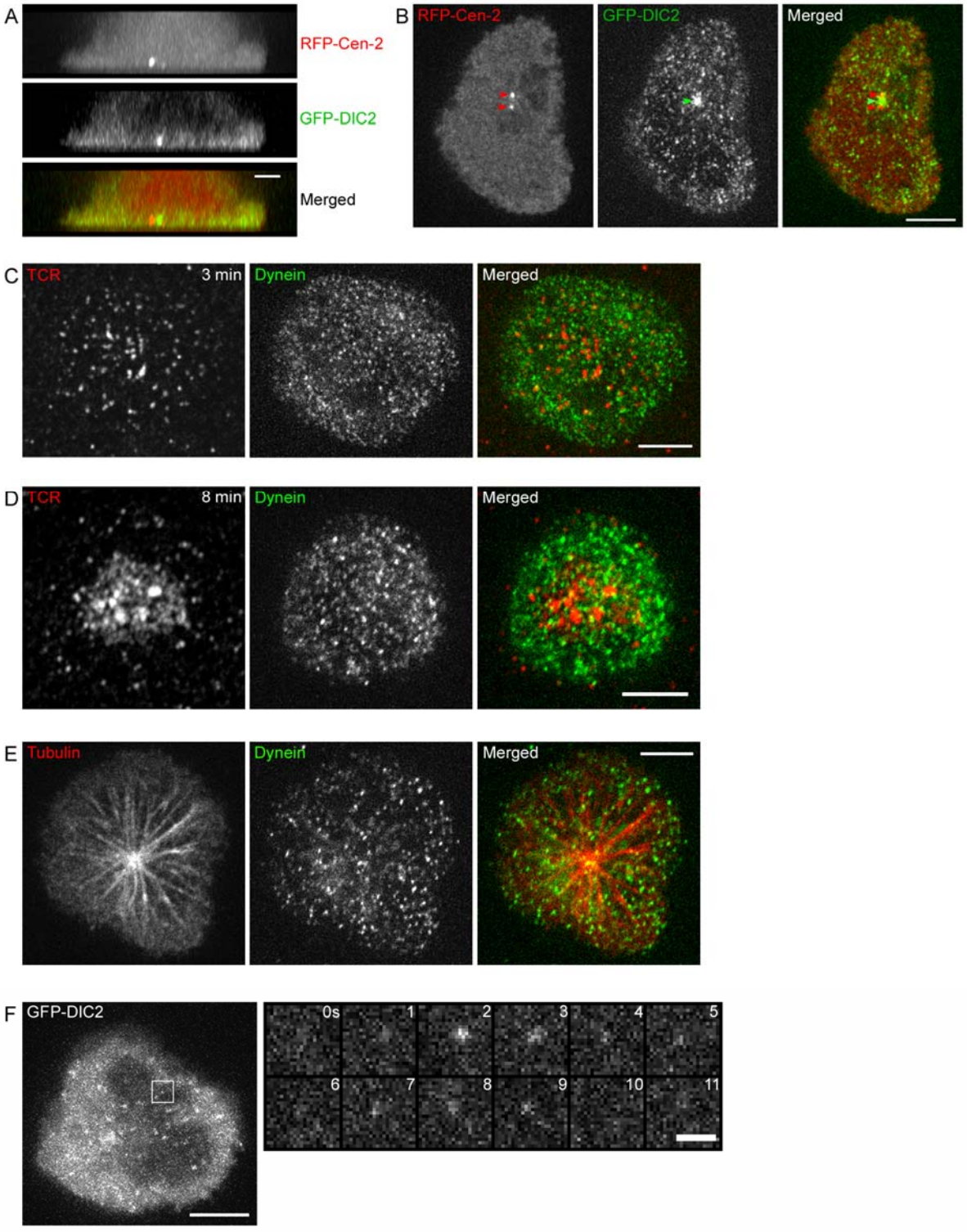
A
RFP-Cen-2
GFP-DIC2
Merged
B
RFP-Cen-2
GFP-DIC2
Merged
C
TCR
3 min
Dynein
Merged
D
TCR
8 min
Dynein
Merged
E
Tubulin
Dynein
Merged
F
GFP-DIC2
0s
1
2
3
4
5
6
7
8
9
10
11

accumulation of dynein near the centrosome was consistent both in intensity and duration, we observed a more transient localization of dynein spots elsewhere at the IS. Specifically, the appearance of these cortical dynein spots were relatively short-lived (average lifetime of 4.0 $\pm$ 2.5 sec, 100 MCs, 4 cells; Fig. 17 F), and did not show lateral movement during their appearance at the IS (see time lapse in Fig. 17 F [right]). Furthermore, in Jurkat cells expressing eGFP-DIC2 and mCherry-Tubulin, and engaged on the planar bilayer substrate, we observed a modest co-localization between dynein clusters and MTs at the IS (40.3%, 4 cells; see Fig. 17 E), indicating that at any given time, some of the cortically bound dynein clusters may bind and pull on MTs, and that the dynamic localization of dynein is not dependent on attachment to MTs. Moreover, these results suggest that cortical force generation at the IS is mediated stochastically by numerous, short-lived clusters of cortically bound dynein.

f. Inhibition of dynein impairs MTOC movement during the polarization phase and blocks the docking phase of MTOC repositioning

To test the contribution of dynein in cortical force generation at the IS during MTOC repositioning, we inhibited dynein using overexpression of the CC1 portion of the dynactin subunit p150 (CC1 DN), which has been shown to inhibit dynein function *in vivo* without noticeable effects on dynactin structure and stability (Quintyne *et al*., 1999; King *et al*., 2003). CC1 overexpression is thought to inhibit dynein by competing for the common binding site on the dynein IC for LIS1/NUDE(L) and dynactin, thus disrupting the regulation of dynein activity (Quintyne *et al.*, 1999; King *et al.*, 2003). Conflicting results have been reported regarding the effect of dynein inhibition on MTOC repositioning in T cells. Previous study by Sanchez-Madrid and colleagues showed that dynein inhibition, using dynactin overexpression and siRNA knockdown of dynein HC, leads to severe disruption of MTOC repositioning in Jurkat T cells engaged to SEE-coated Raji B cells (Martin-Cofreces *et al.*,

2008), while Hashimoto-Tane *et al*. reported that MTOC repositioning was normal in dynein-inhibited primary T cells conjugated to a planar bilayer substrate (Hashimoto-Tane *et al.*, 2011). However, these studies did not observe dynamic MTOC movements (they measured MTOC positions in fixed T cells) and did not distinguish between the polarization and docking phases of MTOC repositioning. Thus, we sought to analyze centrosome movements during the two phases of MTOC repositioning in dynein-inhibited Jurkat cells using the optical trap system.

In RFP-CC1 DN-overexpressing cells, we observed a modest decrease in 'APC/Full Repositioning' events (63.6%, n=11 cells; see 'CC1 DN' in Fig. 18 A), accompanied by an increase in partial MTOC repositioning events (27.3%; see 'CC1 DN' in Fig. 18 A) compared to WT cells (4.1%; see 'WT +SEE' in Fig. 15 B). However, the dynamics of MTOC repositioning during the polarization phase was impaired, with a 59.6% reduction in the rate of MTOC movement (1.32 $\pm$ 0.82 μm/min [CC1 DN] vs. 3.26 $\pm$ 0.77 μm/min [WT]; see 'Polarization Phase' in Fig. 18 B; $p<0.001$). In addition, while the MTOC movement during the polarization phase was directionally persistent in WT cells, (see left side of Fig. 16 A), MTOC movement in RFP-CC1 DN-overexpressing cells was interrupted by pauses and reverse movements of the centrosome away from the synapse, as evidenced by the flat and upward slopes, respectively, observed in the time lapse montage (white arrowheads point to pauses and reverse movements in Fig. 18 D). Together, these results indicate that dynein is required for the rapid and directionally persistent movement of the centrosome during the polarization phase of MTOC repositioning. With regard to the remaining MTOC movement observed in dynein-inhibited cells, we cannot ascertain whether it results from residual dynein activity, or from a different cortical force generating mechanism altogether at the IS.

Next, we observed the effect of dynein inhibition on MTOC movements during the docking phase of repositioning. WT Jurkat cells showed consistent 'docking' of their centrosome at the IS, as evidenced by the close approximation of the centrosome to the

Figure 18. The effect of dynein and LIS 1 inhibition on MTOC repositioning.

(A) Percentage of repositioning events in CC1 DN and LIS1 DN Jurkat cells conjugated to +SEE Raji cell using the optical trap system. (B) Rates of MTOC repositioning during the repositioning and docking phase in WT, CC1 DN, and LIS1 DN Jurkat cells conjugated to +SEE Raji cell using the optical trap system. (C) The average MTOC distance away from the synapse in the final minute of conjugation observed in WT, CC1 DN, and LIS1 DN Jurkat cells. (D) Time lapse montage of GFP-Cen-2 in a CC1 DN-overexpressing Jurkat cell conjugated to +SEE Raji cell. The plane of conjugation is marked by the yellow line. (E) Time lapse montage of RFP-Cen-2 and GFP-LIS1-DN in a LIS-DN-overexpressing Jurkat cell conjugated to +SEE Raji cell. The plane of conjugation is marked by the yellow line. Time and distance of the time lapse montages are indicated to the right and bottom, respectively. Numbers of cells analyzed are indicated inside the bars in A and B.

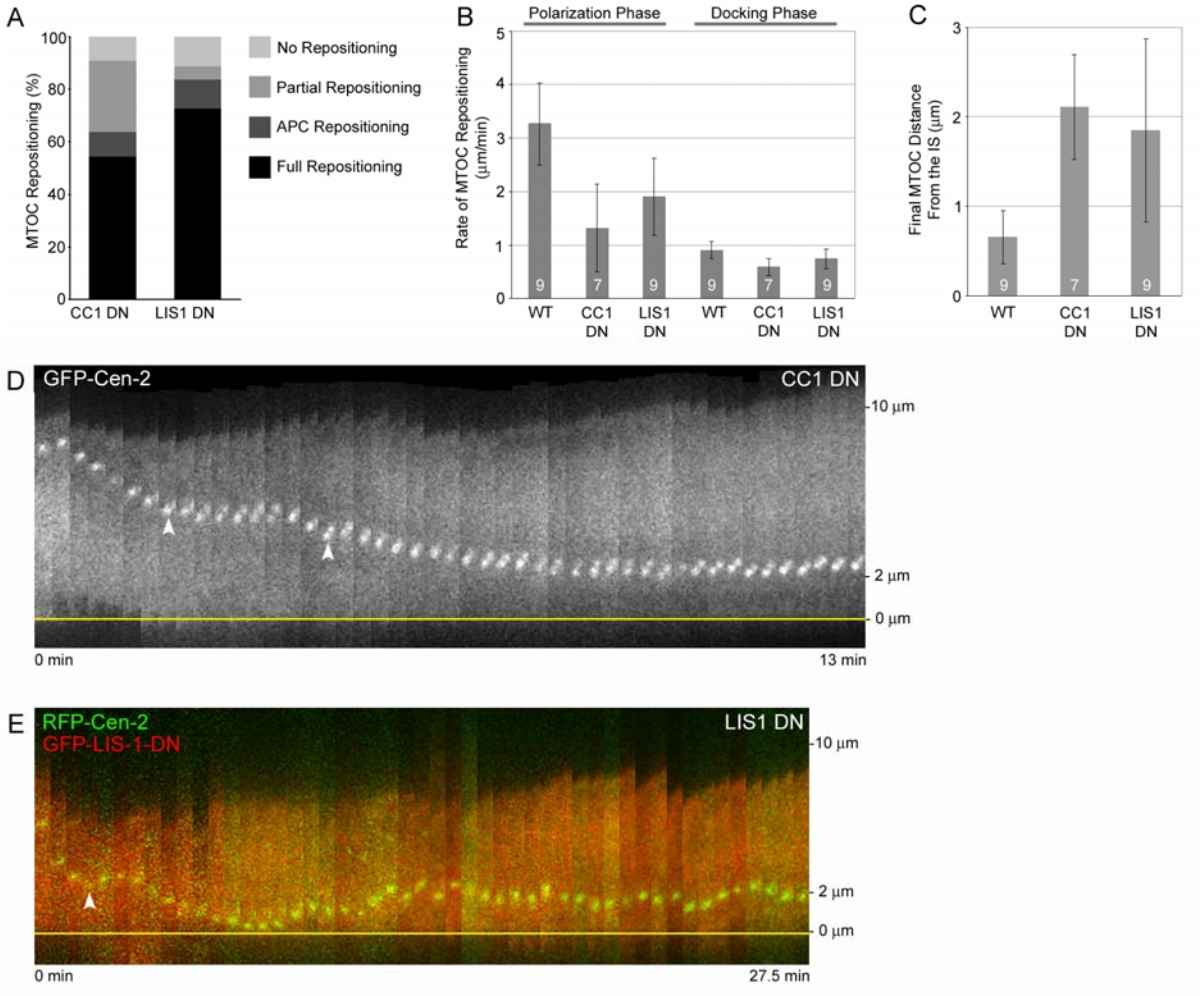

synaptic membrane after completion of its docking phase movement (see right side of the time lapse montage in Fig. 16 A), and the small average distance observed between the MTOC and the synapse during the final minute of conjugation (0.66 ± 0.30 μm, see 'WT' in Fig. 18 C). In contrast, the docking phase was inhibited in RFP-CC1 DN-overexpressing cells, with the centrosome movement being stalled at the transition point, as evidenced by the time lapse montage (see right side of Fig. 18 C), and by the average distance of the MTOC from the synaptic membrane during the final minute of conjugation (2.11 + 0.59 μm, see 'CC1 DN' in Fig. 18 C; $p<0.001$), which closely matches the measured distance of the transition point in WT cells (2.25 μm, Fig. 16 C). We note here that inhibition of the docking phase of MTOC repositioning likely accounts for the increased level of 'Partial Repositioning' events observed in dynein-inhibited cells (see 'CC1 DN' in Fig. 18 A). While entry into the docking phase was severely disrupted with CC1 DN overexpression, on a few occasions we observed brief MTOC movements past the transition point during conjugation with the +SEE Raji cell. We note, however, that these movements never resulted in centrosome docking and accounted for only 4% of total MTOC movements near the transition point. Quantification of these short-lived "docking phase" movements showed that MTOC movement during the docking phase in RFP-CC1 DN-overexpressing cells was slower compared to WT cells (0.58 + 0.16 μm/min [CC1 DN] vs. 0.90 + 0.16 μm/min [WT]; see 'docking phase' in Fig. 18 A, $p<0.05$). In all, these results show that dynein is required for the rapid, directionally persistent movement of the centrosome during the polarization phase, and transition into the docking phase of MTOC repositioning. Moreover, these results are consistent with the involvement of dynein in cortical force generation at the IS during MTOC repositioning in T cells.

g. **Inhibition of LIS1 impairs MTOC movement during the polarization phase and disrupts prolonged centrosome docking during the docking phase**

Having established the requirement for dynein, we next sought to test the role of the dynein regulatory protein, LIS1, in MTOC repositioning in T cells. R. Vallee and colleagues have reported that LIS1 is required for the persistent force generation of dynein under high load (McKenney *et al.*, 2010), and that inhibition of LIS1 disrupts spindle repositioning during mitosis in mammalian cells (Faulkner *et al.*, 2000) and nuclear and MTOC repositioning during migration in neural progenitor cells (Tsai *et al.*, 2005; Tsai *et al.*, 2007). Thus, we asked whether regulation of dynein activity by LIS1 is also required for MTOC repositioning in T cells. To inhibit LIS1 in Jurkat T cells, we utilized overexpression of the self-associating N-terminal portion of LIS1 (LIS1 DN), which has been reported to selectively inhibit LIS1 without disrupting the endogenous localization of the dynein complex and other regulatory proteins (Tai *et al.*, 2002; Tsai *et al.*, 2005). The inhibitory effect of LIS1 DN overexpression is thought to result from the formation of heterodimers between the endogenous, full length LIS1 and the LIS1 DN fragment which show a weak affinity for the binding sites on dynein (Tai *et al.*, 2002).

In GFP-LIS1 DN-overexpressing Jurkat cells, we observed a normal percentage of 'Full/APC Repositioning' events (83.3%, n=18 cells; see 'LIS1 DN' in Fig. 18 A) compared to WT cells (see 'WT +SEE' in Fig. 15 B). However, the dynamics of MTOC repositioning during the polarization phase was impaired, with a 41.6% reduction in the rate of MTOC movement (1.90 $\pm$ 0.71 μm/min [CC1 DN] vs. 3.26 $\pm$ 0.77 μm/min [WT]; see 'Polarization Phase' in Fig. 18 B; $p<0.002$). Also, similar to CC1 DN overexpression, MTOC movement in LIS1 DN-overexpressing cells was interrupted by pauses and reverse MTOC movements, as evidenced by the time lapse montage (see example of a reverse movement [white arrowhead] in Fig. 18 E). Moreover, docking of the MTOC was disrupted in LIS1-inhibited cells, as evidenced by the separation between the MTOC and the synaptic membrane shown in the time lapse montage (see right side of Fig. 18 E), and the increased average distance of the MTOC from the IS during the final minute of conjugation in GFP-LIS1 DN-

overexpressing cells (1.84 ± 1.02 μm; see 'LIS1 DN' in Fig. 18 C; $p<0.005$). In contrast to the stalled MTOC movement at the transition point between the two phases observed with CC1 overexpression, we observed movement of the centrosome past the transition point in GFP-LIS1 DN-overexpressing cells, leading to docking of the centrosome at the IS (see movement of the MTOC toward the synaptic membrane [marked by the yellow line] in the time lapse montage in Fig. 18 E). The rate of MTOC movement during the docking phase in LIS1-inhibited cells was only slightly reduced compared to WT cells (0.73 ± 0.19 μm/min [LIS1 DN] vs. 0.90 ± 0.16 μm/min [WT]; see 'Polarization Phase' in Fig. 18 B; $p<0.05$). However, these cells were unable to maintain docking of the MTOC at the synaptic membrane, as the MTOC retreated back to the transition point after apparent docking at the IS (see MTOC movement after contact with the synaptic membrane in Fig. 18 E) and meandered near the transition point for the remainder of the conjugation process (see right side of the time lapse in Fig. 18 E). We observed this inability to maintain centrosome docking in 60% of LIS1-inhibited cells. Together, these results show that LIS1 is required for the rapid and processive movement of the MTOC during the polarization phase, and maintenance of centrosomal docking at the synaptic membrane during the docking phase of MTOC repositioning. Furthermore, our results are consistent with the idea that LIS1 is required for dynein-mediated transport of high-load cargo (i.e. centrosome and the associated MT array), as proposed by R. Vallee and colleagues, and suggest that the two phases of MTOC repositioning require differential regulation of dynein activity in T cells.

IV. Discussion

Static observations of fixed conjugates in previous studies have suggested that T cell activation is a multi-step process, involving polarization of the centrosome toward the synaptic interface, followed by docking of the centrosome and associated effector molecules at the synaptic membrane for directed secretion (Jenkins *et al*., 2009; Stinchcombe *et al*.,

2006). Using an optical trap system of T cell-APC engagement, we were able to show partial defects in MTOC repositioning in LFA-1-defiecient Jurkat cells, and show for the first time distinct kinetic phases of MTOC repositioning in T cells. Specifically we showed that the rate of MTOC movement during the initial polarization phase is ~3 fold faster than the subsequent docking phase, and that a transition between the phases occurs reproducibly at a distance of ~2 μm from the synaptic interface. We were also able to perform high resolution imaging of cortical dynein at the IS using planar bilayer engagement of T cells. In contrast to previous reports, a relatively uniform distribution of cortical dynein spots were observed at the IS, without localization to specific SMAC regions. Furthermore, we defined the role of dynein in MTOC repositioning by showing that the rapid and persistent movement of the MTOC during the polarization phase and MTOC movement past the transition point require dynein. Lastly, we report for the first time the involvement of LIS1 in MTOC repositioning in T cells, and showed that LIS1 is required for rapid movement of the MTOC during the polarization phase, and maintenance of centrosomal docking at the IS during the docking phase of MTOC repositioning in T cells.

a. Optical trap-controlled activation of T cells

The optical trap has become a useful tool for the study of cell biology, allowing intricate measurement and manipulation of small objects. Moreover, the optical trap has been utilized to allow consistent temporal and spatial control over the T cell engagement process. In the report by Cahalan and colleagues, optically trapped polystyrene beads coated with anti-TCR antibodies were used to test different locations along a polarized T cell for sensitivity to T cell activation (Wei *et al.*, 1999). The optical trap and antibody-coated beads, likewise, were utilized in separate in-vitro experiments to probe the mechano-sensory properties of the TCR, and activation of LFA-1 receptors in T cells (Chen *et al.*, 2007; Kim *et al.*, 2009). Although antibody-coated beads were initially tested in our system,

we observed that the bead, once engaged to the Jurkat cell, frequently escaped the optical trap and repositioned toward the centrosome, giving us very little information about the dynamics of the MTOC repositioning event. Moreover, using an APC allowed engagement of the full repertoire of adhesion molecules, accessory receptors, and lateral movement of ligand-bound receptors at the T cell-APC interface, which are needed for sustained T cell activation. Interestingly, Davis and colleagues have also used the optical trap to engage natural killer (NK) cells with target cells to perform high resolution imaging of the cytoskeletal dynamics at the NK synapse (Oddos *et al.*, 2008; Brown *et al.*, 2011), confirming the advantages of the optical trap system in studying the lymphocyte activation process.

b. The two phases of MTOC movement during T cell activation

The rapid movement of the MTOC toward the site of TCR stimulation has been reported in previous live-imaging studies by M. Huse and colleagues using their photoactivation system and by M. Poenie and colleagues using modulated polarization microscopy (Kuhn and Poenie, 2002; Huse *et al.*, 2007; Quann *et al.*, 2009). Moreover, the rates of MTOC repositioning in these studies (approximately ~3 μm/min in Quann *et al*., 2009; 3.55 + 1.07 μm/min in Kuhn and Poenie, 2002) closely match the fast rate of MTOC movement observed during the polarization phase in our study (3.26 $\pm$ 0.77 μm/min). However, the subsequent docking phase of MTOC movement was not detected in these reports. In regard to the studies by Huse and colleagues, immobilized coverslip substrates were used in their photoactivation system, which inhibits maturation of the IS in engaged T cells (Huse *et al.*, 2007; Quann *et al.*, 2009). We suspect that IS maturation, and the resulting formation of concentric SMAC domains, are required for the docking phase of MTOC repositioning in T cells. Furthermore, a 3 μm-wide cortical region was photoactivated by the laser beam, perhaps obscuring the final docking phase movement of the MTOC, which consistently occurs at a distance of ~2 μm from the site of TCR stimulation. As for the

study by M. Poenie and colleagues, their analysis of centrosomal dynamics in CTLs did not include movement of the MTOC within a distance of ~4.0 μm from the IS and, therefore, could not detect the final docking phase movement (Kuhn and Poenie, 2002). We note, however, that the existence of a distinct docking phase in MTOC repositioning has been suggested in recent imaging studies using fixed CTL-target cell conjugates by G. Griffiths and colleagues (Jenkins *et al.*, 2009; Tsun *et al.*, 2011). In particular, Lck signaling was shown to be required for centrosomal docking at the IS, as the centrosome in Lck-deficient CTLs was consistently polarized toward, but not docked at the synaptic interface (Tsun *et al.*, 2011), similar to the effect of dynein inhibition observed in our study. Also, while we agree with their assessment that the docking step likely represents an important checkpoint during T cell activation, instances of transient docking observed in LIS1-inhibited cells suggest that centrosomal docking requires continued maintenance, contrary to the all-or-none commitment of the T cell to effector function suggested by Griffiths and colleagues.

c. The role of LFA-1 integrins in MTOC repositioning

While LFA-1 integrin receptors were initially identified as a possible anchor for cortical force generators at the IS (Kuhn and Poenie, 2002), the follow-up study by Combs *et al*. reported that LFA-1-deficient Jurkat cells (JB2.7) repositioned their MTOC normally after conjugation with SEE-coated Raji cells (Combs *et al.*, 2006). The latter result contrasts with our finding, as well as with an earlier report by Poenie and colleagues (Kuhn *et al.*, 2001), which show that JB2.7 cells are partially defective in MTOC repositioning. The difference may lie in the methods used to assay MTOC repositioning in T cells. While Poenie and colleagues imaged the centrosome in fixed Jurkat T cells conjugated to +SEE Raji B cells at random contact points, we used the optical trap to always contact the T cell opposite the position of the MTOC. It may be possible that the high MTOC polarization levels reported by Combs *et al.* resulted from ‘background repositioning’ due to the random

method of Jurkat T cell conjugation. In addition, static assays using fixed T cell-APC conjugates lack dynamic information about the MTOC repositioning process and do not offer the sensitivity required for detection of partial defects in MTOC repositioning. Given these issues, spatial and temporal control over T cell activation, and dynamic imaging capability are needed for more detailed studies of cytoskeletal polarization processes in T cells. Moreover, further studies using alternative methods to modulate LFA-1 activity (function-blocking antibodies, siRNA knockdown, chimeric expression, etc.) are needed to understand the contribution of LFA-1 integrin signaling to MTOC repositioning in T cells.

d. Generation of cortical pulling force at the IS

Previous imaging studies have suggested the involvement of a cortical force generator that captures and pulls MTs toward the IS during T cell activation (Kuhn and Poenie, 2002). Our observations of synaptic membrane invaginations provide striking evidence of such cortical pulling force at the IS. Interestingly, similar membrane invaginations have been reported during spindle repositioning in the *C. Elegans* embryo (Redemann *et al.*, 2010). After partial depletion of non-muscle myosin 2 using RNAi, numerous membrane invaginations were observed, aligning along MTs and requiring cortical force generation mediated by the dynein complex. Importantly, since these invaginations indicated the location of cortical force generators along the membrane, they were able to deduce the distribution and quantity of cortical force generators anchored at the membrane during asymmetric cell division. In the same vein, based on the observation that membrane invaginations originate at the IS center, we can infer that cortical pulling forces are concentrated near the center of the synaptic interface during MTOC repositioning in T cells.

e. The localization of dynein at the IS

Dynein is thought to drive cortical force generation at the IS in T cells. Support for this idea comes partly from imaging studies that show accumulation of dynein in a ring-shaped pattern near the contact site in conjugated cells, coinciding with the dSMAC region of the IS (Combs *et al.*, 2006). These results contrast with the uniform distribution of cortical dynein spots observed in our study and, to a certain extent, in the study by Hashimoto-Tane *et al.* (Hashimoto-Tane *et al.*, 2011). Moreover, clusters of dynein have been detected in limited images of Jurkat-Raji cell conjugates (Martin-Cofreces *et al.*, 2008). Possible reason for the difference in dynein localization patterns reported in Combs *et al*. and our study may be the substrates used to engage the T cells. While conjugation of T cells with APCs offers the most physiologically relevant system for studying the T cell activation process, 3-D reconstruction of the T cell-APC conjugate typically yields images with poor resolution due to increased diffraction along the axial plane. Moreover, the synapse is not uniform at the axial plane of the conjugation site, thus it is difficult to image the IS in a single plane using T cell-APC conjugates. Furthermore, even though Jurkat cells expressing low levels of GFP-DIC were imaged in our studies, we noticed a high level of background signal when imaging GFP-DIC at the IS, presumably reflecting a large pool of unanchored cytoplasmic dynein, which may be difficult to separate from the signals for cortically-bound dynein in 3-D reconstructed cells. Given that the distribution of molecules at the IS in planar bilayer-engaged T cells closely resembles that of APC-engaged cells, and given that limited number of dynein clusters were observed in Jurkat-Raji cell conjugates, we argue that the uniform dynein spots observed at the planar bilayer report cortically anchored dynein at the IS. However, as recent advances in imaging techniques allow increased resolution in both lateral and axial planes of imaging, high resolution imaging of dynein in T cell-APC conjugates need to be performed to confirm the uniform distribution of cortical dynein spots at the IS. Moreover, to prove that the dynein spots imaged using GFP-DIC are reporting functional dynein complexes at the IS, we plan to generate a stable line of Jurkat cells

expressing low levels of GFP-DIC, which will be used to test whether exogenously expressed GFP-DIC co-sediments with the endogenous 20S dynein complex on a sucrose gradient.

f. The role dynein in MTOC repositioning in T cells

Further support for the functional involvement of dynein in MTOC repositioning comes from inhibition studies showing that overexpression of p50-dynamitin, as well as siRNA knockdown of dynein HC results in a severe disruption of MTOC repositioning in Jurkat T cells (Martin-Cofreces *et al.*, 2008). While we used similar methods to inhibit dynein (overexpression of the CC1 portion of p150 dynactin and siRNA knockdown of dynein HC [see below]), and while our results are in agreement with the important role of dynein in the MTOC repositioning process, significant differences exist between our study and the report by Martin-Cofreces *et al*. First, they observed a severe reduction in the levels of MTOC repositioning in dynein-inhibited cells using a static assay, while we see only a minor reduction in the overall percentage of MTOC repositioning events (though the kinetics of MTOC movement during the polarization phase and entry into docking phase are inhibited [see below]). We note that a recent study by Hashimoto *et al.* also reported a normal percentage of MTOC repositioning in dynein-inhibited primary T cells engaged and fixed on a planar bilayer substrate. Second, in the live imaging of dynein-inhibited Jurkat cells by Martin-Cofreces *et al*., MTOC movement was reported to be completely inhibited, whereas we see a slower, less persistent movement of the MTOC toward the IS. Lastly, they did not detect the biphasic movement of the MTOC in WT cells, or the effect of dynein inhibition on the docking phase of MTOC movement, as observed in our study.

With regard to the discrepancy in the percentage of MTOC repositioning events, though Martin-Cofreces *et al.* did not explain the scoring criteria used to assay MTOC repositioning, it is possible that 'Partial Repositioning' events were filtered out by their

scoring system, since the MTOC becomes stalled at the transition point before entry into the docking phase. In addition, as the speed of MTOC repositioning is reduced in dynein-inhibited cells, the length of the imaging time may not have been long enough to capture full MTOC repositioning events in their study. Furthermore, since Sanchez-Madrid and colleagues imaged the centrosome in fixed Jurkat T cells conjugated to +SEE Raji B cells at random contact points, it is possible that the partial reduction in "Full Repositioning" events was obscured by the high levels of "background" repositioning inherent in such static assays. With regard to the discrepancy in the kinetics of MTOC movement and entry into docking phase in dynein-inhibited cells, the difference may again lie in the methods used to image MTOC repositioning in T cells. In the study by Martin-Cofreces *et al*., live imaging was performed during chance encounters between the Jurkat T cells and +SEE Raji cells while crawling on the coverslip substrate. As mentioned above, without temporal and spatial control over the T cell conjugation process, it is difficult to image full MTOC repositioning events consistently and dynamically. Thus, it is not surprising that their live-imaging data consisted of only two videos showing MTOC movement in dynamitin-overexpressing cells, and that the two kinetic phases were not detected in their live-imaging of WT Jurkat cells.

Currently, inhibition experiments using siRNA knockdown of dynein HC are being performed to complement the results observed with CC1 DN-overexpression. Preliminary experiments using siRNA knockdown of dynein HC in Jurkat T cells have shown, indeed, MTOC movements are slower and less persistent during the polarization phase and that entry into the docking phase is inhibited, confirming the effects observed with CC1 overexpression. Additional experiments in primary T cells will be needed to confirm the functional role of dynein in MTOC repositioning in T cells.

g. The role of dynein regulatory proteins in MTOC repositioning in T cells

The role of dynein regulatory complexes in MTOC repositioning has not been previously examined in T cells. As the emerging paradigm in dynein regulation suggests differential and competing regulation of dynein activity by LIS1/NUDE(L) and dynactin, and as minus-end directed vesicle/organelle transport requires association of dynein with these regulatory proteins, MTOC repositioning in T cells likely involves regulation by LIS1/NUDE(L) and dynactin. Regarding the role of the LIS1/NUDE(L) complex, our results show that LIS1 is required for the rapid and persistent movement of the MTOC during the polarization phase, and maintenance of centrosome docking during the docking phase. Parallel to LIS1 DN overexpression, experiments using shRNA knockdown of LIS1 are being performed to alternatively inhibit LIS1 in Jurkat T cells. Regarding the role of dynactin, unpublished results by Poenie and colleagues indicate that MTOC repositioning is normal in dynactin-inhibited T cells (Dissertation work by Sarah Youngsun Tan, 2010, University of Texas, Austin). However, since the dynamics of MTOC movement during the two repositioning phases have not been observed in dynactin-inhibited T cells, live-imaging studies are needed in order to compare directly with the effects of LIS1 inhibition on MTOC repositioning. We plan to do so using siRNA knockdown of the p150 dynactin subunit to inhibit dynactin and the optical trap system to engage dynactin-inhibited Jurkat T cells.

h. Conclusion

In this study, we introduced a method to induce MTOC repositioning in T cells with temporal and spatial control using an optical trap. Using this approach, we were able to probe the dynamics of MTOC movements, as well as the contribution of dynein and LIS1 to the MTOC repositioning process in T cells. Specifically, we showed that the MTOC repositioning event occurs in two distinct kinetic phases, with the transition between the phases occurring at a distance of ~ 2 μm from the synaptic interface. Moreover, we observed strong evidence of cortical force generation at the IS, as the synaptic interface

became sharply invaginated when MTOC movements were impeded in T cells. Furthermore, our inhibition experiments showed that dynein and LIS1 are required for fast and persistent movement of the MTOC during the polarization phase, and entry into and maintenance of centrosome docking during the docking phase of MTOC repositioning. Together, these results indicate that dynein and LIS1 are important components of the cortical pulling force driving MTOC repositioning in T cells. Lastly, as the MTOC repositioning event is critical for effector function in T cells, the molecular mechanisms behind the two phases of centrosome movement, and the regulation of centrosome docking at the IS represent important areas to be explored in future investigations.

V. Materials and Methods

Cell culture and transfection

E6.1 and JCAM2.5 Jurkat T cells (gifts from L. Samelson, NCI, NIH), JB2.7 Jurkat T cells (gift from M. Poenie, University of Texas, Austin) and Raji B cells (gift from J. Martina, NHLBI, NIH) were maintained at 37^{o}C in IMDM media (Invitrogen, #12440) supplemented with fetal bovine serum (Sigma-Aldrich, #F0392), sodium pyruvate (Invitrogen, #11360), L-glutamine (Invitrogen, #25030), Penicillin-Streptomycin (Invitrogen, #15140), and MEM non-essential amino acids solution (Invitrogen, #11140). Cells were replated every 48 hrs at a concentration of 2.0 x 10^5 cells/ml for all Jurkat cell lines and 5.0 x 10^5 cells/ml for the Raji B cells. Transfections were performed by nucleofection using cells at a concentration of 1.0 x 10 cells/ml, 1-3 μg of plasmid DNA, Amaxa Kit V (Lonza-Amaxa), and the electroporation protocol for Jurkat T cells.

Plasmids and reagents

Centrin-2 tagged with mGFP or mRFP were gifts from J. Martina (NHLBI, NIH). The dynein intermediate chain 2 construct tagged with mGFP was a gift from K. Pfister (Department of

Cell Biology, School of Medicine, University of Virginia). The Farnesyl construct tagged with mRFP was a gift from J. Donaldson (NHLBI, NIH). The N-terminus dominant negative construct of LIS1 tagged with mGFP was a gift from R. Vallee (Department of Pathology and Cell Biology, Columbia University). The dominant negative CC1 portion of p150 dynactin construct tagged with mRFP was a gift from T. Shroer (Department of Biology, Johns Hopkins University). The LFA-1α construct tagged with mGFP was a gift from M. Kim (Department of Microbiology and Immunology, University of Rochester). Fluo-4 AM was purchased from Molecular Probes/Invitrogen (# F14217). Staphylococcal Enterotoxin E was purchased from Toxin Technology (#ET 404). PHK26 dye for cell membrane labeling was purchased from Sigma Aldrich (#MINI26-1KT).

Planar lipid bilayer substrate

Liposomes were prepared and glass-supported planar lipid bilayers were formed essentially as described previously (Dustin *et al*., 2007). Liposomes were created using a mixture of DOPC (Avanti Polar Lipids, #850375C), biotin-CAP-PE (1% molar ratio) (Avanti Polar Lipids, #180061C), and DOGS-NTA (1% molar ratio) (Avanti Polar Lipids, #790528C) lipids. The anti-CD3ε antibody (Biovest International, # OKT3) was mono-biotinylated and labeled with fluorescent dyes following the protocol of Carrasco *et al.* (Carrasco *et al.*, 2004). A flow chamber was assembled by initially attaching two layers of double-sided tape to the sides of a glass slide. To create a bilayer within the flow cell, a 1.5 µl drop of liposomes was deposited on the glass slide in between the strips of double-stick tape, and then a glass coverslip that has been washed in Piranha solution (70% [v/v] sulfuric acid [Fisher, #A300] and 30% [v/v] hydrogen peroxide [Fisher, #H325]) was placed on top of the glass slide across the double-stick tape, simultaneously allowing a single planar bilayer to form on the coverslip surface and creating a flow chamber. 200 µl of HEPES buffer saline was then flowed through the chamber to wash away remaining liposomes, followed by 100 µl of a

blocking solution containing 5% (w/v) casein (Sigma, #C5890) to block non specific sites. Next, a 1:2 ratio of mono-biotinylated anti-CD3ε antibody labeled with either Alexa-647 or rhodamine-X (10 µg/ml) and streptavidin (Sigma, #85878) were added to the flow chamber to conjugate the anti-CD3ε antibody with the biotin-CAP-PE lipids in the bilayer. Similarly, His-tagged ICAM-1, either unlabeled or labeled with Alexa-647 (0.5 µg/ml), was added to the flow chamber to conjugate with the DOGS-NTA lipids in the bilayer. The uniformity and lateral mobility of lipids in the bilayers was accessed by imaging the diffusion of His-tagged ICAM-1 molecules labeled with Alexa-647 on the surface of the bilayer. For fixation of Jurkat cells on planar lipid bilayer substrates, they were flown into the bilayer chamber and incubated for 3 or 8 min at 37^{o}C and then fixed for 15 min in a solution containing 4% (w/v) paraformaldehyde (Polysciences, Inc., #00380), 1x PBS (pH 7.4) (Quality Biological, Inc., #119-069-101).

Optical Trap Design

We built a simple optical trap, modeled after an early design by Steven Block (vol. II, sec. 7, *Cells: A Laboratory Manual*, CSHL Press). A Nd:YVO4 laser of 4 W continuous power at 1064 nm wavelength provides the IR beam, a Uniblitz shutter gates the laser to a 10x beam expander, a ½ λ waveplate coupled with a polarized beam splitter attenuates the laser power, and an additional 2x Keplerian beam expansion allows complete filling of the back focal plane of the objective. Also, two mirrors in the pathway enable manual steering of the beam, and the beam splitter permits addition of a second beam for dual optical trapping in the future. Lastly, the IR Objective lens, either 60x at NA1.40, 100x at NA 1.42, or 150x at NA 1.45, then focuses the beam onto the specimen stage, forming a gradient required for optical trapping. Multiple trials showed that, indeed, we could trap polystyrene latex beads minimally at 1 mW of laser power and large lymphocytes at 25 mW.

Optical Trap System of Jurkat Cell Engagement

Raji B cells were incubated in cell culture media containing 2 μg/ml SEE for 1.5 hr at 37^{o}C, and then washed twice with culture media. To create a flow chamber, two strips of double-stick tape were placed on parallel edges of a glass slide, and then a #1.5 glass coverslip coated with fibronectin (Sigma, #F2006) was placed on top of the glass slide across the double-stick tape. Jurkat cells were introduced into the flow chamber and allowed to adhere to the fibronectin-coated coverslip for 2 min at 37^{o}C. The chamber was placed on the microscope stage and the adhered Jurkat cell expressing the appropriate reporter was selected. Raji cells were first chilled on ice for 5 min, and then introduced into the flow chamber. The chilling prevented attachment of the Raji cells to the fibronectin coverslip for ~30 sec, providing a brief window in time to trap a Raji cell. The optical trap was, then, turned on, focused on a nearby floating Raji cell, and controlled to bring the trapped Raji B cell opposite the centrosome of the adhered Jurkat cell. The optical trap was turned off and imaging began immediately after contact between the Jurkat T cell and SEE-coated Raji B cell. Jurkat cells were imaged for 30 min following engagement with the Raji B cell, at 15 sec/ frame unless indicated otherwise.

Image acquisition

Images were acquired using either a 60x (1.40 NA), 100x (1.42 NA), or 150x (1.45 NA) objective on an Olympus IX81 microscope fitted with a Yokogawa CSU-X1 spinning disk confocal unit and a QuantEM: 512SC camera (Photometrix). Images were analyzed using MetaMorph software. For dynamic imaging of Jurkat cells on the planar bilayer substrate, we loaded cells into a flow chamber containing the planar bilayer, placed the chamber on the microscope stage, identified cells which were well engaged and spread, then began imaging immediately. In general this process took 2 min. These time lapse images were acquired at 4 sec/frame over a duration of 5 min, unless indicated otherwise. For

simultaneous imaging of fluorescent molecules in the bilayer and in the cortex of the Jurkat cell, imaging was performed at the plane of the bilayer. For dynamic imaging, the temperature of the stage was maintained at 37^{o}C using a Nevtek stage heater. For imaging of calcium fluxes, Jurkat cells were loaded with Fluo-4 AM as described in the Molecular Probes product information sheet, and stimulated using coverslip substrates. The Prior NanoScan Z stage controller was used to take 4D time-lapse images of these cells before and after contact with stimulatory coverslip substrates. The relative intensities of Fluo-4 fluorescence over time were calculated using the region measurement tool in MetaMorph software. For imaging of TCR MCs, we utilized a planar bilayer containing unlabeled His-ICAM-1 and mono-biotinylated anti-CD3ε antibody labeled with Alexa-647.

Analysis of MTOC movement

For measurement of the distance of the MTOC from the IS in GFP- or RFP-Cen-2 expressing cells, a line was drawn at plane of contact between the Jurkat and Raji cells observed in the brightfield image and the line was transferred to the corresponding Cen-2 image using MetaMorph software. The distance from the center of the GFP- or RFP-Cen-2 spot to the line at the plane contact was measured, and this procedure was repeated to measure the MTOC distance from the synapse for each frame of the image stack. For Jurkat cells expressing GFP-Cen-2 and RFP-Farnesyl, The GFP and RFP image stacks were combined using MetaMorph software, and the distance from the center of the GFP-Cen-2 spot to the RFP-Farnesyl line at the contact site was measured for each image of the stack. For the assay of repositioning events, MTOC movements were scored as Full, Partial, or No Repositioning based on the smallest distance of the MTOC from the IS measured in the image stack. For calculation of the instantaneous speed of MTOC movement, the measured MTOC distance from the IS in a single image was subtracted from the previous image, and divided by the lapsed time between the two images. Instantaneous speeds of

MTOC movement calculated at >2.25 μm distance of the MTOC from the IS were averaged to give the polarization phase speed per cell, and at <2.25 μm distance of the MTOC from the IS were averaged to give the docking phase speed per cell.

VI. Acknowledgements

We would like to thank Jose Martina for help with cell culture, transfection protocols, and plasmids, Richard Vallee for LIS1 constructs and shRNA oligos, Minsoo Kim for LFA-1 constructs, Martin Poenie for the JB2.7 Jurkat cell line, Rajat Varma for generous help with bilayers and advice on T cells, Yasuharu Takagi and Kier Neuman for help with building the optical trap, and Lawrence Samelson for E6.1 and JCAM2.5 Jurkat cell lines.

VII. References

Adames, N.R., and Cooper, J.A. (2000). Microtubule interactions with the cell cortex causing nuclear movements in Saccharomyces cerevisiae. J Cell Biol *149*, 863-874.

Brown, A.C., Oddos, S., Dobbie, I.M., Alakoskela, J.M., Parton, R.M., Eissmann, P., Neil, M.A., Dunsby, C., French, P.M., Davis, I., and Davis, D.M. (2011). Remodelling of cortical actin where lytic granules dock at natural killer cell immune synapses revealed by super-resolution microscopy. PLoS Biol *9*, e1001152.

Burakov, A., Nadezhdina, E., Slepchenko, B., and Rodionov, V. (2003). Centrosome positioning in interphase cells. J Cell Biol *162*, 963-969.

Chang, J.T., Palanivel, V.R., Kinjyo, I., Schambach, F., Intlekofer, A.M., Banerjee, A., Longworth, S.A., Vinup, K.E., Mrass, P., Oliaro, J., Killeen, N., Orange, J.S., Russell, S.M., Weninger, W., and Reiner, S.L. (2007). Asymmetric T lymphocyte division in the initiation of adaptive immune responses. Science *315*, 1687-1691.

Chen, H.D., Ge, K.K., Li, Y.M., Wu, J.G., Gu, Y.Q., Wei, H.M., and Tian, Z.G. (2007). Application of optical tweezers in the research of molecular interaction between lymphocyte function associated antigen-1 and its monoclonal antibody. Cell Mol Immunol *4*, 221-225.

Combs, J., Kim, S.J., Tan, S., Ligon, L.A., Holzbaur, E.L., Kuhn, J., and Poenie, M. (2006). Recruitment of dynein to the Jurkat immunological synapse. Proc Natl Acad Sci U S A *103*, 14883-14888.

Faulkner, N.E., Dujardin, D.L., Tai, C.Y., Vaughan, K.T., O'Connell, C.B., Wang, Y., and Vallee, R.B. (2000). A role for the lissencephaly gene LIS1 in mitosis and cytoplasmic dynein function. Nat Cell Biol *2*, 784-791.

Gomes, E.R., Jani, S., and Gundersen, G.G. (2005). Nuclear movement regulated by Cdc42, MRCK, myosin, and actin flow establishes MTOC polarization in migrating cells. Cell *121*, 451-463.

Gomez, T.S., Kumar, K., Medeiros, R.B., Shimizu, Y., Leibson, P.J., and Billadeau, D.D. (2007). Formins regulate the actin-related protein 2/3 complex-independent polarization of the centrosome to the immunological synapse. Immunity *26*, 177-190.

Gonczy, P., Pichler, S., Kirkham, M., and Hyman, A.A. (1999). Cytoplasmic dynein is required for distinct aspects of MTOC positioning, including centrosome separation, in the one cell stage Caenorhabditis elegans embryo. J Cell Biol *147*, 135-150.

Gundersen, G.G. (2002). Evolutionary conservation of microtubule-capture mechanisms. Nat Rev Mol Cell Biol *3*, 296-304.

Hashimoto-Tane, A., Yokosuka, T., Sakata-Sogawa, K., Sakuma, M., Ishihara, C., Tokunaga, M., and Saito, T. (2011). Dynein-driven transport of T cell receptor microclusters regulates immune synapse formation and T cell activation. Immunity *34*, 919-931.

Huse, M., Klein, L.O., Girvin, A.T., Faraj, J.M., Li, Q.J., Kuhns, M.S., and Davis, M.M. (2007). Spatial and temporal dynamics of T cell receptor signaling with a photoactivatable agonist. Immunity *27*, 76-88.

Jenkins, M.R., Tsun, A., Stinchcombe, J.C., and Griffiths, G.M. (2009). The strength of T cell receptor signal controls the polarization of cytotoxic machinery to the immunological synapse. Immunity *31*, 621-631.

Kim, S.T., Takeuchi, K., Sun, Z.Y., Touma, M., Castro, C.E., Fahmy, A., Lang, M.J., Wagner, G., and Reinherz, E.L. (2009). The alphabeta T cell receptor is an anisotropic mechanosensor. J Biol Chem *284*, 31028-31037.

King, S.J., Brown, C.L., Maier, K.C., Quintyne, N.J., and Schroer, T.A. (2003). Analysis of the dynein-dynactin interaction in vitro and in vivo. Mol Biol Cell *14*, 5089-5097.

Kuhn, J.R., and Poenie, M. (2002). Dynamic polarization of the microtubule cytoskeleton during CTL-mediated killing. Immunity *16*, 111-121.

Kuhn, J.R., Wu, Z., and Poenie, M. (2001). Modulated polarization microscopy: a promising new approach to visualizing cytoskeletal dynamics in living cells. Biophys J *80*, 972-985.

Kuhne, M.R., Lin, J., Yablonski, D., Mollenauer, M.N., Ehrlich, L.I., Huppa, J., Davis, M.M., and Weiss, A. (2003). Linker for activation of T cells, zeta-associated protein-70, and Src homology 2 domain-containing leukocyte protein-76 are required for TCR-induced microtubule-organizing center polarization. J Immunol *171*, 860-866.

Martin-Cofreces, N.B., Robles-Valero, J., Cabrero, J.R., Mittelbrunn, M., Gordon-Alonso, M., Sung, C.H., Alarcon, B., Vazquez, J., and Sanchez-Madrid, F. (2008). MTOC translocation modulates IS formation and controls sustained T cell signaling. J Cell Biol *182*, 951-962.

McKenney, R.J., Vershinin, M., Kunwar, A., Vallee, R.B., and Gross, S.P. (2010). LIS1 and NudE induce a persistent dynein force-producing state. Cell *141*, 304-314.

Oddos, S., Dunsby, C., Purbhoo, M.A., Chauveau, A., Owen, D.M., Neil, M.A., Davis, D.M., and French, P.M. (2008). High-speed high-resolution imaging of intercellular immune synapses using optical tweezers. Biophys J *95*, L66-68.

Quann, E.J., Liu, X., Altan-Bonnet, G., and Huse, M. (2011). A cascade of protein kinase C isozymes promotes cytoskeletal polarization in T cells. Nat Immunol *12*, 647-654.

Quann, E.J., Merino, E., Furuta, T., and Huse, M. (2009). Localized diacylglycerol drives the polarization of the microtubule-organizing center in T cells. Nat Immunol *10*, 627-635.

Quintyne, N.J., Gill, S.R., Eckley, D.M., Crego, C.L., Compton, D.A., and Schroer, T.A. (1999). Dynactin is required for microtubule anchoring at centrosomes. J Cell Biol *147*, 321-334.

Redemann, S., Pecreaux, J., Goehring, N.W., Khairy, K., Stelzer, E.H., Hyman, A.A., and Howard, J. (2010). Membrane invaginations reveal cortical sites that pull on mitotic spindles in one-cell C. elegans embryos. PLoS One *5*, e12301.

Sancho, D., Vicente-Manzanares, M., Mittelbrunn, M., Montoya, M.C., Gordon-Alonso, M., Serrador, J.M., and Sanchez-Madrid, F. (2002). Regulation of microtubule-organizing center orientation and actomyosin cytoskeleton rearrangement during immune interactions. Immunol Rev *189*, 84-97.

Sedwick, C.E., Morgan, M.M., Jusino, L., Cannon, J.L., Miller, J., and Burkhardt, J.K. (1999). TCR, LFA-1, and CD28 play unique and complementary roles in signaling T cell cytoskeletal reorganization. J Immunol *162*, 1367-1375.

Splinter, D., Tanenbaum, M.E., Lindqvist, A., Jaarsma, D., Flotho, A., Yu, K.L., Grigoriev, I., Engelsma, D., Haasdijk, E.D., Keijzer, N., Demmers, J., Fornerod, M., Melchior, F., Hoogenraad, C.C., Medema, R.H., and Akhmanova, A. (2010). Bicaudal D2, dynein, and kinesin-1 associate with nuclear pore complexes and regulate centrosome and nuclear positioning during mitotic entry. PLoS Biol *8*, e1000350.

Stinchcombe, J.C., and Griffiths, G.M. (2007). Secretory mechanisms in cell-mediated cytotoxicity. Annu Rev Cell Dev Biol *23*, 495-517.

Stinchcombe, J.C., Majorovits, E., Bossi, G., Fuller, S., and Griffiths, G.M. (2006). Centrosome polarization delivers secretory granules to the immunological synapse. Nature *443*, 462-465.

Stowers, L., Yelon, D., Berg, L.J., and Chant, J. (1995). Regulation of the polarization of T cells toward antigen-presenting cells by Ras-related GTPase CDC42. Proc Natl Acad Sci U S A *92*, 5027-5031.

Tai, C.Y., Dujardin, D.L., Faulkner, N.E., and Vallee, R.B. (2002). Role of dynein, dynactin, and CLIP-170 interactions in LIS1 kinetochore function. J Cell Biol *156*, 959-968.

Tsai, J.W., Bremner, K.H., and Vallee, R.B. (2007). Dual subcellular roles for LIS1 and dynein in radial neuronal migration in live brain tissue. Nat Neurosci *10*, 970-979.

Tsai, J.W., Chen, Y., Kriegstein, A.R., and Vallee, R.B. (2005). LIS1 RNA interference blocks neural stem cell division, morphogenesis, and motility at multiple stages. J Cell Biol *170*, 935-945.

Tsun, A., Qureshi, I., Stinchcombe, J.C., Jenkins, M.R., de la Roche, M., Kleczkowska, J., Zamoyska, R., and Griffiths, G.M. (2011). Centrosome docking at the immunological synapse is controlled by Lck signaling. J Cell Biol *192*, 663-674.

Wei, X., Tromberg, B.J., and Cahalan, M.D. (1999). Mapping the sensitivity of T cells with an optical trap: polarity and minimal number of receptors for Ca(2+) signaling. Proc Natl Acad Sci U S A *96*, 8471-8476.

CHAPTER 4

CONCLUDING REMARKS AND FUTURE DIRECTIONS

I. Overview

The process of T cell activation involves a complex orchestration of cytoskeletal components. In this study, we show that TCR stimulation results in the reorganization of F-actin into radially symmetric LP and LM networks at the IS, and that the cortical actin flow generated by these networks drives the inward movement of receptor clusters at the IS. In concert with actin reorganization, the MTOC becomes polarized toward the APC, aligning MT minus ends and associated cargo toward the center of the IS for directed secretion. Our results show that this MTOC repositioning process is biphasic, involving signaling by LFA-1 and TCR, and cortical force generation mediated by dynein and LIS1. In all, our study highlight the critical roles of cytoskeletal components in T cell function, and indicate that Jurkat T cells could serve as a robust general model system for studying cytoskeletal dynamics and regulation.

II. What is the role of formin-generated actin filaments at the IS?

Our observations raise new questions about the conserved mechanisms of cytoskeletal regulation and function. For one, numerous filopodial-like ribs undergoing rapid actin retrograde flow are revealed by treatment with low-dose CD, representing a population of actin structures that are resistant to the inhibitory action of CD at low levels of treatment. If, indeed, these filopodial-like ribs are endogenous structures embedded within the LP actin

network, their contributions to TCR MC transport in the LP/dSMAC and acto-myosin II filament formation in the LM/pSMAC need to be examined in future experiments.

We speculate that these intra-lamellipodial, filopodial-like ribs serve as preferential tracks for TCR MC transport in the LP/dSMAC. We often observed prolonged periods of radial movement along the outside rim of the IS before TCR MCs initiated movement into the LP/dSMAC, suggesting that not all areas of the LP actin network allow inward movement of TCR MCs. In addition, we observed instances when multiple TCR MCs moved sequentially along the same linear path in the LP/dSMAC, suggesting that preferential tracks exist in the LP/dSMAC for TCR MC transport. As the LP network in metazoan cells is thought to consist of a dendritic actin network nucleated by the Arp2/3 complex and filopodial actin filaments nucleated by formins (Chhabra and Higgs, 2007), inhibition experiments targeting the two classes of actin nucleators at the IS are needed to test our hypothesis. Furthermore, as the mechanistic coupling between the TCR MCs and cortical actin networks is thought to be transient and dissipative (Kaizuka *et al.*, 2007; DeMond *et al.*, 2008; Yu *et al.*, 2010), the binding strength between the respective actin network (dendritic or filopodial actin) and TCR MCs needs to be investigated. It is possible that the parallel, bundled actin filaments of filopodial-like ribs are preferable substrates for TCR MCs than the angled, branched filaments of the dendritic actin network.

III. How does F-actin reorganize at the border between the LP/dSMAC and LM/pSMAC?

According to the dendritic model of actin nucleation, dendritic actin filaments become depolymerized at the rear to generate actin monomers, which become sequestered and recycled back to the leading edge for actin polymerization (Pollard and Borisy, 2003). In our study, strong accumulation of F-actin is observed at the border between the LP/dSMAC and LM/pSMAC in Jas-treated cells, suggesting that robust depolymerization of F-actin normally

occurs at the rear of the LP/dSMAC. This conclusion is consistent with studies in other cell types showing that ~90% of LP actin depolymerizes at the rear of the LP (Ponti *et al.*, 2004). Given that the dendritic actin network is essentially a closed loop system, and that most dendritic actin filaments become depolymerized and recycled back to the leading edge, we speculate that formin-generated actin filaments in the LP/dSMAC (i.e. filopodial-like ribs) serve in part as the precursors for acto-myosin II arc formation in the LM/pSMAC.

Formins are unique among actin nucleating proteins in their ability to accelerate the elongation of actin filaments, and in their ability to serve as barbed end polymerization machines while remaining associated with the barbed ends of growing actin filaments (Chhabra and Higgs, 2007; Chesarone *et al.*, 2010). As the mechanism of formin-mediated actin elongation is thought to occur through alternating contacts between the FH2 domains of the formin dimer to the actin subunits of a growing filament, the barbed ends of actin filaments are effectively shielded from capping proteins during formin-mediated actin elongation (Chesarone *et al.*, 2010). This is consistent with the continued actin retrograde flow observed in filopodial-like ribs in the presence of low-dose CD, which is thought to inhibit actin polymerization by capping the free barbed ends of actin filaments (Carlier *et al.*, 1986). Furthermore, as formins are thought to bundle actin filaments (Chhabra and Higgs, 2007; Chesarone *et al.*, 2010), the generation of parallel, crosslinked filaments should confer greater stability to these bundled actin structures. We imagine that the bundled, parallel filaments comprising the filopodial-like ribs resist severing by ADF/cofilin at the rear of the LP, and continue their treadmilling movement into the LM region, where they become associated with bipolar myosin II filaments to form contractile acto-myosin II arcs. Our observation that GFP-actin does not report the acto-myosin II arcs in the LM/pSMAC is consistent with this idea, as it has been recently shown that GFP-actin cannot be incorporated into formin-generated actin filaments (Chen *et al.*, 2012). Since mDIA1 and FMNL1 have been shown to be the dominantly expressed formins in T cells (Gomez *et al.*,

2007), specific inhibition of these two formins using shRNA knockdown, as well as general inhibition of formins using SMIFH2 need to be performed to test the role of formins in the assembly of acto-myosin II filaments during T cell activation.

IV. What is the "diffusion" barrier for LFA-1 clusters at the pSMAC-cSMAC border?

Results from our study, as well as the study by Kaizuka *et al*., indicate that TCR MCs are able to pass through, while LFA-1 integrin clusters are blocked at the border between the cSMAC and pSMAC regions (Kaizuka *et al.*, 2007). R. Vale and colleagues suggest that differential coupling between TCR and LFA-1 clusters to the cortical actin network is the basis for the selective transport of TCR MCs into the cSMAC (Kaizuka *et al.*, 2007). Specifically, once formed, TCR MCs are not dependent on the cortical actin network and can continue centripetal movement into the actin-depleted cSMAC region, while LFA-1 clusters require the cortical actin network as a structural scaffold, and therefore become disassembled when acto-myosin II arcs are disassembled at the pSMAC-cSMAC boundary. Alternatively, Groves and colleagues suggest that the differential localization of TCR and LFA-1 clusters at the IS is due to the relative size of these clusters, and showed using multivalents antibodies that artificially enlarged LFA-1 clusters can compete with TCR MCs for placement in the cSMAC region (Hartman *et al.*, 2009; Hartman and Groves, 2011). Our results are consistent with the model proposed by Vale and colleagues, as we observe accumulation of LFA-1 clusters at the LM/pSMAC-cSMAC border, movement of TCR MCs between successive acto-myosin II arcs in the LM/pSMAC, and rapid, complete disappearance of actin arcs at the rear of the LM/pSMAC, suggesting a strong overlap in the dynamics and behavior of LFA-1 clusters and acto-myosin II arcs at the IS. That said, when the cSMAC region was no longer actin-depleted in BB-treated cells, presumably due to inhibition of actin arc disassembly, LFA-1 clusters were still restricted to the pSMAC ring of

the IS. This observation is inconsistent with the differential coupling model, and suggests that the "diffusion" barrier may not be actin-dependent.

Instead, we speculate that a physical barrier exists at the pSMAC-cSMAC border; possibly a large organelle that binds the cortical components of the TCR MC with high affinity. The Golgi apparatus is a strong candidate, as it becomes repositioned to the center of the IS via association with the MTOC, and as TCR MCs are internalized at the cSMAC, and sorted into multivesicular bodies for eventual degradation (Lee *et al.*, 2003; Stinchcombe *et al.*, 2006; Vardhana *et al.*, 2010). We imagine that pre-Golgi vesicles become associated with TCR MCs and are transported between acto-myosin II arcs in the LM/pSMAC toward the IS center, where it merges with the repositioned Golgi apparatus to form the cSMAC. In this scenario, the tight connection between the Golgi apparatus and TCR MCs at the cSMAC would act as a barrier to restrict movement of actin arcs and LFA-1 clusters into the cSMAC, and possibly contribute to the close apposition of the MTOC to the IS during the docking phase of MTOC repositioning. Live imaging of pre-Golgi vesicles, the Golgi apparatus, and TCR MCs and inhibition experiments targeting the association between TCR MCs and the Golgi apparatus need to be performed to test this hypothesis.

V. How is dynein anchored at the IS cortex?

Different mechanisms of dynein recruitment to the IS have been suggested in previous reports. Results from Poenie and colleagues suggest that dynein is recruited to the IS via association with ADAP at the dSMAC region (Combs *et al.*, 2006). On the other hand, a recent study by Saito and colleagues argued that dynein associates with TCR MCs during T cell activation, implying that dynein should localize to the cSMAC region of the IS (Yokosuka *et al.*, 2005). Our results are inconsistent with these proposed mechanisms of dynein recruitment, as we observe a uniform distribution of dynein at the IS, without preference for specific SMAC regions and without strong co-localization with TCR MCs.

However, as MTOC repositioning is dependent on TCR stimulation, and as proximal TCR signaling components are also implicated in MTOC repositioning, it is possible that dynein associates indirectly with TCRs at the IS. Live imaging of cortical dynein with TCR adaptor proteins, such as SLP76 and LAT, and molecules involved in downstream TCR signaling, such as PKCθ, will be needed to address this question. Lastly, to identify the cortical receptor for dynein at the IS in T cells, Jurkat cells bound to stimulatory substrates will be unroofed and rapidly fixed to retain the cortical dynein at the IS, and co-immunoprecipitation-coupled mass spectrometry will be used to identify the associated proteins.

VI. What is the mechanism of cortical force generation at the IS?

Studies of spindle positioning in yeast and *C. elegans*, and MTOC repositioning in migrating fibroblasts, have identified two mechanisms for MT pulling at the cortex in cells (Gundersen, 2002; Burakov *et al.*, 2003; Manneville and Etienne-Manneville, 2006; Tanaka and Desai, 2008). The first mechanism involves the pulling force driven by MT depolymerization coupled with MT plus end-attachment to the cortex. This may be the major mechanism for asymmetric spindle positioning in the *C. elegans* embryo, where depolymerizing MT ends are held at the cortex via cortical attachment factors (Gundersen, 2002; Kaltschmidt and Brand, 2002; Manneville and Etienne-Manneville, 2006). The second mechanism involves the pulling force driven by the minus end-directed movement of cortically anchored dynein motors along MTs. Studies in budding yeast show that translocation of the nucleus and spindle into the bud neck occurs through such 'MT capture and sliding' mechanism, driven by dynein localized at the bud cortex via the cortical receptor, Num1 (Adames and Cooper, 2000; Gundersen, 2002). However, recent *in vitro* results by Laan *et al*., indicate that dynein can also be involved in MT depolymerization-mediated force transduction, as cortical dynein bound on microfabricated barriers were shown to capture

MT plus ends and trigger MT depolymerization, resulting in a strong pulling force on MTs (Laan *et al.*, 2012).

Currently, the mechanism of cortical force generation during MTOC repositioning in T cells is not yet known. Since the two mechanisms of MT pulling (MT depolymerization vs. dynein pulling) require distinct configurations of cortically associated MTs (end-on vs. lateral), we will perform high resolution imaging of MTs at the IS using structured illumination microscopy to test the dominant mechanism of MT pulling during T cell activation. Moreover, live-imaging of cortically associated dynein and MTs will allow us to observe MT plus-end capture or MT sliding events at the IS. Lastly, we plan to perform laser ablation on cortically associated MTs to test whether net shrinking is observed (indicative of MT depolymerization-driven pulling) or whether net MT sliding is observed (indicative of dynein-driven pulling) in ablated MTs at the IS.

VII. References

Adames, N.R., and Cooper, J.A. (2000). Microtubule interactions with the cell cortex causing nuclear movements in Saccharomyces cerevisiae. J Cell Biol *149*, 863-874.

Burakov, A., Nadezhdina, E., Slepchenko, B., and Rodionov, V. (2003). Centrosome positioning in interphase cells. J Cell Biol *162*, 963-969.

Carlier, M.F., Criquet, P., Pantaloni, D., and Korn, E.D. (1986). Interaction of cytochalasin D with actin filaments in the presence of ADP and ATP. J Biol Chem *261*, 2041-2050.

Chen, Q., Nag, S., and Pollard, T.D. (2012). Formins filter modified actin subunits during processive elongation. J Struct Biol *177*, 32-39.

Chesarone, M.A., DuPage, A.G., and Goode, B.L. (2010). Unleashing formins to remodel the actin and microtubule cytoskeletons. Nat Rev Mol Cell Biol *11*, 62-74.

Chhabra, E.S., and Higgs, H.N. (2007). The many faces of actin: matching assembly factors with cellular structures. Nat Cell Biol *9*, 1110-1121.

Combs, J., Kim, S.J., Tan, S., Ligon, L.A., Holzbaur, E.L., Kuhn, J., and Poenie, M. (2006). Recruitment of dynein to the Jurkat immunological synapse. Proc Natl Acad Sci U S A *103*, 14883-14888.

DeMond, A.L., Mossman, K.D., Starr, T., Dustin, M.L., and Groves, J.T. (2008). T cell receptor microcluster transport through molecular mazes reveals mechanism of translocation. Biophys J *94*, 3286-3292.

Gomez, T.S., Kumar, K., Medeiros, R.B., Shimizu, Y., Leibson, P.J., and Billadeau, D.D. (2007). Formins regulate the actin-related protein 2/3 complex-independent polarization of the centrosome to the immunological synapse. Immunity *26*, 177-190.

Gundersen, G.G. (2002). Evolutionary conservation of microtubule-capture mechanisms. Nat Rev Mol Cell Biol *3*, 296-304.

Hartman, N.C., and Groves, J.T. (2011). Signaling clusters in the cell membrane. Curr Opin Cell Biol *23*, 370-376.

Hartman, N.C., Nye, J.A., and Groves, J.T. (2009). Cluster size regulates protein sorting in the immunological synapse. Proc Natl Acad Sci U S A *106*, 12729-12734.

Kaizuka, Y., Douglass, A.D., Varma, R., Dustin, M.L., and Vale, R.D. (2007). Mechanisms for segregating T cell receptor and adhesion molecules during immunological synapse formation in Jurkat T cells. Proc Natl Acad Sci U S A *104*, 20296-20301.

Kaltschmidt, J.A., and Brand, A.H. (2002). Asymmetric cell division: microtubule dynamics and spindle asymmetry. J Cell Sci *115*, 2257-2264.

Laan, L., Pavin, N., Husson, J., Romet-Lemonne, G., van Duijn, M., Lopez, M.P., Vale, R.D., Julicher, F., Reck-Peterson, S.L., and Dogterom, M. (2012). Cortical dynein controls

microtubule dynamics to generate pulling forces that position microtubule asters. Cell *148*, 502-514.

Lee, K.H., Dinner, A.R., Tu, C., Campi, G., Raychaudhuri, S., Varma, R., Sims, T.N., Burack, W.R., Wu, H., Wang, J., Kanagawa, O., Markiewicz, M., Allen, P.M., Dustin, M.L., Chakraborty, A.K., and Shaw, A.S. (2003). The immunological synapse balances T cell receptor signaling and degradation. Science *302*, 1218-1222.

Manneville, J.B., and Etienne-Manneville, S. (2006). Positioning centrosomes and spindle poles: looking at the periphery to find the centre. Biol Cell *98*, 557-565.

Pollard, T.D., and Borisy, G.G. (2003). Cellular motility driven by assembly and disassembly of actin filaments. Cell *112*, 453-465.

Ponti, A., Machacek, M., Gupton, S.L., Waterman-Storer, C.M., and Danuser, G. (2004). Two distinct actin networks drive the protrusion of migrating cells. Science *305*, 1782-1786.

Stinchcombe, J.C., Majorovits, E., Bossi, G., Fuller, S., and Griffiths, G.M. (2006). Centrosome polarization delivers secretory granules to the immunological synapse. Nature *443*, 462-465.

Tanaka, T.U., and Desai, A. (2008). Kinetochore-microtubule interactions: the means to the end. Curr Opin Cell Biol *20*, 53-63.

Vardhana, S., Choudhuri, K., Varma, R., and Dustin, M.L. (2010). Essential role of ubiquitin and TSG101 protein in formation and function of the central supramolecular activation cluster. Immunity *32*, 531-540.

Yokosuka, T., Sakata-Sogawa, K., Kobayashi, W., Hiroshima, M., Hashimoto-Tane, A., Tokunaga, M., Dustin, M.L., and Saito, T. (2005). Newly generated T cell receptor microclusters initiate and sustain T cell activation by recruitment of Zap70 and SLP-76. Nat Immunol *6*, 1253-1262.

Yu, C.H., Wu, H.J., Kaizuka, Y., Vale, R.D., and Groves, J.T. (2010). Altered actin centripetal retrograde flow in physically restricted immunological synapses. PLoS One *5*, e11878.